

GRADUATE DESIGN REPORT  
GEORGIA INSTITUTE OF TECHNOLOGY  
28<sup>TH</sup> ANNUAL AHS  
STUDENT DESIGN COMPETITION 2011



Sylvester Ashok  
Raymond Beale  
Bhanu Chiguluri  
Michael Jones  
Jeewoong Kim  
Jonathan Litwin  
Marc Mugnier  
Jaikrishnan Vijayakumar  
Xin Zhang



**“ODYSSEY”  
MULTI-MISSION AIRCRAFT**

**DEPARTMENT OF AEROSPACE ENGINEERING  
GEORGIA INSTITUTE OF TECHNOLOGY  
ATLANTA, GA, 30332**

**AND**

**UNIVERSITY OF LIVERPOOL**

**28TH ANNUAL AMERICAN HELICOPTER SOCIETY STUDENT DESIGN COMPETITION  
GRADUATE CATEGORY**

Sylvester Ashok PhD Candidate  
[sylvester\\_ashok@gatech.edu](mailto:sylvester_ashok@gatech.edu)

Raymond Beale - Graduate Student  
AE 8900 – Special Problem  
[rbeale@gatech.edu](mailto:rbeale@gatech.edu)

Bhanu Chiguluri - Undergraduate Student  
AE 4359 – Rotorcraft Design II  
[bhanu89@gatech.edu](mailto:bhanu89@gatech.edu)

Michael Jones – PhD Candidate  
(University of Liverpool)  
[michael.jones@liverpool.ac.uk](mailto:michael.jones@liverpool.ac.uk)

Jeewoong Kim - Graduate Student  
AE 6334 – Rotorcraft Design II  
[jkim677@gatech.edu](mailto:jkim677@gatech.edu)

Jonathan Litwin - Undergraduate Student  
AE 4359 – Rotorcraft Design II  
[jlitwin3@gatech.edu](mailto:jlitwin3@gatech.edu)

Marc Mugnier - Graduate Student (Team leader)  
AE 8900 – Special Problem  
[marc.mugnier@supaero.org](mailto:marc.mugnier@supaero.org)

Jaikrishnan Vijaykumar – Graduate Student  
AE 6334 – Rotorcraft Design II  
[Jvijaykumar3@gatech.edu](mailto:Jvijaykumar3@gatech.edu)

Xin Zhang – PhD Candidate  
AE 6334 – Rotorcraft Design II  
[xaxtoo@gatech.edu](mailto:xaxtoo@gatech.edu)

Dr. Daniel P. Schrage – Principal Advisor and Instructor  
AE 6334 – Rotorcraft Design II (SPRING 11)  
[daniel.schrage@aerospace.gatech.edu](mailto:daniel.schrage@aerospace.gatech.edu)

### **Acknowledgements**

The Odyssey design team would like to acknowledge the following people and thank them for their assistance and advice during the entire project:

Dr Daniel P. Schrage – Professor, Department of Aerospace Engineering, Georgia Institute of Technology

Dr Dimitri N. Mavris – Director of ASDL, Department of Aerospace Engineering, Georgia Institute of Technology

Dr Lakshmi Sankar – Regents Professor, Department of Aerospace Engineering, Georgia Institute of Technology

Dr. Emre Gunduz – Postdoctoral fellow, Department of Aerospace Engineering, Georgia Institute of Technology

Dr Byung-Young Min – Postdoctoral fellow, Department of Aerospace Engineering, Georgia Institute of Technology

Wg. Cmdr. Martin Mayer

Mr Alex Robledo

Mr Tom Lawrence

Mr Mike Roberts

Mr Robert Loewy

Mr Apinut Sirirojvisuth

Mr Mike Osmon

Ms Tiffany Adams

### **Special Acknowledgments**

The Odyssey design team would like to thank especially Mr Etienne Baer for his unique contribution to the project and Mr Robert Scott and his team for their valuable support on the cost analysis.

## TABLE OF CONTENTS

TABLE OF CONTENTS.....	IV
LIST OF FIGURES.....	VI
LIST OF TABLES.....	VIII
ACRONYMS.....	IX
NOMENCLATURE .....	X
GENERAL INTRODUCTION .....	1
ODYSSEY KEY FEATURES AND TECHNOLOGIES .....	4
ODYSSEY SPECIFICATIONS.....	5
TOP-LEVEL REQUIREMENTS .....	6
<b>APPENDIX A     VEHICLE CONFIGURATION AND SELECTION .....</b>	<b>7</b>
A.1. <i>Helicopter Missions</i> .....	7
A.2. <i>Cabin configuration</i> .....	9
A.3. <i>Additional requirements</i> .....	10
A.4. <i>Initial concept selection</i> .....	15
A.5. <i>Hub selection and IBC system</i> .....	16
A.6. <i>Comparison between HH-60G Pavehawk and Odyssey</i> .....	18
<b>APPENDIX B     CONCEPT INITIAL SIZING AND PERFORMANCE.....</b>	<b>19</b>
B.1. <i>Initial sizing</i> .....	19
B.2. <i>Performance evaluation</i> .....	20
B.3. <i>Initial Performance without the auxiliary propulsion</i> .....	22
<b>APPENDIX C     MAIN ROTOR GEOMETRY AND AIRFOIL DESIGN .....</b>	<b>23</b>
C.1. <i>Rotor radius selection and optimization</i> .....	23
C.2. <i>Airfoil selection</i> .....	25
C.3. <i>Taper ratio and linear twist selection</i> .....	27
C.4. <i>Final blade planform design</i> .....	30
<b>APPENDIX D     FUSELAGE DESIGN .....</b>	<b>31</b>
D.1. <i>Validation of the CFD code</i> .....	31
D.2. <i>Drag Analysis</i> .....	32
D.3. <i>Fuselage aerodynamics and forces</i> .....	34
<b>APPENDIX E     AUXILIARY PROPULSION DESIGN .....</b>	<b>36</b>
E.1. <i>Final Design Configuration</i> .....	38
<b>APPENDIX F     ENGINE DESIGN .....</b>	<b>40</b>
F.1. <i>Baseline engine GE CT701C</i> .....	40
F.2. <i>Rubberized engine</i> .....	40
F.3. <i>Single Engine Hover Ceiling</i> .....	40
F.4. <i>Final Engine configuration</i> .....	42
<b>APPENDIX G     ODYSSEY PERFORMANCE SUMMARY .....</b>	<b>45</b>
G.1. <i>Power curves</i> .....	45
G.2. <i>Speed performance with All Engines On (AEO)</i> .....	47

G.3.	Engine failure condition performance .....	48
G.4.	Payload Range diagram.....	50
G.5.	Performance summary .....	51
<b>APPENDIX H</b>	<b>WEIGHT BREAKDOWN AND MATERIAL SELECTION .....</b>	<b>52</b>
H.1.	Weight calculation of the fuel system .....	52
H.2.	Material selection .....	52
H.3.	Stealth mode.....	54
H.4.	Empty weight breakdown.....	55
<b>APPENDIX I</b>	<b>YAW CONTROL AND GURNEY FLAPS .....</b>	<b>56</b>
<b>APPENDIX J</b>	<b>DRIVE SYSTEM.....</b>	<b>59</b>
J.1.	Requirements.....	59
J.2.	Conceptual Design .....	59
J.3.	Gear Train Sizing.....	60
J.4.	Optimization Setup .....	61
J.5.	Optimization results.....	63
J.6.	Controller design.....	65
<b>APPENDIX K</b>	<b>STRUCTURAL ANALYSIS AND ROTOR DYNAMICS .....</b>	<b>67</b>
K.1.	V-n Diagram.....	67
K.2.	Rotor Structural Dynamics.....	67
K.3.	Active Vibration Control.....	71
K.4.	Airframe Structural Integrity .....	71
<b>APPENDIX L</b>	<b>NOISE EMISSION.....</b>	<b>73</b>
L.1.	Applicability of ICAO Stage 4 Noise emission.....	73
L.2.	Noise level requirements .....	73
L.3.	Aeroacoustics code WOPWOP .....	74
<b>APPENDIX M</b>	<b>HANDLING QUALITIES AND FLIGHT CONTROLS .....</b>	<b>77</b>
M.1.	FLIGHTLAB Model .....	77
M.2.	Handling Qualities and Piloted Simulation .....	78
M.3.	Mission Task Elements.....	83
M.4.	Overall Pilot Assessment.....	88
M.5.	Recommendations for future design iteration.....	89
<b>APPENDIX N</b>	<b>AVIONICS.....</b>	<b>90</b>
N.1.	Generation and distribution architecture .....	90
N.2.	Avionics and cockpit features .....	90
<b>APPENDIX O</b>	<b>COST ANALYSIS.....</b>	<b>91</b>
O.1.	Development cost .....	92
O.2.	Recurring cost and acquisition cost .....	94
O.3.	Direct operating cost .....	95
<b>APPENDIX P</b>	<b>CERTIFICATION CONSIDERATIONS AND TIMEFRAME .....</b>	<b>97</b>
<b>CONCLUSIONS AND RECOMMENDATIONS .....</b>		<b>99</b>
<b>REFERENCES.....</b>		<b>100</b>

## LIST OF FIGURES

Figure 0-1: GeorgiaTech Integrated Product and Process Development Methodology [45].....	1
Figure 0-2: Advanced rotorcraft design concepts considered [11] .....	2
Figure 0-3: US Armed Forces HH-60G Pavehawk [48].....	2
Figure 0-4: Integrated Rotorcraft Design tool .....	3
Figure 0-5: Future roadmap for the Army Aviation [9].....	3
Figure A-1: Odyssey Area coverage and ground ambulance coverage .....	7
Figure A-2: Cabin configuration with three transverse stretchers .....	9
Figure A-3: Cabin configuration with 6 passengers .....	9
Figure A-4: Quality Function Deployment (QFD) matrix.....	13
Figure A-5: Prioritization Ranking of the two scales .....	15
Figure A-6: Concepts scores vs. two scales.....	15
Figure A-7: Final relative score of the concepts.....	16
Figure A-8: Individual Blade Control system on Odyssey’s main rotor .....	17
Figure A-9: Morphological matrix of Odyssey .....	18
Figure B-1: Rf method for Rotorcraft/VSTOL Aircraft synthesis [43] .....	19
Figure B-2: sizing results for the three primary missions.....	20
Figure B-3: Power required vs. Airspeed for the.....	20
Figure B-4: Initial Performance for mission 2 without aux propulsion .....	22
Figure C-1: ModelCenter's Design Explorer environment framework.....	23
Figure C-2: Rotor diameter sensitivity analysis using the Rf method [26] .....	24
Figure C-3: Advancing side Mach number vs. Tip speed at 250 kts .....	24
Figure C-4: Mach number and advance ratio at sea-level vs. Airspeed .....	25
Figure C-5: SC1095 Airfoil profile .....	25
Figure C-6: Airfoil simple trade study.....	25
Figure C-7: Pitching coefficient at 250 kts.....	26
Figure C-8: Lift to drag ratio at 250 kts at sea-level.....	27
Figure C-9: CT trim vs. CP .....	29
Figure C-10: Figure of Merit at sea-level vs. taper ratio and linear twist.....	29
Figure C-11: Final Blade Planform design of Odyssey .....	30
Figure D-1: Pressure coefficient distribution on the ROBIN fuselage .....	31
Figure D-2: Odyssey fuselage and hub drag evaluation with CFD code.....	32
Figure D-3: Streamline velocity with the pusher propeller disengaged.....	32
Figure D-4: Streamline velocity with the pusher proeller engaged .....	33
Figure D-5: Bodyframe .....	34
Figure D-6: Airloads vs. angle of attack.....	35
Figure D-7: Airloads vs. sideslip angle .....	35
Figure D-8: Variation of the flat plate drag area vs. angle of attack.....	35
Figure E-1: Propeller system design process.....	36
Figure E-2: Ideal Thrust Available from a 5 ft Diameter Propeller.....	36
Figure E-3: Local Thrust Coefficient for a Ducted and Unducted Propeller Blade.....	37
Figure E-4: 5 ft diameter propeller design trade study .....	38
Figure E-5: Odyssey propeller system’s off-design performance .....	39
Figure E-6: Ducted Configuration with horizontal stabilizer .....	39
Figure E-7: Dual counter-rotating blades .....	39
Figure E-8: Pusher propeller configuration (rear view).....	39
Figure F-2: Impact of ceiling on the fuel consumption .....	41
Figure F-1: Impact of ceiling on the design gross weight .....	41
Figure F-3: Impact of ceiling on the DOC.....	42
Figure F-4: T700 GE701C.....	42
Figure F-5: Power available of Odyssey's engine vs. altitude and atmospheric condition .....	44
Figure G-1: Power curve at sea-level for mission 1 .....	45
Figure G-2: Power curve in military HOT DAY conditions for mission 1 .....	46
Figure G-3: Power curve at sea-level for mission 2 .....	46

Figure G-4: Power curve for mission 2 in military Hot Day conditions.....	47
Figure G-5: RoC at maximum takeoff gross weight.....	48
Figure G-6: Autorotative index derived for several helicopters and Odyssey .....	49
Figure G-7: Payload range diagram at max TOGW .....	50
Figure H-1: Odyssey fuel system weight calculation .....	52
Figure H-2: Odyssey gear housing in Graphite-Epoxy material.....	52
Figure H-3: Starflex of Odyssey's main rotor.....	53
Figure H-4: Odyssey engine and transmission mounts .....	53
Figure H-5: Odyssey Primary structure .....	53
Figure H-6: Pusher structure and duct frame.....	54
Figure H-7: Odyssey empty weight breakdown .....	55
Figure I-1: Differential collective in high power state.....	56
Figure I-2: Differential collective in low power state.....	56
Figure I-3: VR-7 Airfoil with Double Gurney ( $x/c=0.9$ , $h/c=0.025$ ).....	57
Figure I-4: Gurney Flaps on the main rotor blade under CATIA .....	57
Figure I-5: Dynamic Simulation of Gurney flaps yaw control power .....	58
Figure I-6: ADS-33 Requirements for moderate amplitude yaw heading changes .....	58
Figure J-1: Concept of planetary CVT [3].....	59
Figure J-2: Transmission schematic .....	60
Figure J-3: Optimization setup .....	61
Figure J-4: Face gear finite element analysis in ANSYS .....	64
Figure J-5: Ring gear and clutch bands actuators .....	64
Figure J-6: Power Electronic Module architecture .....	66
Figure K-1: Vn diagram .....	67
Figure K-2: Axial Strength of blades .....	68
Figure K-3: Lag stiffness of main rotor blades.....	68
Figure K-4: Flap stiffness of main rotor blades.....	69
Figure K-5: RCAS Blade model.....	69
Figure K-6: Hover fanplot at 310 RPM (Tip speed: 650 ft/s).....	70
Figure K-7: Forward flight fanplot at 215 RPM (Tip speed: 450 ft/s) .....	70
Figure K-8: Predicted pilot 4/rev vibration [49].....	71
Figure L-1: Rotor blade formed by a series of four structured patches [22].....	74
Figure L-2: Odyssey's main rotor blade .....	74
Figure L-3: Odyssey's pusher propeller blade .....	75
Figure L-4: Single observer point during PSU WOPWOP processing .....	75
Figure L-6: Thickness noise level for the pusher propeller .....	76
Figure L-5: Thickness noise level for the main rotor only .....	76
Figure M-1: CSGE screen .....	77
Figure M-2: Bare Airframe Poles of Odyssey .....	79
Figure M-3: Cyclic Control channels of Odyssey .....	80
Figure M-4: Collective, Pedal and Throttle Control Channels of Odyssey .....	80
Figure M-5: aircraft response to longitudinal doublet control input.....	80
Figure M-6: Trimmed flight control positions.....	81
Figure M-7: Poles of dutch roll oscillation.....	81
Figure M-8: Poles of longitudinal pitching oscillation.....	81
Figure M-9: Maximum achievable Roll Quickness.....	82
Figure M-10: Maximum achievable Pitch Quickness .....	82
Figure M-11: Arrangement for hover MTE.....	83
Figure M-12: Comparison of CHR for several aggression pull maneuvers.....	86
Figure M-13: Comparison of CHR for several aggression hover turn maneuvers .....	86
Figure M-14: Comparison of CHR several aggression roll step maneuvers .....	87
Figure M-15: Arrangement of throttle and collective controls .....	88
Figure N-1: Odyssey's cockpit and avionics.....	90
Figure O-1: Odyssey's development cost (in 2011 USD).....	92
Figure O-2: Monte Carlo simulation of the RDTE cost .....	93
Figure O-3: Drive system cost decomposition vs. manufacturing method.....	94

Figure O-4: Odyssey Average unit cost vs. production units .....	95
Figure O-5: Average Production cost breakdown .....	95
Figure O-6: Operations and Support Cost .....	96
Figure O-7: Sensitivity analysis of the fuel price's impact on the O&S cost .....	96
Figure P-1: FAA Type certificate process .....	97
Figure P-2: Tentative Development schedule and certification timeframe .....	98

## LIST OF TABLES

Table A-1: Overall Evaluation Criterion for Odyssey and baseline vehicle.....	14
Table A-2: Comparison of the baseline HH-60G Pavehawk vs. Odyssey.....	18
Table C-1: Optimized Rotor geometry at first iteration .....	23
Table C-2: Lift and drag coefficients at 250 kts .....	27
Table C-3: Material properties of the Main Rotor System .....	30
Table D-1: Drag coefficients of the Robin fuselage .....	31
Table D-2: Assumptions, streamline visualization and drag coefficients.....	32
Table D-3: Comparison of flat plate drag area with and without the fan .....	33
Table D-4: Drag build-up and estimation of the flat plate drag area .....	34
Table D-5: CG position of Odyssey .....	34
Table E-1: Odyssey Propeller System Design Specifications .....	38
Table F-1: Characteristics of Odyssey's engine .....	44
Table G-1: Odyssey Performance summary .....	51
Table H-1: Material selection for the fuselage section .....	54
Table J-1: Transmission Design inputs.....	60
Table J-2: Optimization parameters.....	62
Table J-3: Gear material properties .....	62
Table J-4: Genetic Algorithm setup.....	63
Table J-5: Drive system weight breakdown .....	63
Table J-6: Odyssey Transmission results .....	64
Table K-1: Main rotor vibrations.....	72
Table L-1: PSU WOPWOP Assumptions .....	75
Table L-2: Noise level calculation for Odyssey .....	76
Table M-1: Rotor configuration .....	77
Table M-2: Total Vehicle Mass and Inertia Values.....	78
Table M-3: Odyssey control power .....	82
Table M-4: Odyssey control power predicted handling qualities levels.....	82
Table M-5: Precision Hover MTE Tolerances .....	83
Table M-6: Emergency Pull-Up MTE Tolerances .....	84
Table M-7: Hover Turn MTE Tolerances .....	84
Table M-8: Speed Conversion MTE Tolerances .....	85
Table M-9: Speed Conversion MTE Tolerances .....	85
Table M-10: Summary of Cooper-Harper Ratings awarded.....	89
Table O-1: Life-cycle cost decomposition .....	91
Table O-2: Existing aircraft used for the validation of the Bell PC model.....	91
Table O-3: Bell PC model general inputs.....	92
Table O-4: Possible manufacturing process for each part .....	94
Table O-5: Final manufacturing combination .....	94

## ACRONYMS

6K95	Military Hot Day conditions (6,000 ft and 95 degrees Fahrenheit)
A/C	Aircraft
AEO	All Engines On
AVC	Active Control Vibration
BERP	British Experimental Rotor Program
CAD	Computer Aided Design
CAE	Computer Aided Engineering
CAM	Computer Aided Manufacturing
CBEM	Combined Blade Element Momentum (theory)
CE	Concurrent Engineering
CIRADS	Concept Independent Rotorcraft Analysis and Design Software
CVT	Continuously Variable Transmission
DER	Designated Engineering Representatives
DOC	Direct Operating Cost
DoE	Design of Experiments
ESF	Engine Scaling Factor
FFSO	Full Factorial Sub-Optimizer
FW	Face Width
GA	Genetic Algorithm
HIGE	Hover In Ground Effect
HOGE	Hover Out of Ground Effect
ICAO	International Civil Aviation Organization
IDG	Integrated Drive Generator
IPPD	Integrated Product and Process Development
IPR	Intermediate Rated Power
IRP	Intermediate Rated Power
LCC	Lifecycle Cost
MCI	Mission Capability Index
MCP	Maximum Continuous Power
MCP	Maximum Continuous Power
MRP	Maximum Rating Power
MTBF	Mean Time Between Failure
MTTR	Mean Time To Repair
NCI	Noise Comfort Index
O&S	Operations and Support (cost)
OEC	Overall Evaluation Criterion
OEI	One Engine Inoperative
OEM	Original Equipment Manufacturer
PEM	Power Electronic Module
PSCP	Project Specific Certification Plan
QFD	Quality Function Deployment (matrix)
RCAS	Rotorcraft Comprehensive Analysis System
RDTE	Research, Development, Testing and Evaluation (cost)
Rf	Fuel fraction method
RFP	Request for Proposal
RWST	Rotary Wind Structures Technology (program)
SABP	Self Aligning Bearingless Planetary
SAR	Search and Rescue
SFC	Specific Fuel Consumption
SI	Safety Index
SMR	Single Main Rotor
TRL	Technology Readiness Level

## NOMENCLATURE

$\psi$	Helical angle
A	Disk area
Acq	Acquisition price
AF	Activity Factor
alt	Altitude
$A_\pi$	Equivalent flat plate drag area
b	Number of blades per main rotor
B	Pusher propeller number of blades
c	Average chord
$C_d$	Drag coefficient
$C_{d0}$	Zero lift drag coefficient
chord <sub>n±</sub>	Chord of a segment n
$C_L$	Lift coefficient
$C_M$	Pitch moment coefficient
$C_T$	Thrust coefficient
cutout	Cutout percentage
D	Drag of the vehicle
DOC	Direct Operating cost
$d_p$	Pitch diameter
$E_{pw}$	Excess power
g	Gravity acceleration
hp <sub>mec</sub>	Mechanical power
ihp	Main rotor Induced power
$I_R$	Main Rotor Moment of Inertia
M	Gear material
$m_g$	Gear ratio / mechanical advantage
MI	Manufacturability Index
$M_n$	Blade station of segment n
n	Number of blade elements (BEM theory)
$n_1:n_2$	Taper ratio
$N_{Approach}$	Noise during approach
$N_{eng}$	Number of engines
NI	Interior noise
$N_{og}$	Number of gears
$N_{Overflight}$	Over-flight noise
$N_t$	Number of fuel tanks
$N_{TO}$	Noise at takeoff
ocd	Outer cone distance
$p, g$	Pinion, gear (superscript)
Payload	Payload weight
$P_c$	Probability that the failure is catastrophic
$P_d$	Diametral Pitch
$P_{det}$	Probability of being detected
$P_f$	Probability of an in-flight failure
$P_{hit}$	Probability of being hit
php	Parasite power
$P_{kill}$	Probability of being killed
$P_{srv}$	Probability of surviving a catastrophic crash
R	Gas constant
r	Local radius
R	Main Rotor radius
$R_1$	Range in Mission 1 configuration
$R_2$	Range in Mission 2 configuration
$R_3$	Range in Mission 3 configuration

RDTE	RDTE cost
Rhp	Main rotor profile power
rhp	Total power
RoC	Rate of climb
$r_p$	Penalty factor
$S_b$	Bending stress
$S_{ba}$	Allowable bending stress
$S_c$	Contact stress
$S_{ca}$	Allowable contact stress
Surv	Survivability
T	Main rotor thrust
$t_{k/e}$	Time to recognize engine failure
$T_{std}$	Temperature standard at a given altitude
$V_{aux}$	Auxiliary Fuel tank volume
$V_{be}$	Best endurance speed
$V_{br}$	Best range speed
$V_d$	Rate of descent
$V_{fus}$	Fuselage Fuel tank volume
$V_{MCP}$	Maximum cruise speed at MCP
W	Vehicle Weight
$W_f$	Fuel Weight
$W_{gs}$	Gearset weight
$w_p$	Weight penalty function
Z	Height above the ground
$\Delta T$	Temperature gap with standard atmosphere
$\Delta x$	Blade element width (BEM theory)
$\eta_{mec}$	Mechanical efficiency
$\eta_{prop}$	Propeller efficiency
$\theta$	Local pitch angle
$\Lambda$	In-ground effect correction factor
$\lambda_i$	Inflow ratio
$\lambda_{i,n}$	Inflow ratio on segment n
$\mu$	Advance ratio
$\rho$	Air density
$\rho_0$	Air density at sea-level
$\sigma$	Main rotor solidity
$\sigma_n$	Local solidity of a segment n
$\Omega$	Main Rotor angular speed

## GENERAL INTRODUCTION

The Request for Proposal for the 28th Annual AHS/Industry Student Design Competition for a Multi-Mission Aircraft has led to a configuration analysis of several rotorcraft designs. This report aims to validate and present the technical specifications for a coaxial compound helicopter as the best design to satisfy the range, flight speed and weight requirements of the aircraft. Perhaps the most innovative and creative aspect of aerospace engineering is during the conceptual design of a new aircraft system. The configuration synthesis consists of putting together parts, elements, or disciplines so as to form a whole. Engineers must assess and evaluate the best first level analysis from aerodynamics, propulsion, weight control, design, and cost to combine them in order to obtain an aircraft configuration able to perform the required mission. In the process of doing this, the most important variables will be parametrically analyzed and the controlling ones selected. As such, helicopters in production today may be referred to as a baseline design. Rotorcrafts are a trade between hover performance and forward flight speed. However, technology advancements are required to achieve higher forward flight speeds and cargo requirements. A design parametric sensitivity evaluation will provide the best configuration for the missions based on the parameters this design team has chosen to optimize. Essentially we have been tasked with combining the most efficient aerodynamic design and propulsion elements necessary to perform the missions at the lowest cost and weight, following the Georgia Tech Integrated Product and Process Development (IPPD) methodology [45] for rotorcraft preliminary design, as shown in Figure 0-1.

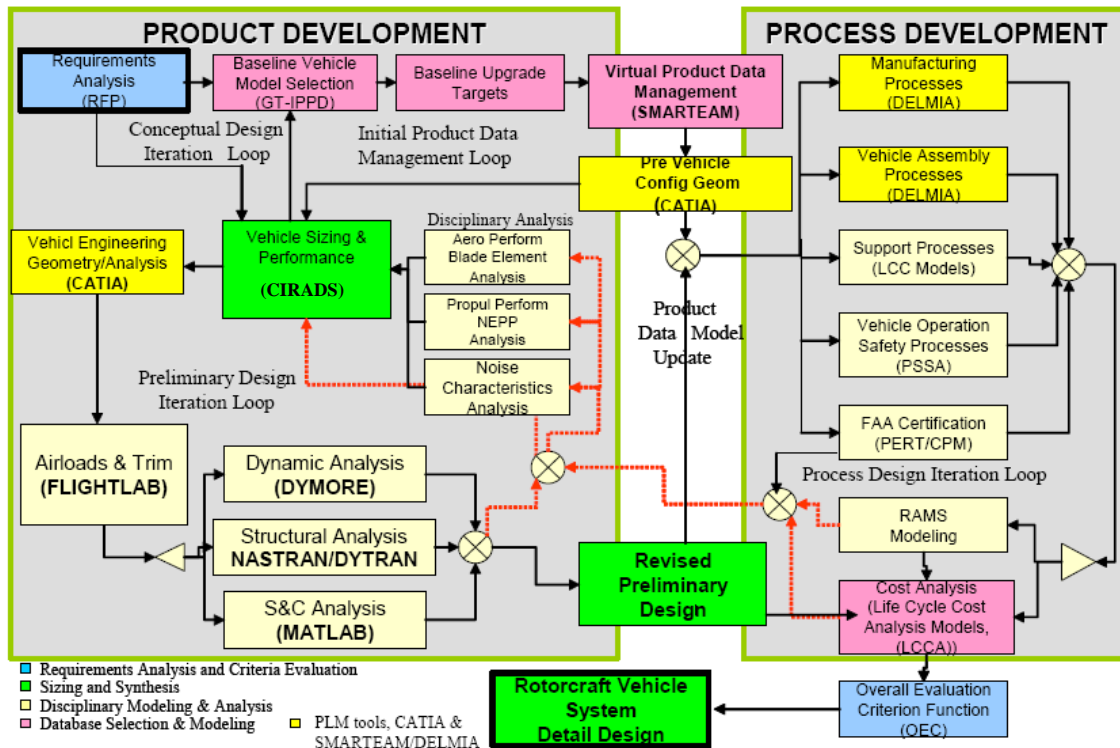


FIGURE 0-1: GEORGIATECH INTEGRATED PRODUCT AND PROCESS DEVELOPMENT METHODOLOGY [45]

In order to evaluate different rotorcraft configurations from an objective point of view, specific criteria, which capture the key product and process characteristics, need to be established from the problem definition. There are many metrics that can be employed within an Overall Evaluation Criterion (OEC) to ensure that the rotorcraft is being evaluated on the criteria most relevant to the missions and performance requirements. During the conceptual design phase the Georgia Tech teams worked on several concepts to meet the AHS mission requirements and selected the most competitive vehicle configurations for the preliminary design stage. This selection has been conducted by using a strict and fair comparison with the

key parameters that drove the conceptual and preliminary design. The concepts included an advanced helicopter, a single main rotor compound helicopter, a coaxial compound helicopter, an advanced tandem rotor compound and a tilt rotor, as shown in Figure 0-2.

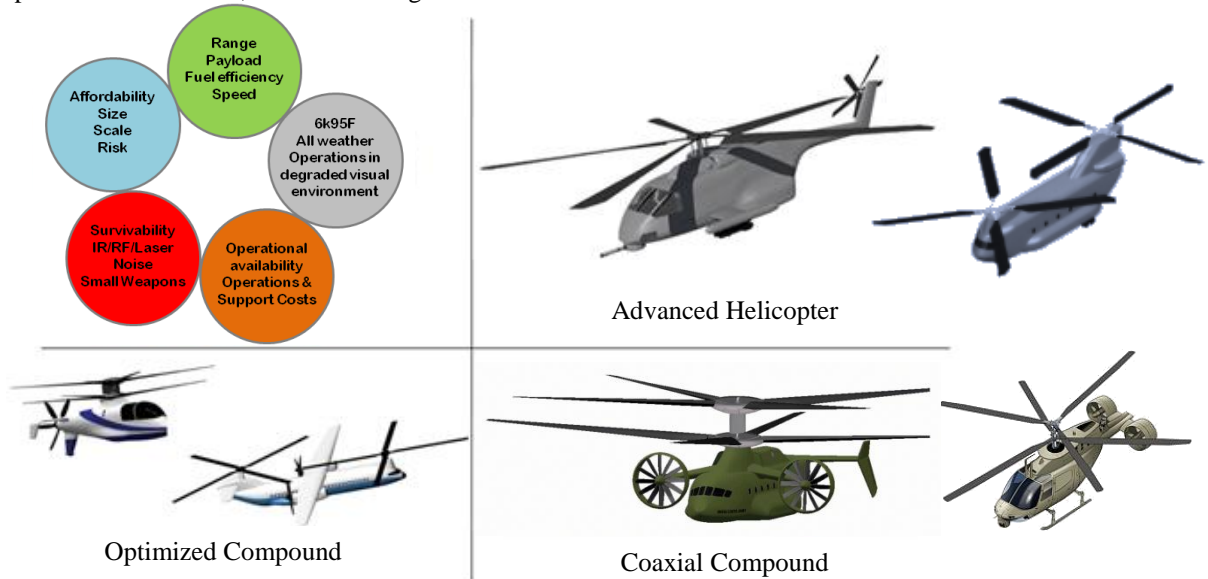


FIGURE 0-2: ADVANCED ROTORCRAFT DESIGN CONCEPTS CONSIDERED [11]

The ability to reach high speed cruise and maintain desirable hover capabilities is an ongoing challenge to rotorcraft designers. The coaxial compound design provides many attractive qualities for the flight envelope, assuming reductions in coaxial hub drag are available or measurable via technology gap considerations. All coaxial helicopters poses the unique quality of offloading retreating blades, allowing for optimization of lift production from the advancing blades, significantly attenuating the high drag and torque generated. The pusher configuration allows the vehicle to unload the lift generated by the main rotors in forward flight and provides enough forward propulsion to reach higher cruise speed. These constraints have been driving most of the research efforts of the industry in the domain of vertical-lift capability vehicles.

This report aims to provide details about the design of a coaxial compound helicopter to perform the mission profiles set by the 28th Bell AHS competition. The objective is to validate and present the preliminary design of this vertical lift vehicle and highlight the tradeoff analysis required to make this concept feasible. Currently the US Armed Forces, excepting the Marine Corps, primarily utilize variants of the Sikorsky UH-60 Blackhawk for Combat Search and Rescue, Insertion, and Resupply missions. For this reason, the SAR version of this helicopter, the HH-60G Pavehawk shown in Figure 0-3, has been selected as the baseline vehicle for our study. Though a capable helicopter, the Pavehawk does have a number of shortcomings and is nearing the end of its original lifetime. One of this rotorcraft's shortcomings is the many variants employed by the four services in order to accomplish these three missions as well as many other missions. Currently, the US military employs ten variants of the HH-60 most of which accomplish several missions beyond their primary mission. The only real exception to this is the dedicated medical evacuation aircraft and the VIP transport aircraft (the only variant utilized by the US Marine Corps). The variants decrease the availability of aircraft and increase the HH-60 systems operational and acquisition cost, requiring more airframes.



FIGURE 0-3: US ARMED FORCES HH-60G PAVEHAWK [48]

Unfortunately, this rotorcraft does not accomplish future missions to the satisfaction of the US Armed Forces. Several shortcomings arise in the airspeed and payload accomplished by the HH-60G. The dash speed is limited for the same reason as other conventional helicopters by transonic tip speed at very high advance ratio and blade stall on the retreating side. The internal payload is also limited, though external loads allow for a much higher payload. These performance limits, added to the many variants required to effectively accomplish different missions, result in an aircraft that is not sufficient for the US Military forces. This report details the completion of the Integrated Product and Process Development (IPPD) Methodology shown in Figure 0-1. The initial Rf method [44] was used to conduct initial sizing analysis in terms of horsepower and gross weight, each component of the vehicle was optimized in the Preliminary Design Iteration Loop. The integrated Rotorcraft Design tool had to be implemented in a parametric design environment to conduct this project, as shown in Figure 0-4.

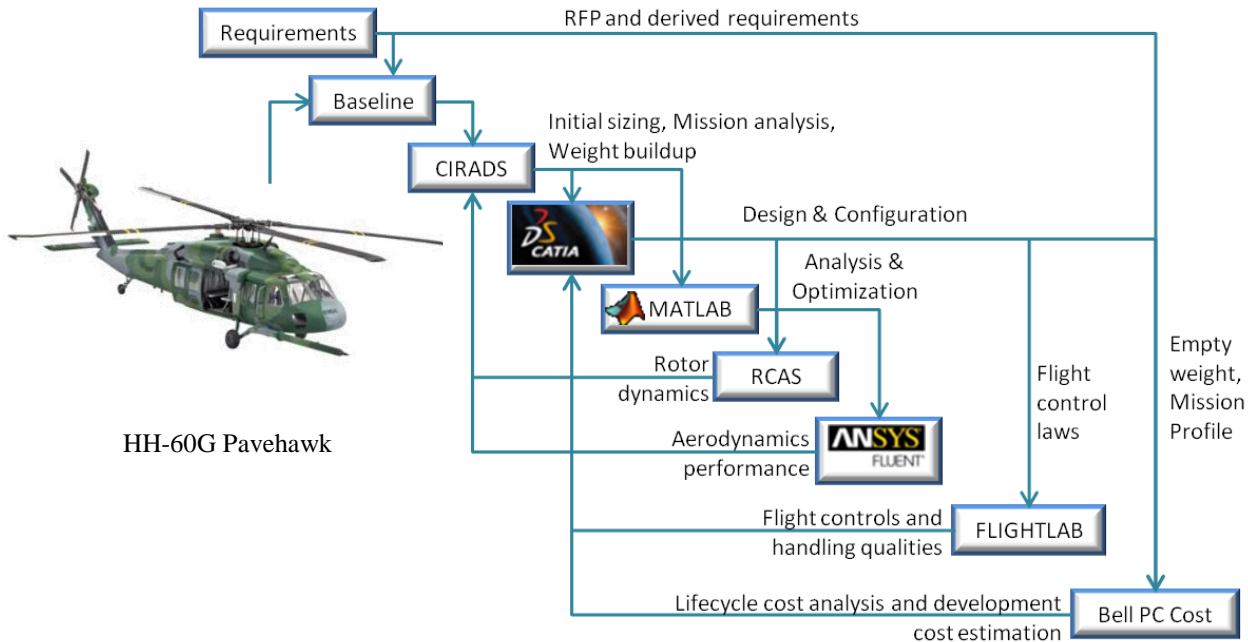


FIGURE 0-4: INTEGRATED ROTORCRAFT DESIGN TOOL

The future roadmap for the army aviation is shown in Figure 0-5 [9]. The replacement of the current multi-role transport helicopter UH-60 and its variants is scheduled for 2030 and the Army is looking for a new vehicle able to perform a large variety of missions depicted by the RFP. Due to the lack of specific requirements regarding the timeframe in the RFP, Odyssey should perform its first flight by 2025 for an entry in service as early as possible. Consequently, a number of key technologies which present a low Technology Readiness Level (TRL) today can be implemented by 2025.

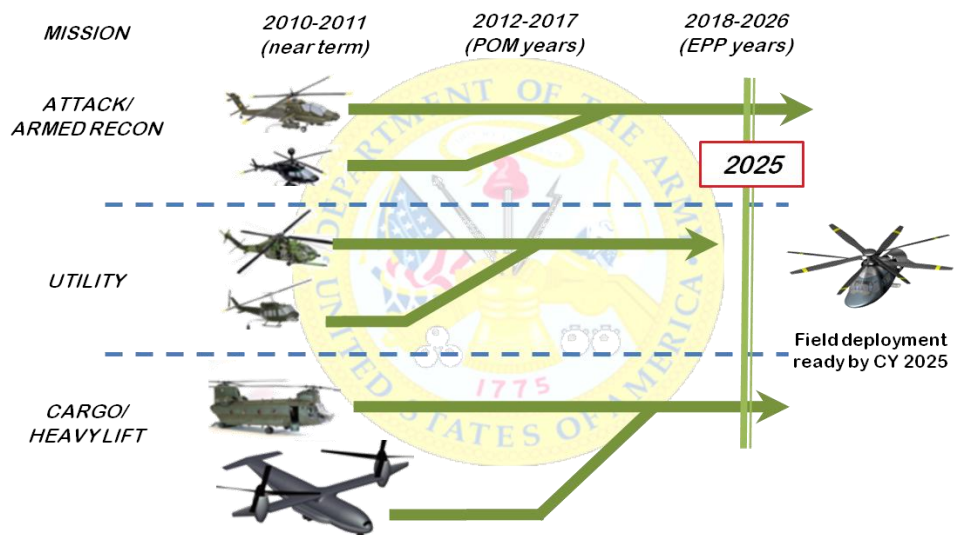
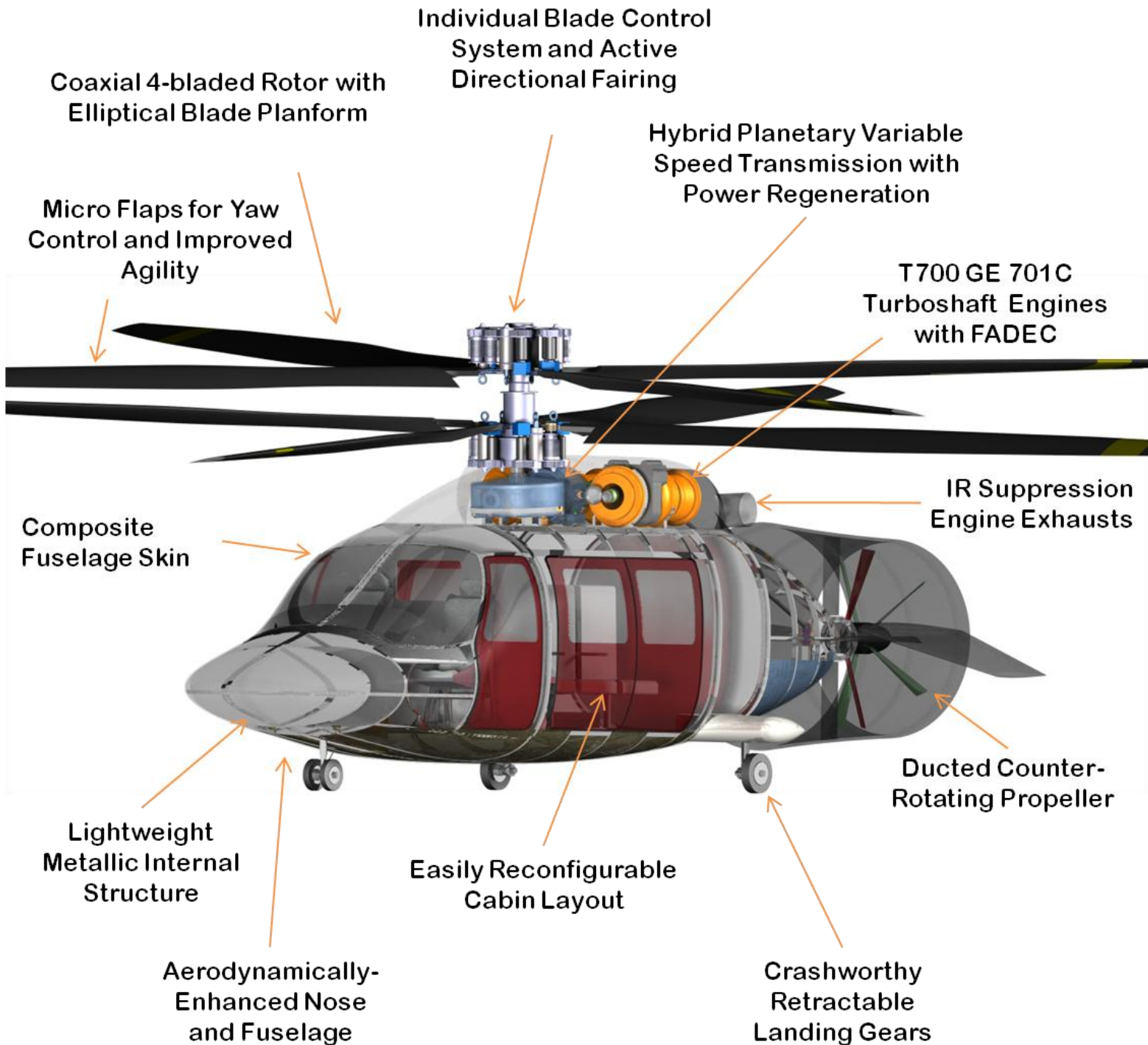
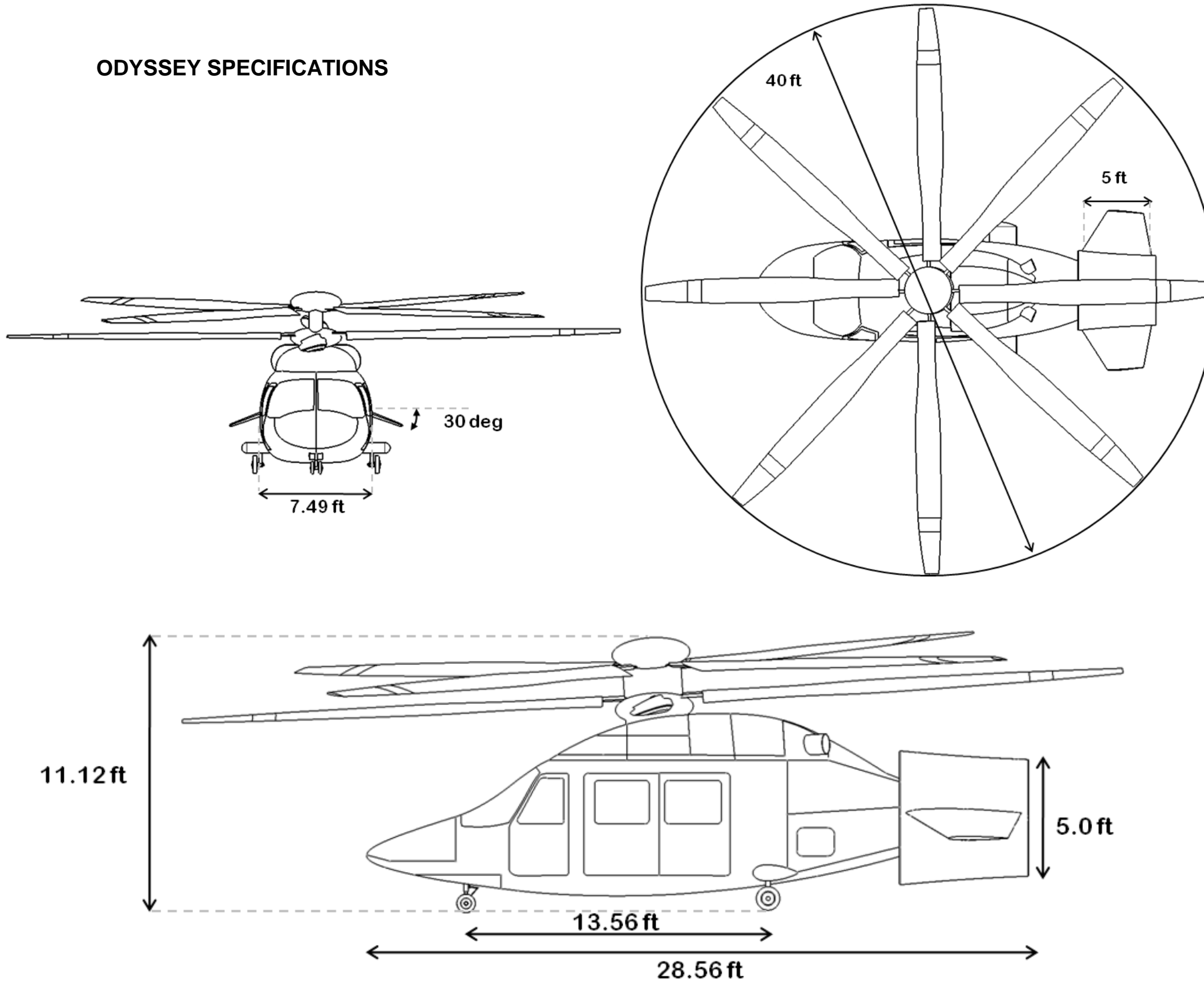


FIGURE 0-5: FUTURE ROADMAP FOR THE ARMY AVIATION [9]

## ODYSSEY KEY FEATURES AND TECHNOLOGIES



**ODYSSEY SPECIFICATIONS**



**ODYSSEY SPECIFICATIONS**

**DIMENSIONS**

Length overall	28.56 ft	8.7 m
Overall height	11.12 ft	3.38 m
Fuselage width	7.49 ft	2.3 m
Rotor diameter	40 ft	12.2 m
Cabin volume	309 ft <sup>3</sup>	8.7 m <sup>3</sup>
Disk Loading	11.97 lbs/ft <sup>2</sup>	58.44 kg/m <sup>2</sup>

**PROPULSION AND DRIVE SYSTEM**

2 x T700 GE 701C Turboshaft with FADEC and Hybrid Continuously Variable Speed Transmission

**ENGINE RATING**

IRP 30 min	2 x 1,678 shp	2 x 1,251 kW
MCP	2 x 1,550 shp	2 x 1,155 kW
OEI 2 ½ min	1,809 shp	1,348 kW

**WEIGHT**

Max TOGW	15,020 lbs	6,812 kg
Empty	8,470 lbs	3,841 kg
Max Payload	4,000 lbs	1,814 kg
Typical EMS equipment	2,100 lbs	952 kg
Fuel	2,120 lbs	961 kg
Crew	800 lbs	362 kg

**CAPACITY**

4 crew (1 Pilot, 1 Co-pilot, 1 Crew Chief, 1 Flight Engineer)

3 stretchers + 2 medical attendants or up to 6 passengers + equipment

**PERFORMANCE (ISA, S.L., MGW)**

Max Range	642 nm	1,187 km
Max Endurance	4.0 hr	
Dash speed IRP	246 kts	455 km/h
Max Cruise Speed V <sub>MAX</sub>	239 kts	442 km/h
Best range speed V <sub>BR</sub>	134 kts	248 km/h
Best endurance speed V <sub>BE</sub>	77 kts	142 km/h
Figure of Merit	0.84	
Service ceiling	19,500 ft	5,943 m
Absolute ceiling	20,100 ft	6,126 m

**TOP-LEVEL REQUIREMENTS**

Requirement	Target Value	Comments	Method/ Tool <sup>1</sup>	Section
VTOL	Yes	Coaxial configuration for vertical takeoff and landing capability	B	A.4.
Cabin	Reconfigurable <30 min	Reconfigurable cabin for the primary missions in less than 30 minutes for deployability	B/CATIA	A.2.
Multi-mission	3 missions	Sizing of the vehicle to perform three primary missions	A/CIRADS	A.1.
Crew	4 permanent	1 pilot / 1 copilot / 1 Chief Cabin / 1 Operational crew	B/CATIA	A.2.
6K95 HOGE	Possible using MCP	Hover capability of the vehicle in military Hot Day conditions at max TOGW	A/MATLAB	G.1.
Rubber Engine	GE CT 701C	Rubberize the baseline engine for the HH-60G Pavehawk		F.2.
Detectability	Minimize	Minimize Infrared signature and radar signature for increased survivability in hostile environments	C	H.3.
Operability	Three times a week	Operating costs calculation was based on this assumption	A/ Excel	O.3.
Costs	Minimize	(RDTE) costs, Specific Fuel Consumption (SFC) and operating cost must be minimized	A/ Bell PC model	Appendix O
Reserve fuel	45 minutes	FAR Part 91.151 reserve fuel at night, in VFR conditions [16]	A/CIRADS	B.1
Self-Deployability	1,500 nm	Internal additional fuel tanks may be required to perform this mission	A/MATLAB	G.4.
Speed and ceiling	Maximize	Maximize cruise speed to perform Mission 1 within 'Golden Hour' and maximize ceiling performance	A/MATLAB	G.2.
Overflight Noise	95.33 EPNdB	Effective Perceived Noise measured when aircraft flies over at cruise speed and at 500 ft	A/WOPWOP	L.3.
Approach noise	98.33 EPNdB	Effective Perceived Noise measured from 60 ft away while hovering	A/WOPWOP	L.3.
Take-off noise	95.33 EPNdB	Effective Perceived Noise measured one mile away during cruise	A/WOPWOP	L.3.
Hub technology	IBC	Optimize hub selection for performance, safety and reliability	B	A.5.

Requirement	Target Value	Comments	Method/ Tool	Section
Achieve Yaw control	ADS 33E Section 3.3.6	Peak yaw rate to change in heading shall meet the limits specified in ADS thanks to micro flaps	S/ FLIGHTLAB	Appendix I
Handling Qualities	Level 1&2	Achieve Level 1 and Level 2 handling qualities specified by ADS 33E Section 3	S/ FLIGHTLAB	M.2.
Hover stability	ADS 33E	Perform Mission Tasks Elements analysis to conduct stability assessment	S/ FLIGHTLAB	M.3.
Reliability/ Maintenance	Minimize cost and time	Maximize Mean Time Between Failures and minimize Mean Time To Repair	C	A.3.
Autorotation maneuver	$t_{ke} > 1.5s$	Give the pilot enough time to recognize engine failure to safely engage autorotation maneuver	A/MATLAB	G.3.
OEI rate of climb	150 ft/s	One Engine Inoperative (OEI) requirement is defined by FAR Part 29.67 [16]	A/MATLAB	G.3.
OEI HIGE 6K95	Hover capability	HIGE capability in emergency power rating with one engine inoperative at 6K95	A/MATLAB	F.4.
Safety Index	1	Safety Index (SI) defines how safely a given aircraft will behave during the mission	A/MATLAB	A.3.
Vibrations	Minimize	FAR Part 29.251 The rotorcraft must be free from excessive vibration during normal conditions [18]	A/ANSIS	K.3.
Fatigue	10,000 hrs	Material should be selected to guarantee 10,000 hrs life before replacement	A/Abaqus	H.2.
Transition	Smooth from hover to cruise	The transmission should enable transition and the helicopter shall be controlled and stabilized	A/CATIA Excel	Appendix J
Slowed main rotor	Variable speed transmission	Slowed tip speed via hybrid variable speed transmission. Power Electronic Module shall control the transition regime	A/CATIA Excel	J.6.
Structural load factor	Ultimate load factor	Vn diagram limitation envelope	A/Excel	K.1.
Ground resonance	Avoid	Stiff-inplane blades to avoid n/rev and ground resonance	A/RCAS	K.2.
Blade stability	Dynamic stability	Fan Plot for 4-bladed main rotor. Avoid 3,4,5/rev	A/RCAS	K.2.
TC issuance	By FY2025	First flight by FY2025. Certification Plan and TRL assessment	A	Appendix P

<sup>1</sup> A : Analysis      B : By Design      C : Compliance Statement      S : Simulation

## Appendix A VEHICLE CONFIGURATION AND SELECTION

Several helicopters in production have been selected as design contributors for this next generation configuration. The recent cruise speed record holder, the Sikorsky X2 Technology Demonstrator, will serve as a baseline for the rotor design, including airfoil selection, hub type, and structural load capabilities. As such, blade element theory will be applied to the chosen rotor parameters in order to properly size the rotor to meet the thrust requirements for the heavier AHS configuration. In addition, the Russian coaxial KA 27 and KA 50 provide a comparable weight division for the required missions. This reference will aid in providing a weight breakdown of vehicle components, specific range capabilities and give insight into the factors which limit high speed cruise and long range of these vehicles. Furthermore, the Cheyenne compound helicopter is an example of a single main rotor configuration with a pivoting tail propeller which provides auxiliary propulsion in the form of a pusher rotor. A careful comparison of this compound helicopter to similar mission type standard SMR helicopters will provide additional information concerning weight contributions of the transmission and structural components supplied by the addition of an auxiliary propulsion design. Since time is limited for this initial configuration analysis, an in depth market survey provides baseline estimates for different components of the aircraft. Based on the given mission requirements, a collection of baseline geometries were considered, highlighting the unique qualities of each vehicle. Afterward, several configurations derived from existing designs were run through the Concept Independent Rotorcraft Analysis and Design Software (CIRADS) developed at GeorgiaTech [13], with corresponding estimates for range, cost and reliability for each configuration.

### A.1. Helicopter Missions

The development of Odyssey to fulfill some of the missions beyond the UH-60 offers the possibility for greatly increased capability and efficiency for the US Armed Forces. Performance improvements would be best realized in an increased airspeed and payload. A maximum airspeed close to 240-250 kts would allow Odyssey to return a critical casualty from up to 225 nautical miles away to an advanced care facility within the *Golden Hour*, greatly increasing the likelihood that the casualty will survive. Additionally, outfitting the aircraft specifically for the medical evacuation mission will make rotorcraft an advanced medical vehicle beyond what is currently available. Increasing internal payload decreases the number of aircraft and trips required to resupply and insert troops onto the battlefield during wars. Combat Search and Rescue (CSAR), troop insertion, and resupply are the three primary missions that must be performed by Odyssey.

#### Benefits of the helicopter to the emergency medical service role

The unique characteristics of Odyssey make it well-suited to the role of an emergency vehicle. Vertical takeoff and landing capability, high cruise speed along with a smooth ride allow it to be used where ground transportation or ambulances are inadequate or impossible. Figure A-1 shows the area covered by a ground ambulance and the area covered by one single Odyssey unit. There are several ways to use helicopter in MEDEVAC operations. These include: the transfer of patients from one hospital to another facility, the delivery of advanced medical teams and equipment to the scene of an accident, the retrieval of accident victims and their delivery to centers of medical care, and the rapid transport of blood and organs when time is critical [25].

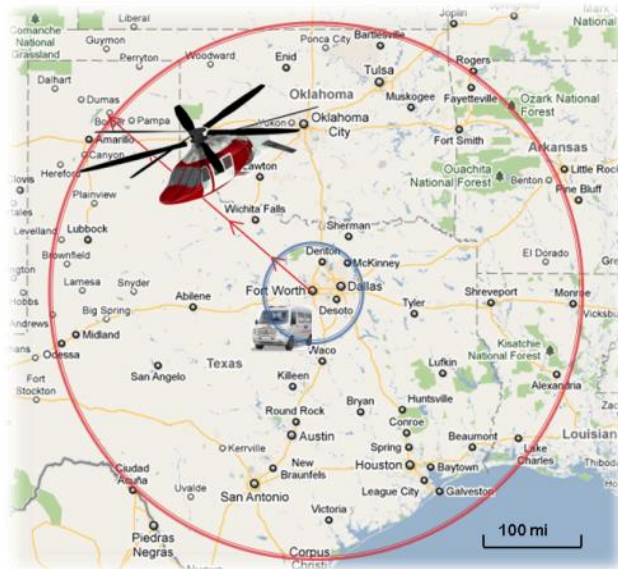


FIGURE A-1: ODYSSEY AREA COVERAGE AND GROUND AMBULANCE COVERAGE

The predominant use of the emergency helicopter in the United States today is as hospital-based, fully equipped air ambulance, that is to say an airborne extension of the emergency room. It is possible to stabilize the patient before transport, either at the scene or at a local hospital, and then provide a high level of medical care enroute to a more relevant specialized medical center.

### **Mission 1 Search and Rescue**

Mission 1 is a typical Search and Rescue (SAR) mission. Preparing for a response to mass disasters, such as major earthquakes or industrial disasters, requires revisions of present local, regional, and national disaster plans. These plans should include the following [37]:

- life-supporting first aid and basic rescue capability of the lay public
- advanced trauma life support and advanced (heavy) rescue capability brought quickly to the scene from local and surrounding (regional) emergency medical services systems
- trauma hospitals sending medical resuscitation teams to, and receiving casualties from, the disaster scene for resuscitative surgery and definitive care

In a scenario where an emergency medical services model is created and designed to mobilize rapid support for local emergency medical services from regional, state, and national resources, the armed forces should help, at least for transport and security. The *Golden Hour* rule states that the first 60 minutes following the mass disaster or the injury are vital to rescue casualties.

The vehicle must carry up to 6 passengers during the inbound leg during 225 nm between 50 and 70 minutes. In order to meet this requirement, we decided to target an initial maximum speed of 225 knots. In this case, the inbound leg would be performed in less than 60 minutes, greatly increasing the probability of saving lives. The starting point of the mission is located at 6,000 ft above the sea-level and the external temperature is 95°F in military Hot Day conditions. The maximum speed requirement during the inbound leg performed when Odyssey carries passengers appears to be the most important constraint for the design of the vehicle, along with the 6K95 HOGE requirement. The weight of the crew was evaluated at 800 lbs, considering the equipment of pilots and cabin crew. The weight of the two empty litters along with two medical personnel and the medical equipment was evaluated at 1,000 lbs. Loiter capability for 30 minutes allows Odyssey to stay at least 30 minutes in the disaster area. The weight of the helicopter during the inbound leg was conservatively evaluated and we assumed that 6 passengers were rescued for a total weight of 2,100 lbs. Since the vehicle must be able to perform this mission in military hot day conditions, the initial sizing was performed by assuming that the helicopter cannot fly below 6,000 ft. Considering similar missions, the altitude of cruise was fixed at 2,000 ft above the ground, which corresponds to 8,000 ft above the sea level in the most challenging environment. Mission 1 is critical for the power sizing and the fuel required since the inbound leg presents a huge challenge for our design and must be performed at Maximum Continuous Power (MCP).

### **Mission 2 Insertion in hostile territory**

Mission 2 is based on the recent military activities in Afghanistan, Iraq or Libya where the US Army must be able to deploy troops in hostile territories and for areas in mountains for example. This mission requires the aircraft to carry a crew of four and six additional soldiers plus equipment totaling a minimum payload of 4000 pounds internal for a minimum distance of 250 nm. Mission 2 is critical for the design gross weight. The cabin configuration had to be optimized to carry six soldiers. We decided to go for a back-to-back seats configuration to facilitate the soldiers' deployment onto the battlefield as shown in page 9. This configuration is very similar to the current cabin configuration of the HH-60G Pavehawk. In addition to keeping the center of gravity in the symmetric plane, this solution provides an easier reconfiguration capability with removable seats.

### **Mission 3 Resupply**

Mission 3 is very similar to the previous mission. The mission profile is exactly the same and the only difference comes from the payload carried. In this mission, the vehicle must carry 3,000 lbs during both outbound and inbound legs. In one way we can assume that the vehicle is unloading logistics and reloading passengers or defective materials. It can also be understood as a resupply mission of 500 nm, carrying the

same payload. The vehicle must be refueled at the end of this unique segment. The cabin configuration is very easy to capture and the seats must be removed to provide as much room as possible to carry logistics and equipment.

## A.2. Cabin configuration

The driving requirements for the cabin configuration were:

- Enable easy loading/unloading operations
- Enable medical personnel interactions with injured passengers on the litters
- Maintain the center of gravity close to the hub axis for stability and control of the rotorcraft
- Enable easy reconfiguration for another mission with removable seats and transportable litters in less than 30 minutes

The pilot and the copilot are seated next to each other to enable easy communication between both. The cockpit cannot be accessed by the cabin members for a maximum protection against inadvertent interactions. The Crew Chief and the Flight Engineer are seated in face of each other in the front of the vehicle and the seats can also be removed in case both crew members are not needed for a specific mission such as self deployment of the vehicle. Sliding doors were retained as the best technical and feasible solution for our concept because it provides the best compromise between rotor clearance and weight savings. In the case of Mission 1, the litters were initially stacked because of space constraint and the second sliding door should have been blocked to ensure the security of the people inside the cabin. The main drawback of this configuration involved center of gravity issues. However, it was decided to opt for a configuration where two litters are stacked and perpendicular to the fuselage's axis. In this case, it was possible to add a third litter for medical use, as shown in Figure A-2. The medical personnel must also be able to interact with the casualties. One medical personnel can seat between the CC and the FE while the other one can seat in the back of Odyssey and access the medical equipment. A third seat is optional in the back to bring another passenger such as a family member or other medical personnel. Figure A-3 shows the cabin configuration with six seats for mission 2.



FIGURE A-2: CABIN CONFIGURATION WITH THREE TRANSVERSE STRETCHERS

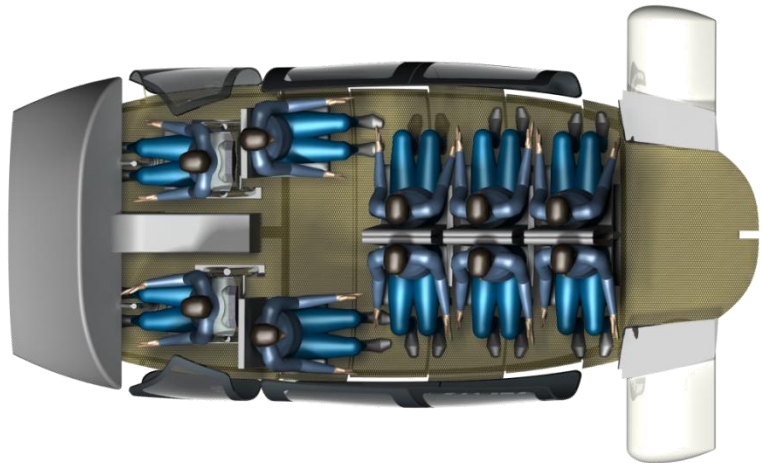


FIGURE A-3: CABIN CONFIGURATION WITH 6 PASSENGERS

### A.3. Additional requirements

The RFP states other requirements for the vehicle. Odyssey must meet the Stage 4 requirements of the International Civil Aviation Organization (ICAO) and the infrared (IR) signature should be reduced as much as possible for military and para-military missions. The top level requirements are summarized page 6. The hovering capability at 6,000 ft and 95 deg Fahrenheit is a strong requirement in terms of power required. At the beginning of the missions, Odyssey gross weight reaches a maximum and requires a lot of power from the engines to sustain hover. The engine recommended for this study is a rubber engine CT7. We decided to use the baseline engine from the HH-60G Pavehawk because we believed our final vehicle characteristics would be close to the baseline. An additional reserve fuel was considered based on the safety requirements stated by the FAR Part 29. Since this vehicle must be deployed in case of mass disasters or war, the maximum range of Odyssey was targeted at 1,500 nm which enables a deployment on the entire US territory. This mission might be performed with additional fuel tanks in the cabin and the vehicle must be ready in 20 minutes. The vibrations of the vehicle must be minimized. The FAR Part 29.251 states that each part of the rotorcraft must be free from excessive vibration during normal conditions [16]. The component life target value was fixed at 10,000 hrs to limit the time and costs spent to change components. Table page 6 shows the primary derived requirements that we tried to meet. The method and the tools used to demonstrate compliance are shown. “B” corresponds to “By design”, “A” stands for “Analysis”, “C” means “Compliance statement” and “S” stands for “Simulation”.

#### Safety Index Criterion

The Survivability Index for civil missions can be derived as shown in Equation 1.  $P_f$  is the probability of an in-flight failure,  $P_c$  is the probability that the failure is catastrophic, and  $P_{sv}$  is the probability of surviving a catastrophic crash. The survivability index must be as close as possible to one.

EQUATION 1

$$Surv = (1 - P_f)(1 - P_c)P_{sv}$$

It is also possible to derive the survivability index for military missions as shown in Equation 2.  $P_{det}$  is the probability of being detected during the mission,  $P_{hit}$  is the probability of being hit by the enemy, and  $P_{kill}$  is the probability of being killed by the missile. Usually the efforts are focused on reducing the radar and infrared signature and enhancing the flares and defensive maneuvers to avoid being hit by a missile.

EQUATION 2

$$Surv = (1 - P_{det})(1 - P_{hit})(1 - P_{kill})$$

The Autorotative Index (AI) is a ratio that includes the most important factors that influence the autorotative performance of a helicopter, such as kinetic energy stored in the rotor, weight of the aircraft, and the rotor disc area [23]. Any rotorcraft that experiences a total loss in power at any point during flight should be capable of performing an autorotation emergency landing. The autorotation is an energy management maneuver where the descent rate and forward speed of the rotorcraft cause the lift vector to tilt forward, driving the rotor, and maintaining the rotor speed with rotational inertial energy. When the aircraft is close enough to its landing surface, the pilot must convert much of the kinetic energy stored in the rotor to thrust, thus slowing the descent rate of the vehicle and allowing for a safe landing. AI used by Bell Helicopter is calculated using Equation 3:

EQUATION 3

$$AI = \frac{I_R \Omega^2}{2W}$$

In this equation  $I_R$  is the main rotor inertia,  $\Omega$  is the rotational speed, and  $W$  is the gross weight. When the vehicle presents high inertia in the rotor and high rotational speed, combined with a low weight and low disc loading, the ratio of kinetic energy stored in the main rotor to the potential energy is much higher, thus

increasing the probability of a safe autorotative maneuver. For coaxial rotor without a directional tail propeller, yaw control in autorotative maneuver is critical and requires much more kinetic energy stored to control the torque and to maintain the stability of the flight. As a consequence, we decided to target a value of 150 which is very close to the Bell helicopters.

The One Engine Inoperative (OEI) requirement is defined by FAR Part 29.67 [16]. The vehicle must be able to sustain a minimum rate of climb of 150ft/s in normal condition at the design gross weight to enable a safe return to base. The remaining engine can operate for 30 minutes at IRP during this operation or maximum contingency power for 2 minutes and a half. The Excess Power EPW defines the ratio of the 30-second OEI power available to the HOGE power required at sea level on a standard day. If an engine fails at any time during flight, the other engine switches to the 30-second OEI mode to provide double power to sustain the flight in safe conditions and to enable the pilot to control his aircraft. It is now possible to define the Safety Index (SI) as derived in Equation 4. The coefficients in front of each term in this equation express the relative importance of the parameters. Their sum must be equal to 1 to normalize the SI.

EQUATION 4

$$SI = 0.8E_{PW} + 0.1 \frac{AI}{150} + 0.1Surv$$

### Mission Capability Index

The Mission Capability Index (MCI) is another engineering parameter to express the aptitude of the aircraft to perform a given mission. Since our vehicle must perform three primary missions, the MCI can be defined by Equation 5. Likewise, the sum of the coefficients in front of each engineering parameter must be equal to 1. The Mean Time Between Failure (MTBF) is defined as the average time before any failure<sup>2</sup> in any part of the rotorcraft occurs and prevents it from performing its mission. The Mean Time To Repair (MTTR) represents the average time required to repair a failed component or device.

EQUATION 5

$$MCI = 0.357 \left[ 0.5 \frac{V_{MCP}}{230} + 0.3 \frac{V_{br}}{140} + 0.2 \frac{V_{be}}{70} \right] + 0.309 \left[ 0.4 \frac{R_1}{225} + 0.3 \frac{R_2}{250} + 0.3 \frac{R_3}{250} \right] + 0.186 \frac{Payload}{4000} + 0.148 \left[ 0.5 \frac{MTBF}{23} + 0.5 \frac{MTTR}{12} \right]$$

<sup>2</sup> Any component or subcomponent that breaks and keeps the aircraft from flying safely constitutes a failure.

### Noise Comfort Index

The stage 4 noise level is an improvement over the stage 3 standards of the ICAO. The Effective Perceived Noise in dB (EPNdB) is used in certification for flyover noise. It includes correction factors for pure tones and for the duration of the noise. Since jet engines are perceived to be noisier than propeller for example, the traditional A-weighting scale in favor of a new scale based on equal loudness [21]. The Noise Comfort Index (NCI) is used to measure the internal and external noise environment as well as the vibrations experienced by the passengers in the rotorcraft and is defined by

Equation 6.  $N_{TO}$  is the noise measured at take-off,  $N_{Approach}$  is the noise measured from 60 ft away during the approach phase,  $N_{Overflight}$  is the overflight noise,  $F$  is the passenger vibration (target:  $0.004f+0.01$  with  $f$  the frequency level per revolution<sup>3</sup>, and  $NI$  the interior noise measured during cruise.

EQUATION 6

$$NCI = 0.461 \left[ 0.35 \left( 1 - \frac{N_{TO} - 95.3}{100} \right) + 0.35 \left( 1 - \frac{N_{Approach} - 98.3}{100} \right) + 0.3 \left( 1 - \frac{N_{Overflight} - 93.3}{100} \right) \right] + 0.274(1 - 10F) + 0.265 \left( 1 - \frac{NI - 50}{100} \right)$$

### Overall Evaluation Criterion

The Overall Evaluation Criterion (OEC) is an engineering parameter used by the Georgia Tech IPPD process to enable comparison between different concepts. The OEC ranks the performance and safety characteristics of a given design and is presented as the ratio of benefits to costs. The OEC is defined by Equation 7.

EQUATION 7

$$OEC = \frac{0.620MCI + 0.202SI + 0.178NCI}{0.4 \frac{RDTE}{369,000,000} + 0.4 \frac{Acq}{8,160,000} + 0.2 \frac{DOC}{2,976}}$$

The coefficients for each of these parameters were derived from the Quality Function Deployment (QFD) matrix shown in Figure A-4. The QFD matrix identifies the key engineering aspects of the overall design. The customer requirements are listed and compared to the engineering feasible solutions. The roof of the QFD, which represents the correlation between the engineering solutions, is not shown in Figure A-4. All the rankings are relative and were based on our experience. The QFD provides a good method of determining rank and numerical solution to the coefficients shown in Equation 7. It can be seen that the design gross weight of the vehicle is a critical parameter, along with power loading, disk loading, MCI and acquisition cost while noise emission and safety, though very important, do not rank as high. However the safety index, the flat plate drag area and the design gross weight rank high on the difficulty scale.

<sup>3</sup> For example, the vibration limit at 1/rev is 0.014, 4/rev limit is 0.026

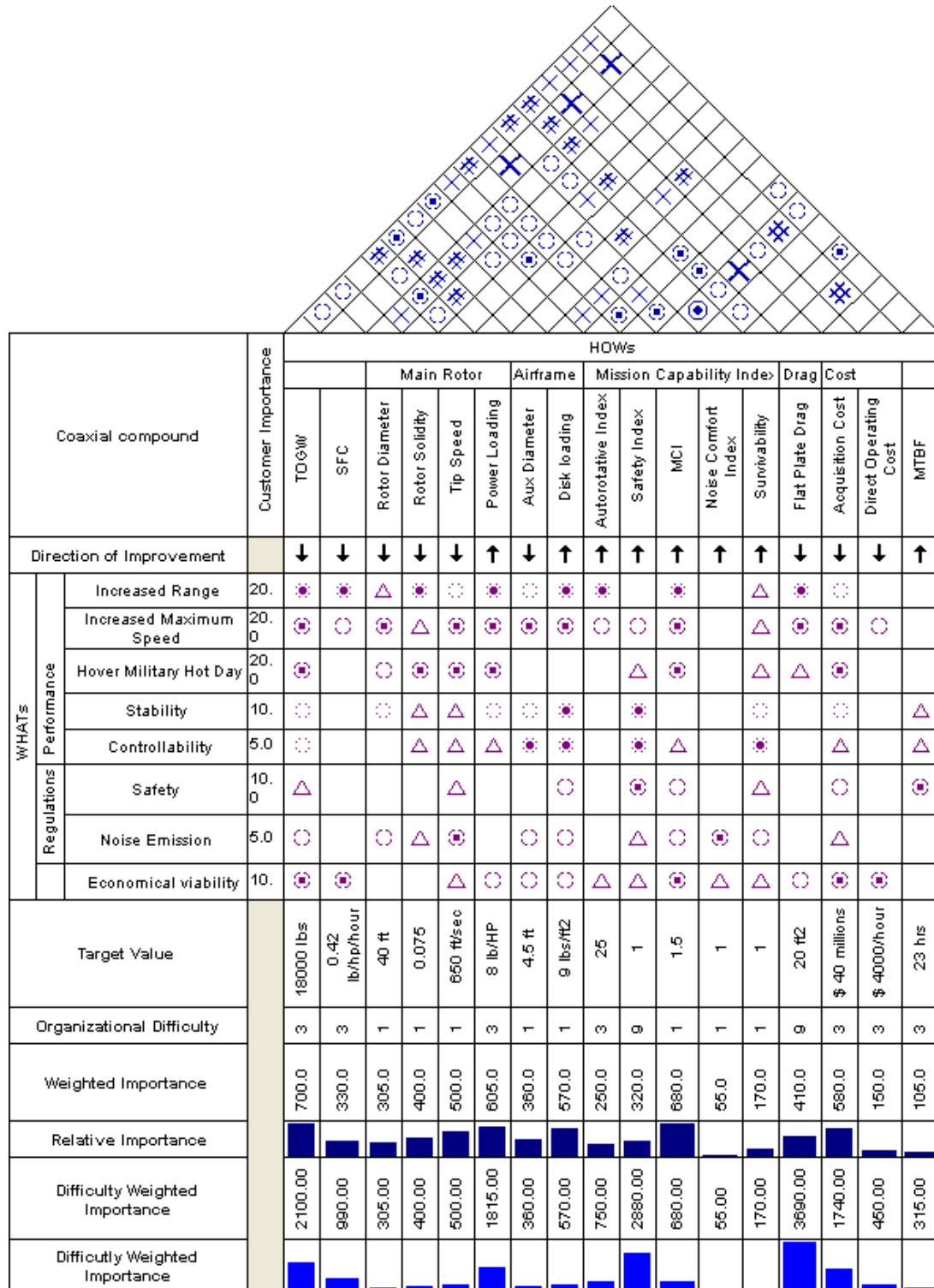


FIGURE A-4: QUALITY FUNCTION DEPLOYMENT (QFD) MATRIX

### Odyssey OEC

A number of parameters are difficult to capture in this preliminary design, such as the MTBF and MTTR, the probability of a catastrophic failure etc... It was possible to run a Monte Carlo simulation on this scenario to calculate the OEC of Odyssey and compare it to the existing HH-60G Pavehawk. For example, normal distributions around the calculated values for the noise comfort index were used, along with uniform distribution for the MTBF and MTTR. Table A-1 shows the calculation of the OEC, done at the very end of the project but presented in this section. It can be seen that the HH-60G Pavehawk presents a very bad OEC due to a very low MCI and Safety Index compared to Odyssey, a larger Cost Index. In the case where data were unavailable for the HH-60G Pavehawk, some values have been assumed identical for both helicopters (such as noise, vibrations, survivability etc) though Odyssey might benefit from technological improvements. This quantitative study shows the overall superiority of Odyssey on the existing HH-60G to perform the primary missions and to meet the top-level requirements.

TABLE A-1: OVERALL EVALUATION CRITERION FOR ODYSSEY AND BASELINE VEHICLE

	Odyssey	HH-60
Safety Index criterion		
$P_f$	0.001	0.001
$P_c$	0.0001	0.0001
$P_{srv}$	0.98	0.98
Surv	0.979	0.979
AI	183	122
$E_{pw}$	1.194	0.693
SI	1.175	0.734
Mission Capability Index		
$V_{mcp}$	239	157
$V_{br}$	134	108
$V_{be}$	77	76
$R_1$	280	120
$R_2$	260	116
$R_3$	270	118
Payload	5000	8000
MTBF	30	30
MTTR	10	10
MCI	1.108	0.965

	Odyssey	HH-60
$N_{TO}$	61.49	61.49
$N_{approach}$	72.78	72.78
$N_{overflight}$	66.25	66.25
F	0.014	0.014
NI	62	78
NCI	1.063	1.021
Cost Index		
RDTE	\$ 369,000,000	\$ 604,000,000
Acq Cost	\$ 8,160,000	\$ 12,800,000
DOC	\$ 2,976	\$ 2,700
CostIndex	1.000	1.464
Overall Evaluation Criterion		
<b>OEC</b>	<b>1.113</b>	<b>0.634</b>

### A.4. Initial concept selection

Multiple concepts were considered during the first phases of the conceptual design. The VTOL capability requirement eliminated several concepts and the ability to hover and autorotate reduced the number of possibilities. Advanced conventional helicopter was considered but quickly eliminated because of the speed requirement. Most conventional helicopters cannot fly above 160 knots and could not have achieved the Golden Hour rule for Mission 1. Tilt rotor and compound helicopter were the remaining candidates. The concept of the tilt rotor did not appear as reasonable because of its size, its lack of autorotation capability and by its complexity. In addition, we felt that the main asset of the tilt rotor was the maximum cruise speed which corresponds only to one of the primary requirements of the RFP. The several concepts of compound helicopter equipped with a pusher to unload the lift of the main rotor in cruise were studied: a Single Main Rotor (SMR), a tandem rotor and a coaxial rotor. In order to rank these concepts, the decision making process was based on the following considerations:

- Autorotative capability
- Complexity
- Maneuverability
- Vibrations
- Power required in cruise
- Preliminary cost analysis
- Noise
- Price
- Weights
- Controllability
- Similarity to the baseline

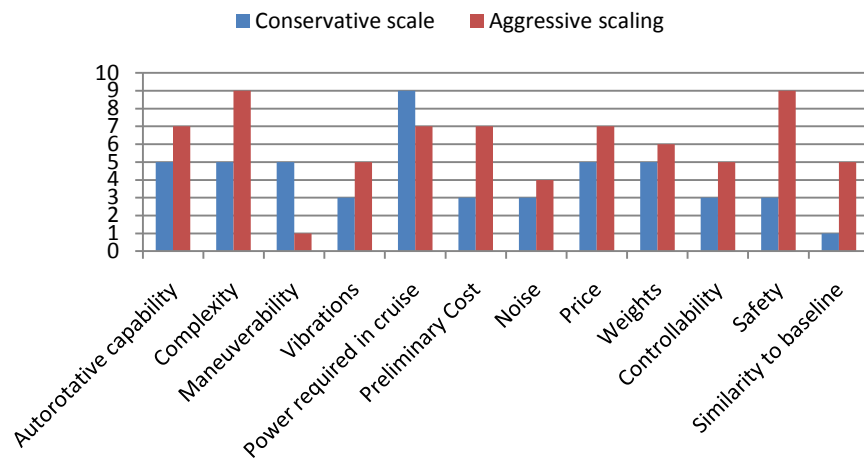


FIGURE A-5: PRIORITIZATION RANKING OF THE TWO SCALES

These criteria were ranked and the prioritization is shown in Figure A-5. The aggressive scale tends to dilute the rankings and dwells on the safety and the complexity level of the vehicle. The conservative scale is mainly based on the amount of power required in cruise and the other criteria are very close to each other.

The scores of each concept are shown in Figure A-6 for both scales. It can be seen that the SMR appears as the best alternative on the aggressive scale, but this concept requires a lot of power to sustain the payload and to meet the speed requirement. As a consequence, this concept falls to the third place in the conservative scale. The tandem rotor was ranked last in both scales and was quickly abandoned.

	Conservative scale				Aggressive scale			
	SMR	Tandem	Coax	Tilt rotor	SMR	Tandem	Coax	Tilt rotor
Autorotative capability	25	5	25	5	35	7	35	7
Complexity	25	15	15	5	45	27	27	9
Maneuverability	15	25	25	15	3	5	5	3
Vibrations	9	15	21	21	15	25	35	35
Power required in cruise	9	27	27	63	7	21	21	49
Preliminary Cost	15	9	9	9	35	21	21	21
Noise	15	9	9	6	20	12	12	8
Price	25	15	25	15	35	21	35	21
Weights	15	15	25	25	18	18	30	30
Controllability	9	15	9	27	15	25	15	45
Safety	9	9	15	15	27	27	45	45
Similarity to baseline	9	3	3	1	45	15	15	5
Total score	180	162	208	207	300	224	296	278
Score normalized	0.237781	0.214003	0.274769	0.273448	0.273224	0.204007	0.269581	0.253188

FIGURE A-6: CONCEPTS SCORES VS. TWO SCALES

### Benefits of the coaxial compound rotor

The average normalized score of each concept are shown in Figure A-7. The coaxial rotor, which significantly increases speed, eliminates tail rotor, and provides a compact and agile body seemed to be the best alternative. The coaxial concept utilizes more of a rotor's lift potential by eliminating retreating side blade stall limits in high speed flight. SMR helicopters must produce equal lift on each side of the disk to keep the rotor level in a satisfactory roll. To compensate for the unequal distribution in relative velocities, larger pitch angles are required on the retreating side than on the advancing side. As higher speeds are reached or higher lift is required by the mission profile, a stalled region develops on the retreating side and produces a dramatic increase in power demand and in control system loads [25].

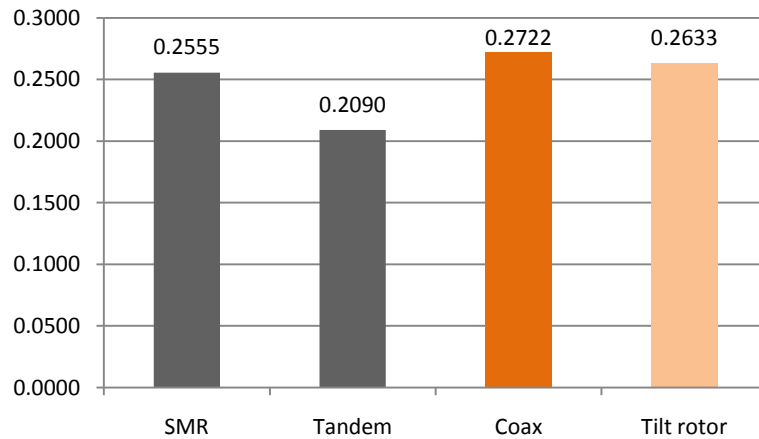


FIGURE A-7: FINAL RELATIVE SCORE OF THE CONCEPTS

Odyssey avoids this phenomenon by using two coaxial, counter-rotating, rigid rotors. As speed increases and advance ratio reaches higher values of 0.6 or 0.7, the lift is transferred to the advancing blades on each side of the disk, producing a balanced rolling moment. Because large inter-rotor rolling moments are generated, a stiff-in-plane blade attachment is used to insure adequate blade tip clearances, along with very high flapping stiffness.

### A.5. Hub selection and IBC system

Since the performance is very sensitive to the overall drag of the helicopter, the hub design had to be addressed early in the conceptual design phase. Using the same procedure described above for the concept selection, the most important characteristics were safety, autorotative index, maneuverability, vibrations, drag, weight, price, noise and direct operative cost. The safety is measured in Mean Time Between Failure (MTBF) and was considered as the most important criterion. Vibrations and drag highly influence the cruise conditions and are fundamental for our concept. The different hub concepts were:

- 1) 3-Blade articulated rotor with a swashplate control
- 2) 4-Blade elastomeric articulated rotor with swashplate control
- 3) 3-Blade hingeless rotor with individual blade control by hydro-mechanical actuators
- 4) 4-Blade bearingless rotor with individual blade control by hydro-mechanical actuators and active faring for low vibrations

Hub design 1 is the standard configuration for coaxial helicopters and has been produced on many existing Kamov rotorcraft. Designed in the early 70s, this 'old-school' concept presents the advantage of being largely documented. The disc area is reduced because the weight of the helicopter is no longer supported by a single main rotor but by two main rotors. The anti-torque system (such as a tail rotor) is no longer required because both rotors spin in contrary directions. However, the articulated rotor is composed of many exposed rotating parts and the hub is significantly increased. The mechanical complexity is also very pronounced.

Hub design 2 is similar to the baseline HH-60G hub design. An increase in number of blades increases the performance of the vehicle in hover and in autorotative maneuver. Noise and vibrations are also reduced in this case. The elastomeric articulated rotor presents a feathering hinge per blade to vary the pitch angle. The collective pitch is controlled by the vertical position of the collective swashplate and the cyclic control is achieved by tilting the swashplate.

Hub design 3 is truly hingeless. The individual control by hydro-mechanical actuators provides significant weight savings and improves the control response for handling qualities. The drag of the hub can be greatly reduced by replacing the articulated hub with bearingless hub, though increasing the price of the vehicle.

Hub design 4 combines the advantages of a 4-blade rotor with a bearingless design. Hover performance, autorotation and noise characteristics are improved. Vibrations are strongly reduced thanks to active control. A stiff-in-plane configuration for Odyssey enables an increase in the stiffness of the blades and thus reduces the vertical distance between the hubs. The IBC system implemented on Odyssey is shown in Figure A-8.

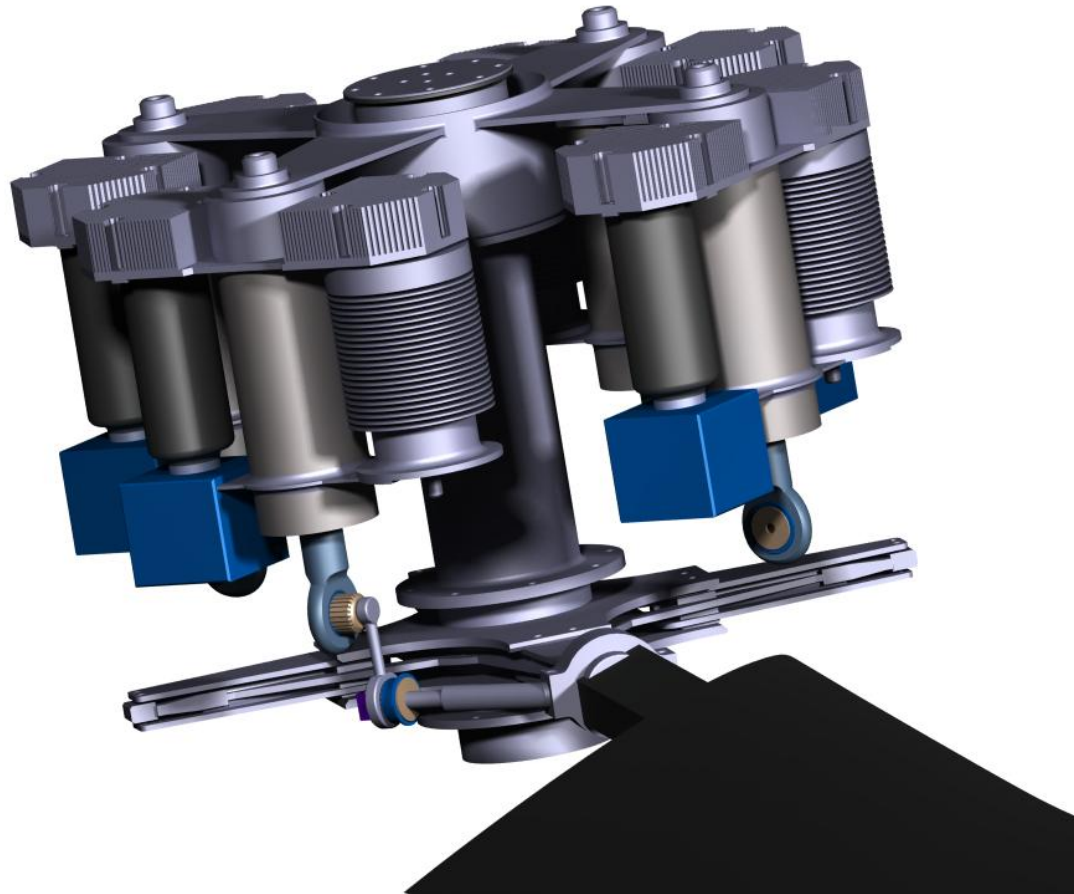


FIGURE A-8: INDIVIDUAL BLADE CONTROL SYSTEM ON ODYSSEY'S MAIN ROTOR

### Rotor shaft angle

In high speed cruise, propulsive force is provided by the auxiliary propulsion. The coaxial main rotor produces only lift. However, the Sikorsky XH-59A flight test data showed that the aerodynamic efficiency of the rotor is highly dependent upon the pitch attitude of the rotor shaft, or upon the built-in shaft tilt angle [1]. A negative built-in shaft tilt (tilted aft) would have resulted in an autorotational mode where the rotor can extract energy from the air flow through the disk. However, such a configuration would have required more thrust from the pusher propeller to compensate the aft tilt of the thrust vector of the main rotor. Tilting the main rotor shaft forward provided extra forward thrust but reduced the main rotor efficiency. Best flight attitude of the X2TD was assumed between -4 and -2 degrees and this is why we designed a forward built-in shaft tilt of -3 degrees on Odyssey [1].

### A.6. Comparison between HH-60G Pavehawk and Odyssey

A quick comparison of Odyssey with the baseline vehicle is shown in Table A-2. The payload capacity of the Pavehawk is largely superior to the requirements of the AHS design. However, the range and speed performance of the HH-60G keep it from meeting the top-level requirements.

TABLE A-2: COMPARISON OF THE BASELINE HH-60G PAVEHAWK VS. ODYSSEY

HH-60G Pavehawk	Odyssey
	
Single Main Rotor	Compound Coaxial Helicopter
Hingeless hub	Bearingless hub with active fearing
Swashplate control	Individual Blade Controls
130 nm radius of action	250 nm radius of action
Max cruise speed of 152 kts	Max cruise speed of 239 kts
10 passengers capacity	6 passengers capacity
15 troop seats	6 troop seats
6 litters	3 litters
2 crew	4 crew

The morphological matrix is presented in Figure A-9. Although the number of alternatives is unlimited, this example shows that more than 322,486,272 combinations can be explored within this matrix. An exhaustive exploration is not possible and the yellow cells show the initial concept selection.

Morphological Matrix							
	Alternatives						
Airframe	1	2	3	4	5	6	Number of alternatives
Material	metal	Aluminum	composite				3
Seating	2 abreast	3 abreast	4 abreast				3
Tail	T-Tail	H-Tail					2
Gear	retractable	non retractable					2
Wing	no wing	fixed low mount	fixed high mount	stowable			4
Power Plant	1	2	3	4	5	6	
Engine	Turboshaft	Turboprop	Turbofan				3
Number of engines	1	2	3	4			4
Transmission	Split-Torque	SABP	Planetary	CVT			4
Avionics	1	2	3	4	5	6	
Control system	Hydraulic	Fly-by-Wire	Fly-by-Light				3
Navigation	VOR/GPS	VOR/ILS/GPS	ILS/GPS				3
Communications	FM/UHF/VHF	FM/UHF/VHF/SAT COM	FM/UHF/VHF/SAT COM/HF	FM/UHF/VHF/SAT COM/HF/RNAV			4
Lift/Thrust	1	2	3	4	5	6	
Number of rotors	2	4	8				3
Main rotor hub	Fully articulated	Hingeless	Bearingless				3
Main rotor Blades	2	3	4				3
Anti-torque	no anti-torque	tail rotor	jet exhaust				3
Aux Fwd Propulsion	pusher	ducted pusher	turboprop	turbojet			4
Number of Aux Prop	1	2					2
Aux prop position	on wings	on fuselage					2
Technology	1	2	3	4	5	6	
Tech adoption	Drag reduction	SFC improvement	Material				3

FIGURE A-9: MORPHOLOGICAL MATRIX OF ODYSSEY

## Appendix B CONCEPT INITIAL SIZING AND PERFORMANCE

In the conceptual design iteration loop presented in Figure 0-1 page 1, the initial vehicle design configuration geometry and the analysis of the requirements are the necessary inputs to the vehicle sizing and performance box. This step consists in sizing the optimum geometry of the vehicle and obtaining the gross weights for the three primary missions. The sizing code uses the Georgia Tech/Hiller Rf method [44], which consists in iterating the fuel weight ratio until convergence of the design gross weight for a given mission. The user specifies the mission, the guessed gross weight of the vehicle and the generic aircraft geometry. A blade element model calculates the rotor performance in hover and in cruise. The fuel required to perform this mission is also calculated by segments and an iterative loop closes the procedure until convergence on a gross weight [13]. The initial guess gross weight was 22,000 lbs (based on the maximum takeoff gross weight of the HH-60G Pavehawk [48]). The optimization program determines an optimal solution to the Rf problem. This program utilizes an iteration process to produce the performance analysis of the helicopter. The general Rf method used for Rotorcraft Synthesis is presented in Figure B-1 [43].

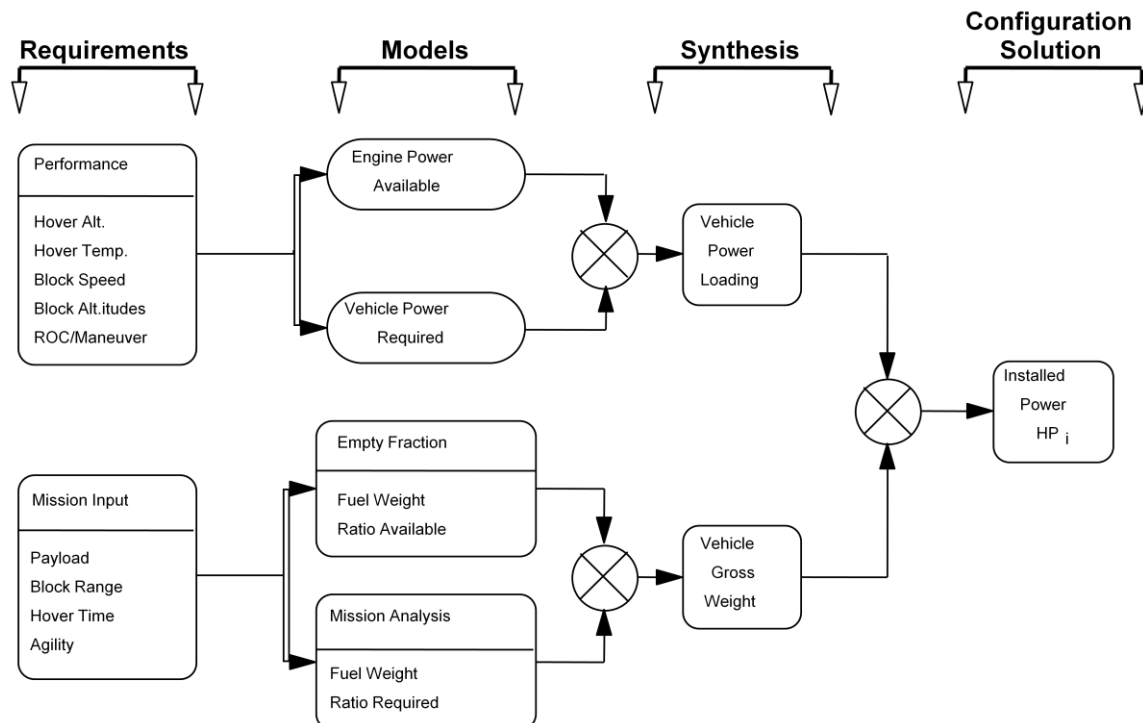


FIGURE B-1: RF METHOD FOR ROTORCRAFT/VSTOL AIRCRAFT SYNTHESIS [43]

### B.1. Initial sizing

Matlab and CIRADS were used to optimize the initial geometry of Odyssey. Since these tools are coupled, along with Excel and CATIA, the automated analysis environment was built using ModelCenter. For the three primary missions, the code was run to converge on a design gross weight, empty weight and fuel weight. The results of this code have proven to be highly accurate when compared to flight test data from the HH-60G. This code was also used by Georgia Tech design teams for preliminary designs in previous successful AHS competitions. For each mission, FAR Part 91.151 states that the vehicle must carry a 45 min reserve fuel at night in VFR conditions [18]. This additional requirement was taken into account in this analysis.

Mission 2 represents the higher constraint in terms of weight because of the heavy payload. The takeoff gross weight of this mission was 16,450 lbs and the empty weight was 8,879 lbs, leading to an empty weight ratio of 0.54. This first study was important to evaluate the empty weight of Odyssey. For the three different design points, the empty weight was very close and it was decided to conduct further sizing iterations to converge towards better results. After the optimization of main rotor blades and empty weight

breakdown, the converging values for Odyssey are presented in Figure B-2. The empty weight ratio of Mission 2 is 0.54 which is acceptable for our design. Mission 1 sized the fuel required to perform the golden hour mission and thus the size of the fuel tanks. According to this first level analysis, the empty weight of the helicopter can be estimated around 8,400 lbs.

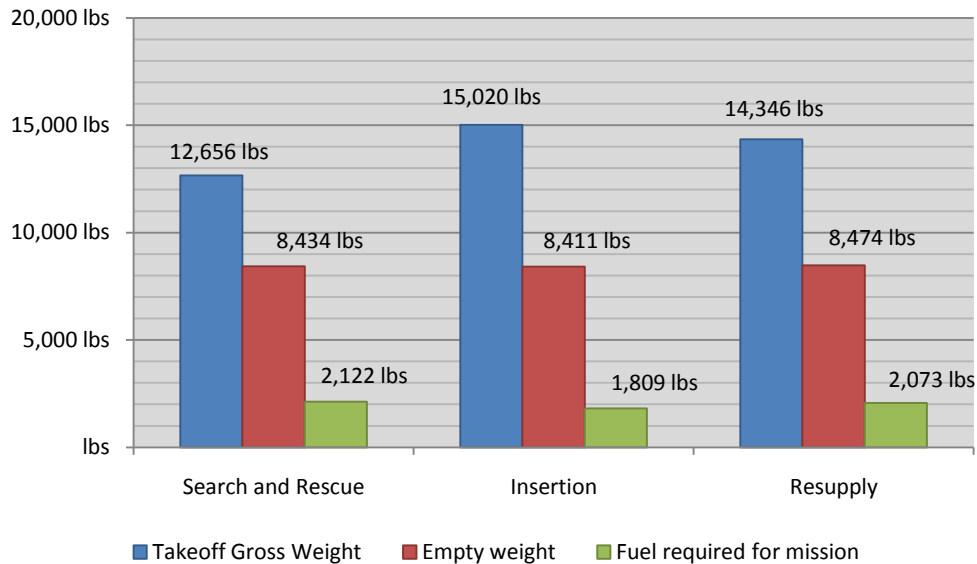


FIGURE B-2: SIZING RESULTS FOR THE THREE PRIMARY MISSIONS

## B.2. Performance evaluation

### Performance validation model

A Matlab code was used to calculate the induced power, the profile power, the accessory power, the gear box power, the parasite power, and the total power required of Odyssey. This code was first validated on the HH-60G Pavehawk. The power graph of the HH-60G Pavehawk at sea-level is presented in Figure B-3. The generated dash speed is 157 kts and the official dash speed is 155 kts (1.2% of error). This code was validated and adapted to a coaxial rotor. A correction factor was used to account for the inflow interference on the bottom rotor. The parasite drag was increased by 18.5% to account for the propeller efficiency, which was expected to be around 81% in this range of speed. In this simulation, we assumed that the pusher propeller would provide the whole forward thrust to move the helicopter in cruise. The equations used are described in the next section of this appendix.

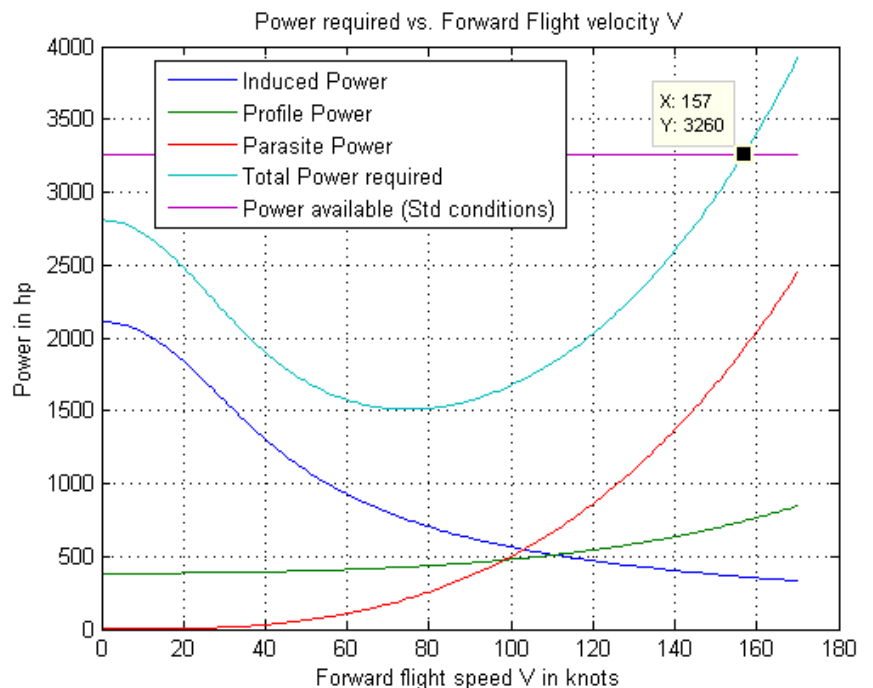


FIGURE B-3: POWER REQUIRED VS. AIRSPEED FOR THE HH-60G PAVEHAWK AT SEA LEVEL

### Power performance model and equations

This section describes the equations and the model developed to calculate the power required of Odyssey. To calculate the performance in Hot Day, the ratio of the air density at 6K95 to the air density at sea-level is necessary. A temperature of 95 deg Fahrenheit at 6,000 ft corresponds to 57.4 deg F over standard temperature at this altitude. Using the standard ICAO pressure-altitude relationship, given by Equation 8, this ratio is 0.7495.

$$\text{EQUATION 8}$$

$$\frac{\rho}{\rho_0} = \frac{P_{std}}{\rho_0 g R (T_{std} + 57.4)}$$

Using the Leishman's definition of the thrust coefficient for a coaxial helicopter [24], it is possible to calculate the induced power, in horsepower, of the coaxial rotor using Equation 9.  $\Omega R$  is the tip speed,  $A$  is the disk area, 1.15 is the empirical tip loss factor to account for swirl losses and tip losses, 1.16 is the empirical correction factor to account for the influence of the upper rotor on the lower rotor inflow [24],  $C_T$  is the thrust coefficient and  $\lambda_i$  is the inflow ratio. This expression is multiplied by two because there are two main rotors.

$$\text{EQUATION 9}$$

$$ihp = 2 \times \rho A (\Omega R)^3 \frac{(1.15 \times 1.16 \times C_T \lambda_i)}{550}$$

The profile power of the two main rotors, in horsepower, is calculated using Equation 10.  $c_{d0}$  is the zero lift drag coefficient of the airfoil,  $\sigma$  is the solidity of the rotor,  $\mu$  is the advance ratio, 4.6 is an empirical factor to account for compressibility effect at high advance ratio [41]. The expression is multiplied by two because there are two main rotors.

$$\text{EQUATION 10}$$

$$Rhp = 2 \times \rho A (\Omega R)^3 \frac{\left( \sigma \frac{c_{d0}}{8} (1 + 4.6\mu^2) \right)}{550}$$

The parasite power of the vehicle is calculated using Equation 11, where  $A_\pi$  is the equivalent flat plate drag area.

$$\text{EQUATION 11}$$

$$php = \rho A (\Omega R)^3 \frac{\mu^3 A_\pi}{2A \times 550}$$

The mechanical gear losses are calculated using Equation 12 where  $\eta_{mec}$  is the mechanical efficiency.

$$\text{EQUATION 12}$$

$$hp_{mec} = (1 - \eta_{mec}) [ihp + Rhp + php]$$

The accessory power  $hp_{acc}$  is evaluated at 5 hp in our case. Then the total power required by the vehicle is given by Equation 13 where  $\eta_{prop}$  is the pusher prop efficiency. The pusher propeller is supposed to provide the thrust to move the vehicle forward in cruise. As a consequence, the pusher must overcome the parasite drag but one must take into account a drag penalty for the pusher propeller efficiency.

$$\text{EQUATION 13}$$

$$rhp = ihp + Rhp + hp_{acc} + hp_{mec} + (2 - \eta_{prop}) php$$

The MATLAB code developed had to take into account the tip speed schedule (linear transition from 650 ft/s to 450 ft/s in the range of 110 kts to 150 kts).

### B.3. Initial Performance without the auxiliary propulsion

Without a pusher propeller configuration, the maximum cruise speed of 250 knots cannot be achieved at sea-level or in military hot day conditions with the installed baseline engine. The max cruise speed for Mission 1 is limited to 232 knots and Odyssey can hover in this configuration. It can also be seen that at sea-level, the OEI rated power is enough to hover and guarantees a large safety margin. However, in Hot Day conditions, the loss of one engine prevents the hovering capability of Odyssey at max gross weight and degrades the safety of the vehicle. The same analysis is shown in Figure B-4 for Mission 2 at maximum takeoff gross weight. The code did not take into account blade stall limits and compressibility effects which usually limit the maximum cruise speed of conventional helicopters. In addition, the compressibility effects at the tip of the blades would limit the maximum cruise speed. Therefore, the predicted performance without auxiliary propulsion was very optimistic. Based on this initial performance evaluation, auxiliary propulsion was definitely required to provide the thrust needed at high speed while the tip speed of the main rotors is reduced in cruise.

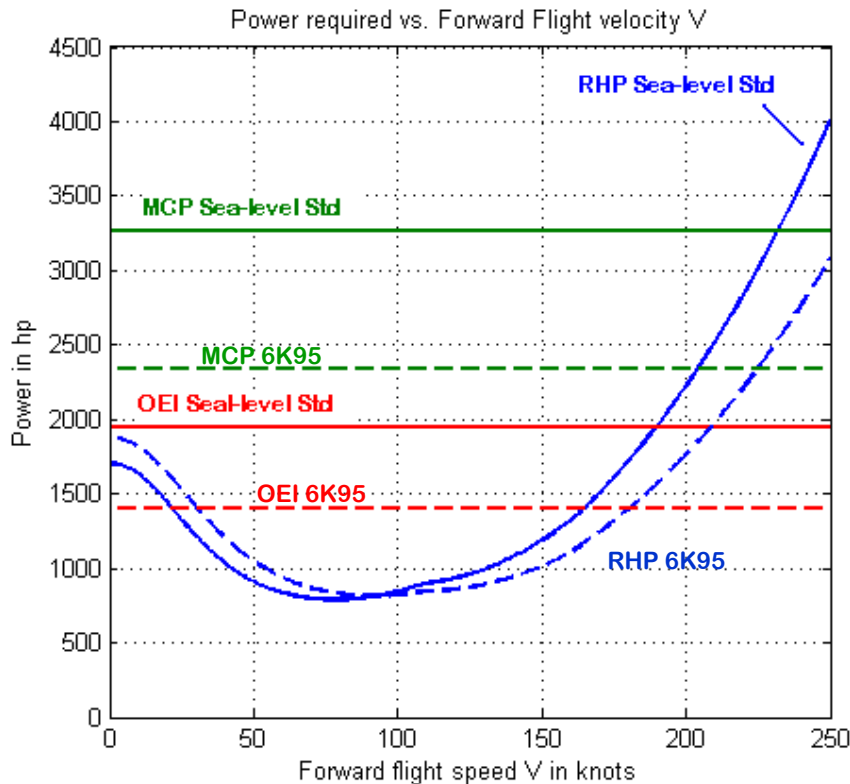


FIGURE B-4: INITIAL PERFORMANCE FOR MISSION 2 WITHOUT AUX PROPULSION

## Appendix C MAIN ROTOR GEOMETRY AND AIRFOIL DESIGN

In the previous design phases, the configuration of the rotorcraft was selected and first level iterations yielded a design gross weight. The optimization of the tip speed, of the rotor geometry, and of the blade section among others is fundamental to improve the performance of the rotorcraft in hover and in cruise. In addition, the reduction of the design gross weight would be anticipated to improve fuel efficiency, power required and costs.

### C.1. Rotor radius selection and optimization

#### ModelCenter's Design Explorer

Due to the team's familiarity with Phoenix Integration's ModelCenter environment, we decided to use an optimizer in Model Center [39]. ModelCenter's Design Explorer, shown in Figure C-1, was linked to the MATLAB code for CIRADS to perform an optimization of gross weight and power required. Variables to optimize and objective functions are identified in the Design Explorer, and then the Design Explorer generates an Orthogonal Array which is used to capture the response of the model's objective (gross weight) in reaction to different design variables. The Orthogonal Array is similar in many ways to a Design of Experiments, except that in this case it can be generated automatically by ModelCenter.

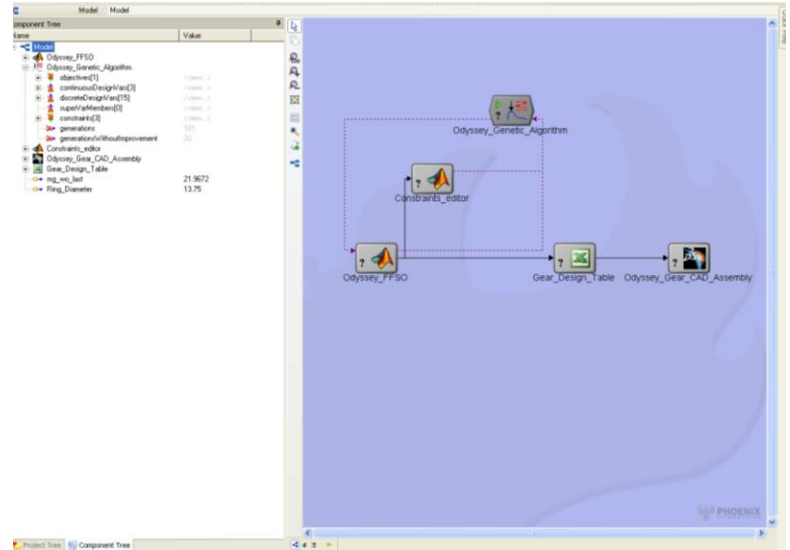


FIGURE C-1: MODELCENTER'S DESIGN EXPLORER ENVIRONMENT FRAMEWORK

The Design Explorer fits a response surface to the results of the cases from the Orthogonal Array. This is an n-dimensional surface represented by the response of gross weight to various design values. The global minimum gross weight is achieved for some unknown combination of design variables. The response surface can be adequately generated from a small number of cases but more cases must be run to identify the globally minimum gross weight. So, after the response surface is generated, the Design Explorer uses a generic gradient descent method to track to the minimum gross weight. This type of method simply follows the trend of decreasing gross weight with any combination of variables, and identifies the values for those design variables which will achieve that desired minimum gross weight. Some of the design variables that we attempted to optimize on apparently were not well defined in CIRADS, and the optimization broke down. In the Design Explorer, if a variable breaks down, it can simply be returned to its baseline value, and omitted from future optimization. If we had used a Design of Experiments, however, as many as 80% of the cases that would have been run would have had meaningless results due to the nonsensical physical accounting of these parameters in CIRADS. Among the most interesting parameters, the rotor diameter and the solidity of the rotor were correctly optimized.

TABLE C-1: OPTIMIZED ROTOR GEOMETRY AT FIRST ITERATION

Rotor Parameter	Value after optimization
Rotor diameter (ModelCenter)	41.01 ft
Rotor diameter (Rf method)	40 ft
Rotor solidity	0.075
Number of blades (per rotor)	4

### Georgia Tech/Hiller Rf method

In addition to this optimization procedure, a sensitivity analysis was conducted on the rotor diameter using the Georgia Tech/Hiller Rf method [44] to validate the rotor diameter and the results are presented in Figure C-2. Minimizing the rotor diameter reduces the downwash effect on the fuselage in hover, the vibrations, and helps to reduce the vertical gap between the hubs, thus reducing the hub drag. The value of 40 ft appears to be the best compromise in terms of diameter and design gross weight. The final results from both the ModelCenter's Design Explorer and Excel are presented in Table C-1. A 4-blade rotor was also recommended by the Design Explorer, comforting our first trade study for the hub design in A.5. page 16.

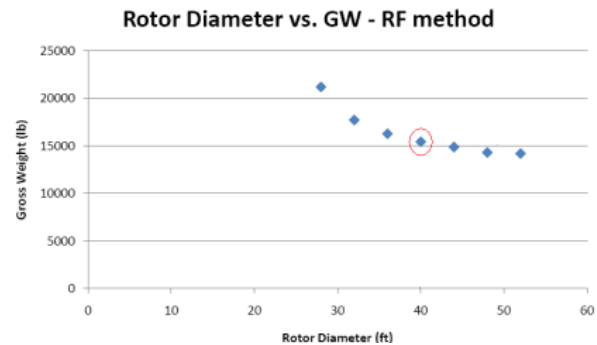


FIGURE C-2: ROTOR DIAMETER SENSITIVITY ANALYSIS USING THE RF METHOD [26]

### Tip speed selection

The tip speed is defined as the speed at the tip of the blades of the main rotor. Blade stall and compressibility effects are usually major constraints at very high speed. Since most helicopters have a fixed rotor diameter, the tip speed is usually linked to the rotational speed of the rotor. On conventional helicopters, this rotational speed is constant and limits the flight envelope of Odyssey. The advance ratio  $\mu$  is defined as the ratio of the forward flight speed to the tip speed  $\Omega R$ .

### Subcritical Mach number in high speed cruise

With a target speed of 250 knots and a radius of 20 ft, it was possible to plot the relative Mach number of the blades as a function of the blade station and of the tip speed, as shown in Figure C-3. It can be seen that a tip speed of 700 ft/s leads to a supersonic section at the tip on the advancing side and this is not desirable. At 250 knots, we desire to limit the transonic effects on the blades which can lead to shocks, vibrations and drag divergence. The transonic effects appear between Mach 0.8 and 1 and the blade should not operate in this region. As a consequence, the tip speed of 450 ft/s was selected at cruise. On the retreating side, it can be seen that almost 90% of the blade is in reverse flow, increasing the drag and resulting in a negative lift. However, with a coaxial rotor, the lack of lift on the retreating side of one rotor is compensated by the lift provided by the advancing side of the other rotor.

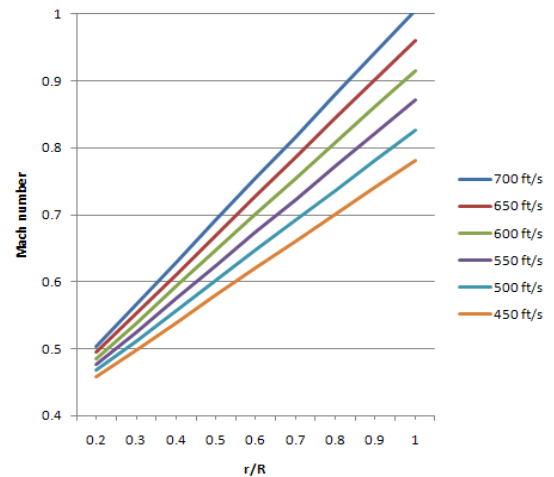


FIGURE C-3: ADVANCING SIDE MACH NUMBER VS. TIP SPEED AT 250 KTS

### Reverse flow region

The same trade study can be conducted at a mid-range speed of 125 knots. At this cruise speed, the tip speed can be up to 650 ft/s to avoid the transonic region on the advancing side. The reverse flow region on the retreating side is limited and the performances of the helicopter at relative low speed are preserved. This study fixed the tip speed of the helicopter at 650 ft/s at low speed (below 125 kts) and 450 ft/s at high speed (above 125 kts). Assuming a smooth transition of rotational speed, the relative Mach number at the tip is also plotted vs. the airspeed in Figure C-4. The transonic region is avoided in the whole flight envelope and the retreating side is never completely in reverse flow mode. The advance ratio is also calculated on this figure. The transition speed corresponds to an advance ratio close to 0.5 which is the usual limit of conventional helicopters.

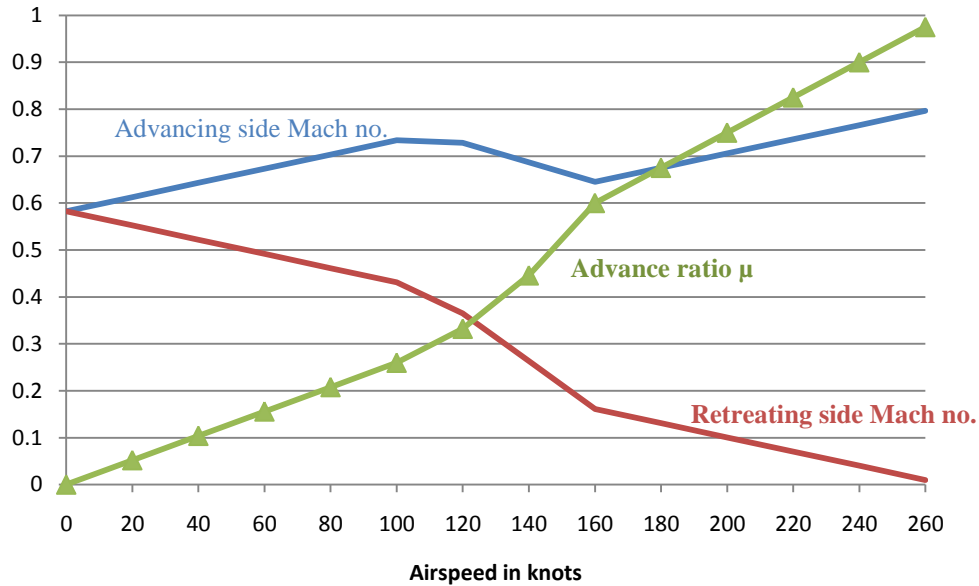


FIGURE C-4: MACH NUMBER AND ADVANCE RATIO AT SEA-LEVEL VS. AIRSPEED

## C.2. Airfoil selection

### Airfoils of the baseline HH-60G Pavehawk

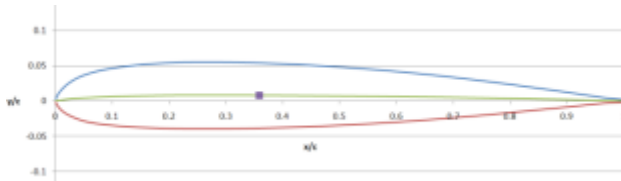


FIGURE C-5: SC1095 AIRFOIL PROFILE

On modern helicopters, the blades use several airfoil sections to optimize the performance. At the same time, non-linear twist enables an increase in the figure of merit of the rotor and taper ratio is also required to reduce the bending moment caused by the lift at the tip. The rotor diameter, solidity and tip speed were all selected in the previous analyses. The baseline HH-60G Pavehawk is equipped with the SC1095 as shown

in Figure C-5 [8]. However it can be noticed that there is a transition area around the middle of the blade and the SC1094 replaces the SC1095.

### Inventory of airfoils

A quick inventory of possible airfoil was based on the Georgia Tech Preliminary Design Program (GTPDP) which is a preliminary design code to obtain a brief overview of the configuration. This code has not been used in our preliminary design due to time constraint and lack of knowledge of this tool. However, the airfoil library of GTPDP was used to evaluate the different airfoils. A simple power study was performed on a tapered blade, with a linear twist angle of -10 degrees and a given configuration of 17,200 lbs. The variable tip speed is accounted for and the results are presented in Figure C-6. It can be seen that the NACA airfoils all present higher power required in hover and at high speed. The Boeing VR7 and VR8 airfoils seem to be clearly better over the entire range of this graph but the SC1095 remains close in terms of performance.

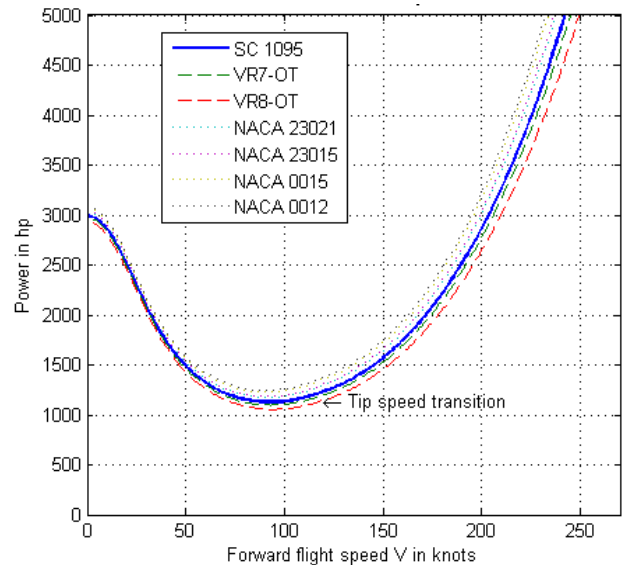


FIGURE C-6: AIRFOIL SIMPLE TRADE STUDY

### Airfoils L/D ratio comparison and selection process

In order to evaluate the airfoils, a MATLAB code was created to compute the effective angle of attack at each blade section on the advancing side at 250 knots. It was then possible to compute the lift to drag ratio of each airfoil. The results are presented in Table C-2 and the plot of the lift to drag ratio of the airfoils is presented in Figure C-8 . Airfoil data table was generated by two potential codes in order to be used in the blade element analysis. The two codes are XFOIL and Transonic Full Potential code. XFOIL was used for subsonic flow analysis ( $M_\infty < 0.7$ ). For high speed, Transonic Full Potential code was used. XFOIL was developed for the design and analysis of subsonic isolated airfoils. XFOIL performs various useful functions such as viscous (or inviscid) analysis of an airfoil, airfoil design and redesign by interactive modification of surface speed distributions, and blending of airfoils.

Transonic Full Potential code computes steady transonic flow past thick airfoils at an angle of attack. The numerical solution involves the following steps:

- Grid generation, where a set of nodes are chosen surrounding the airfoil. The FPE is to be solved at these nodes.
- Discretization, where the FPE is converted into a system of coupled nonlinear algebraic equations,
- Relaxation or iterative solution, where the algebraic equations developed in step are iteratively solved.
- Post-processing, where the surface pressure distribution and the airloads are computed and printed out.

It can be seen that the lift to drag ratio of the three airfoils is degraded from 60% to 90%. A possible solution consisted in adopting an elliptical planform in this region to reduce the profile power. The elliptical planform minimizes the induced drag and the induced power and would participate to increase the lift to drag of the blades in this critical region [10]. In addition to reducing the vibrations, another advantage of the elliptical planform is the improved autorotative index since the blade mass is more distributed out-board, increasing the moment of inertia of the blades. A similar planform was selected over a simple linear tapered planform for the Sikorsky X2 demonstrator [4]. At very high speeds on the retreating side, the drag is high on the inboard region of a linear tapered blade. The chord near the root must be reduced to overcome this phenomenon.

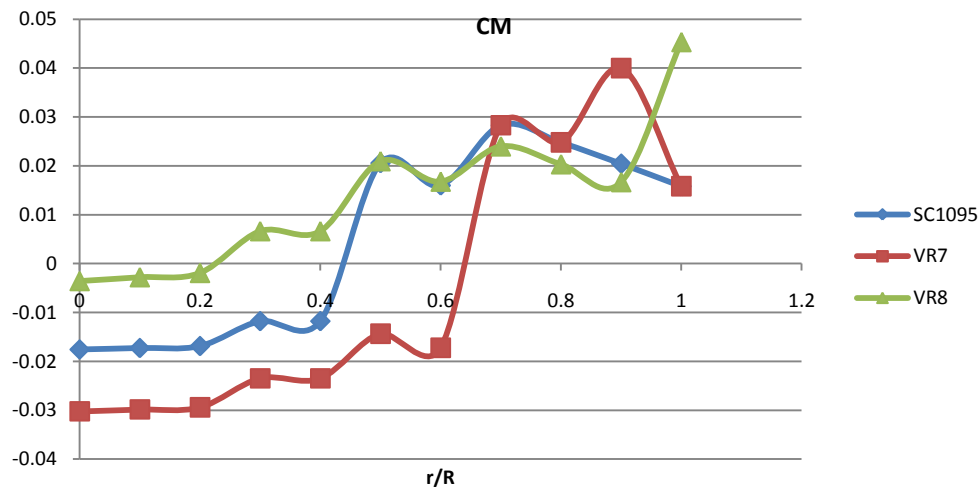


FIGURE C-7: PITCHING COEFFICIENT AT 250 KTS

The BERP tip is specifically designed to increase the rotor performance at very high Mach numbers and at low angle of attack, while reducing the noise emission. Since the loss of lift on the retreating side on one rotor is compensated by the advancing side of the other rotor on a coaxial helicopter, the BERP design was not considered here.

TABLE C-2: LIFT AND DRAG COEFFICIENTS AT 250 KTS

r/R	Mach#	AoA (deg)	Sc1095		VR7		VR8	
			Cd	Cl	Cd	Cl	Cd	Cl
0.1	0.42	6.02	0.9071	0.0172	0.0119	0.9868	0.0132	0.7982
0.2	0.46	6.79	1.1541	0.0387	0.0091	1.1192	0.0154	0.8577
0.3	0.5	7.03	1.1579	0.0395	0.0084	1.1851	0.0241	0.9760
0.4	0.54	6.98	1.1541	0.0387	0.0265	1.3037	0.0358	1.0673
0.5	0.58	6.75	1.0840	0.0416	0.0214	1.2305	0.0372	1.0542
0.6	0.62	6.41	1.0150	0.0333	0.0172	1.1568	0.0284	0.9962
0.7	0.66	5.99	1.0403	0.0618	0.0174	1.1652	0.0223	0.9253
0.8	0.7	5.51	0.9608	0.0504	0.0505	0.9608	0.0325	0.9720
0.9	0.74	4.98	0.8827	0.0408	0.0662	1.1674	0.0262	0.8894
1	0.78	4.43	0.8054	0.0326	0.0327	0.8054	0.0741	1.0591

The lift to drag ratio of the SC1095 is limited compared to the Boeing VR7 and VR8. It can be seen that the VR7 airfoil is very efficient from the root to 70% of the blade radius. Then from 70% to 95%, the VR8 presents a higher lift to drag ratio, along with a lower pitching moment coefficient. In order to maximize the performance of the rotor, the VR7 was picked as the airfoil up to 70% of the radius station, and the VR8 was picked as the airfoil from 70% to the tip. The transition area is the center of the elliptical planform.

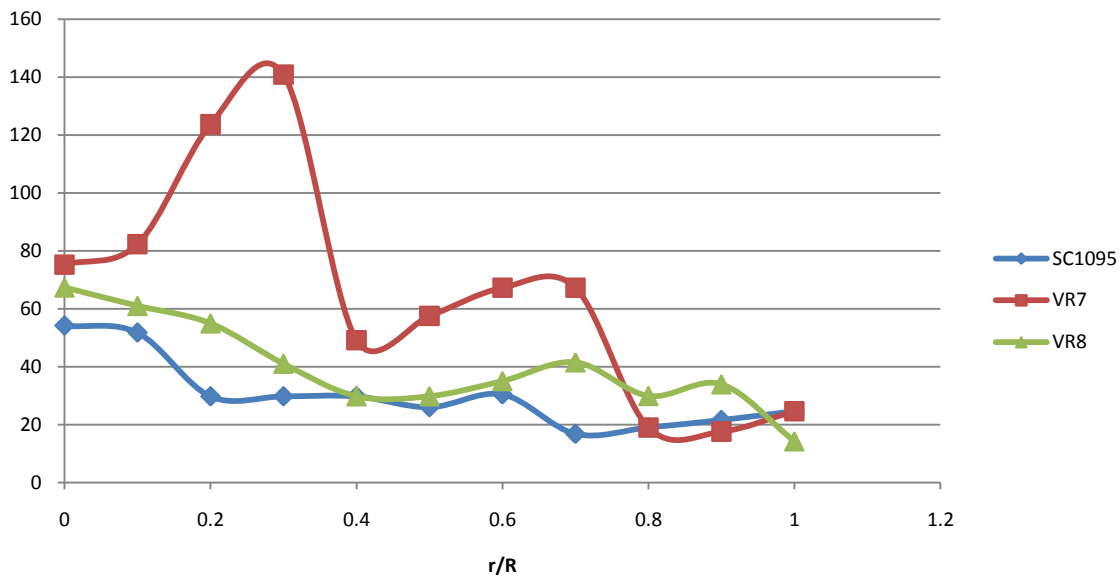


FIGURE C-8: LIFT TO DRAG RATIO AT 250 KTS AT SEA-LEVEL

### C.3. Taper ratio and linear twist selection

#### Hover performance optimizer creation

The previous sections were focused on the optimization of the rotor geometry for maximum cruise speed. However, an important optimization work was also performed to improve the performance of the rotor in hover. The linear twist and the taper ratio were two parameters that were optimized. The Combined Blade Element Momentum (CBEM) theory was used in this problem. The cutout value was fixed at 10% and is similar to the baseline vehicle. The blade of the rotor was decomposed in 10 segments. The radial position was defined as shown in Equation 15. We assumed that the blade could be decomposed in 10 segments with a constant width fixed at  $\Delta x$  given by Equation 14.

EQUATION 14

$$\Delta x = \frac{1 - \text{cutout}}{n} = \frac{0.9}{10} = 0.09$$

EQUATION 15

$$M_n = \text{cutout} + \frac{\Delta x}{2} + (n - 1)\Delta x$$

Then we defined the linear taper ratio by the expression  $n_1:n_2$  where  $n_1c$  is the chord at the root and  $n_2c$  is the chord at the tip. As a consequence, since the area of the blade remains the same for a fixed solidity of the rotor, there is a relationship between  $n_1$  and  $n_2$  as described in Equation 16. It is supposed that the root chord is larger than the tip chord and that the triangular blade (corresponding to  $n_1=2$  and  $n_2=0$ ) is the limiting geometry.

EQUATION 16

$$\frac{n_1 + n_2}{2} = 1$$

The linear twist angle is generally negative. For this study the twist angle  $\theta_w$  varies from 0 (no linear twist angle) to -20 deg. These values are realistic because a higher twist angle would not only challenge the small angle assumption (typically less than 20 deg) used in our equations but would also cause stall effects on the blade for high angles of attack.

It was also necessary to calculate the local solidity of a segment as a function of the taper ratio. The local solidity is the ratio of the area of segment  $n$  multiplied by number of blades over the disk area. For a segment  $n$  the chords are given in Equation 17.

EQUATION 17

$$\text{chord}_{n\pm} = n_1\bar{c} + \frac{(n_2 - n_1)(M_n \pm \frac{\Delta x}{2} - \text{cutout})}{1 - \text{cutout}} \bar{c}$$

Then the local solidity for a given segment  $n$  and a given taper ratio  $n_1:n_2$  is calculated using Equation 18.

EQUATION 18

$$\sigma_n = \frac{b \frac{\text{chord}_{n+} + \text{chord}_{n-}}{2} \Delta x}{\pi R}$$

It was then possible to use the CBEM code. The induced velocity is given by Equation 19. This expression is obtained when we equal the thrust produced by the rotor given by the momentum theory and the thrust calculated by the blade element theory [24].

EQUATION 19

$$\lambda_{i,n} = \sqrt{\left(\frac{\sigma a}{16}\right)^2 + \frac{\sigma a}{8} \theta M_n - \frac{\sigma a}{16}}$$

### Hover performance optimizer's results

It was necessary to compute iteratively the value of the pitch angle  $\theta_{75}$  in order to match the thrust coefficient  $C_T$ . The maximum error allowed was 5%. The results highly depend on this criterion of convergence. For this case the error was minimized and it was not possible to converge with a smaller error

without modifying other parameters such as the increment of the taper ratio or the increment of the linear twist angle. Figure C-9 presents the plot of the power coefficient  $C_p$  vs. the converged value of the thrust coefficient  $C_T$ . For our configuration at 6K95, the ideal value of  $C_T$  was 0.0082 and the pitch angle is calculated by iteration to match this value with an error of 5%. Each data point in this figure represents a different combination of taper ratio and twist angle. It can be seen that our results are very close to the ideal value of 0.0082 (the error is 2%). The value of the local pitch angle for this combination is  $\theta_{75}=0.214$  rad = 12.26 deg, which is a very reasonable value.

The best taper combination seemed to correspond to  $n_1 = 1.1$  and the linear twist was -10 degrees as shown on the 3D map in Figure C-10. In this case the taper ratio was merely 0.81. However it can be seen that the performance of the rotor was degraded when the taper ratio was increased. The triangular blade (corresponding to  $n_1=2$ ) was significantly degrading the hovering performance. The triangular blade cannot be implemented on current helicopters, mainly for manufacturing and structural considerations. Actually the rectangular blade seemed to be pretty efficient in hover in this study. It is not surprising to see that most helicopters have indeed a small taper ratio in reality (close to 0.8).

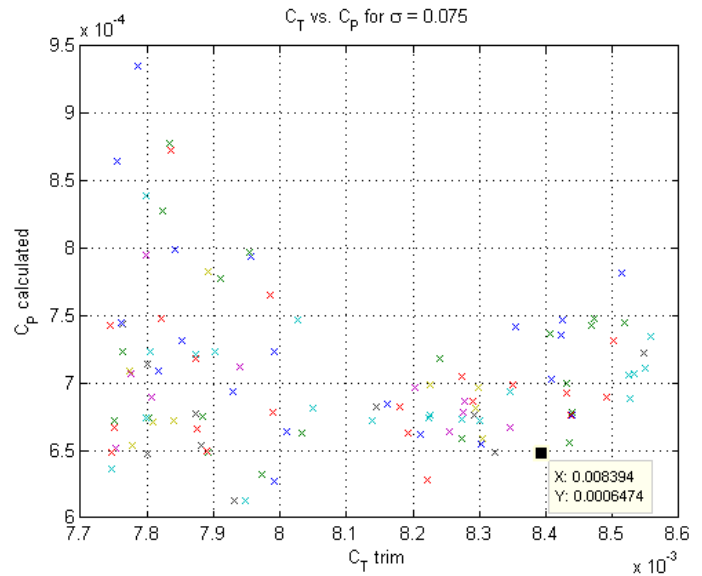


FIGURE C-9: CT TRIM VS. CP

However the figure of merit obtained (0.84) might seem to be a little bit too high. It can be accounted for by the fact that the tip losses and the swirl losses have been neglected in this code. In addition the small angles approximation used to derive the equations is sometimes threatened by the local values. At the same time the expression of  $\lambda_t$  given in Equation 19 leads sometimes to a complex number, meaning that the term inside the square root is negative. As a consequence the flow is going up because the local angle of attack (very sensitive to the twist angle  $\theta_{tw}$  at the root) is negative. This hypothesis is violating the assumptions of the CBEM theory. As a consequence the inflow velocity was supposed to be zero in this case and it can explain that the results presented are different than the reality. A penalty of 5% to account for these assumptions might be realistic, leading to an estimated Figure of Merit of 0.79

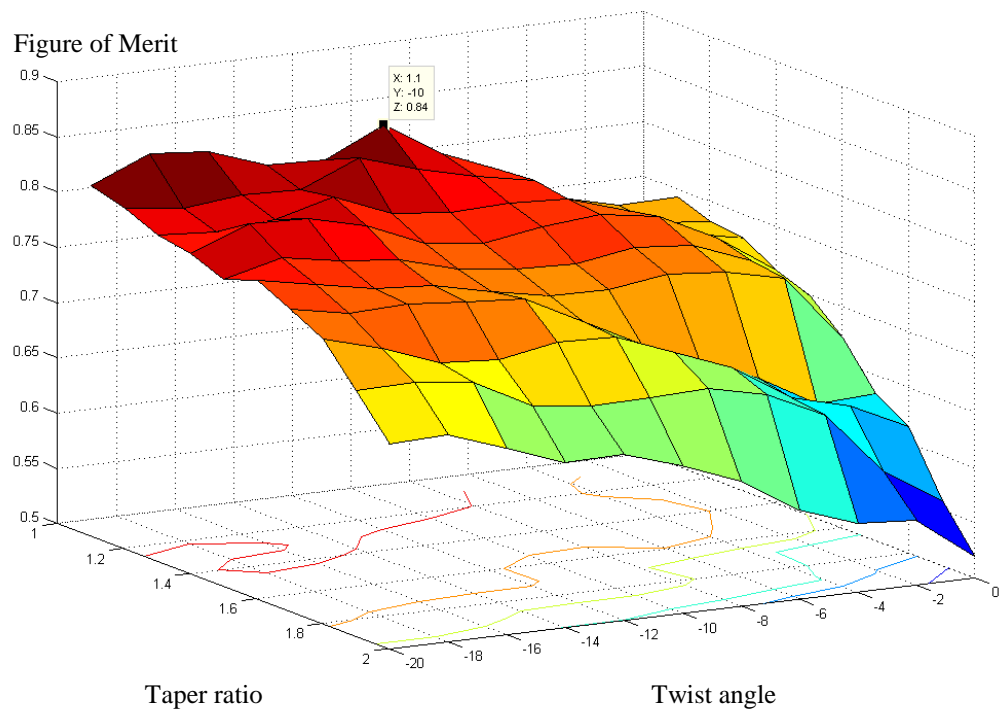


FIGURE C-10: FIGURE OF MERIT AT SEA-LEVEL VS. TAPER RATIO AND LINEAR TWIST

### C.4. Final blade planform design

The main rotor of Odyssey consists in a bearingless hub, VR-7 and VR-8 airfoils, linear twist and taper ratio and an elliptical planform. A root cutout of 10% was necessary to enable the assembly and allow enough room for IBC systems and fairings. The blade has a proper torsional stiffness and a high bending stiffness to maintain the minimum clearance between the two hubs. Most materials used in this blade are configured to be much stiffer than used in helicopter rotor blades. Figure C-11 shows the final blade planform in CATIA along with the main characteristics and dimensions of the blade. A solidity of 0.075 leads to an average chord length of 1.17 ft.

The materials used in the design of the main rotor are listed in Table C-3. The blade properties are essential to calculate the cross-sectional properties including structural properties and inertia properties. Torsional stiffness, bending stiffness, shear center, center of mass, mass per unit span and mass moments of inertia are part of the input file for the dynamic calculations shown in J.6. page 65.

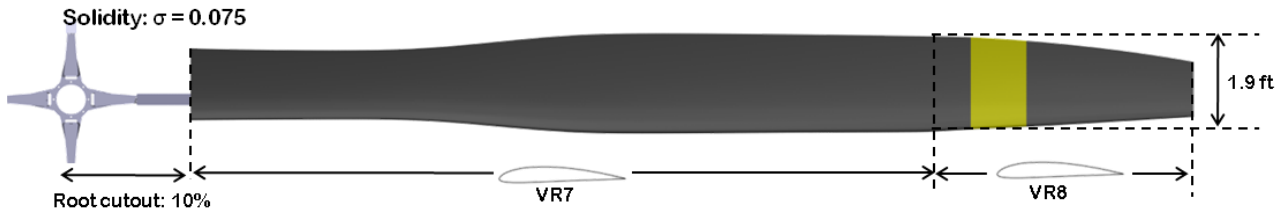


FIGURE C-11: FINAL BLADE PLANFORM DESIGN OF ODYSSEY

TABLE C-3: MATERIAL PROPERTIES OF THE MAIN ROTOR SYSTEM

Subcomponent	Material	Density (slug/ft <sup>3</sup> )	Young's modulus (Pa)	Young's modulus (lbf/ft <sup>2</sup> )
Hub	Tungsten carbide	30.7	1.404E+10	2.02E+12
Bearing	Aluminium oxide	7.66	8.208E+09	1.18E+13
Spar	Graphite fiber	3.01	3.470E+09	4.99E+13
Filling	Aluminium hexweb	0.68	1.238E+05	1.78E+07
Cover	Graphite fiber	3.01	3.470E+05	4.99E+07

## Appendix D FUSELAGE DESIGN

The high speed performances are mainly driven by the overall drag of Odyssey. It was required to develop a confident approach to build the equivalent flat plate drag area to compute the sizing and synthesis of the rotorcraft. In order to achieve this objective, Computational Fluid Dynamics (CFD) code was used and calibrated on existing data. The more accurate the drag buildup model was, the better our initial sizing estimation was. CFD analysis of the body and of the hub was conducted in Fluent 12.1 using grids automatically generated. The drag generated by the landing gear was neglected in high speed because it is retractable.

### D.1. Validation of the CFD code

In order to calibrate the CFD code, a simulation of Fluent 12.1 with a ROBIN fuselage was used and the results were compared with experimental measures [42]. The pusher propeller provides the entire thrust required for forward flight at high speed and the main rotor only provides lift to compensate the weight of Odyssey. As a consequence, the angle of attack of the vehicle in cruise is very close to 0 if there is no built-in-shaft tilt. Computations were performed with a zero angle of attack to simulate the behavior of the fuselage in cruise. The grid used 437,494 tetrahedral cells and 81,730 nodes. The Reynolds number, calculated on the fuselage length, was approximately  $1.6 \text{ E}+6$  at 0.1 Mach number. The distribution of the pressure coefficient CP is presented in Figure D-1.

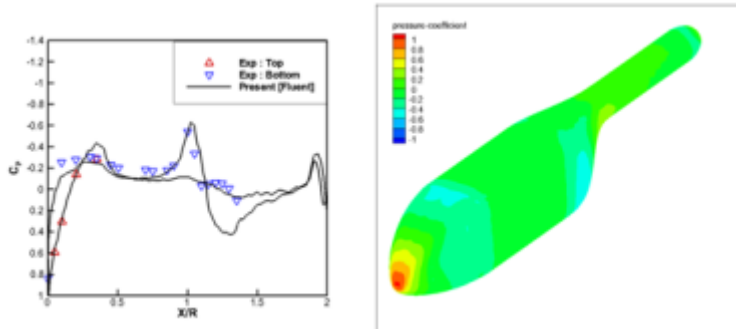


FIGURE D-1: PRESSURE COEFFICIENT DISTRIBUTION ON THE ROBIN FUSELAGE [42]

The results are presented in Table D-2. The predicted drag coefficient given by the CFD code is by far lower than the actual value of the fuselage. Other CFD codes were used to predict the coefficient of pressure distribution and in each case, the predicted value is almost 50% lower than the actual value. A correction factor was required to account for this gap between the computational tool and the actual data.

TABLE D-1: DRAG COEFFICIENTS OF THE ROBIN FUSELAGE

Grid	Unstructured tetrahedral	Cd present	0.105
Flow model	Incompressible flow	Cd overflow [42]	0.114
Turbulence model	K-ε	Cd elsA (SA) [42]	0.109
Mach number	0.1	Cd eIA (KOK) [42]	0.101
Sref	14m <sup>2</sup>	Cd exp	0.145

### CFD model of the fuselage

Once the CFD model was validated on existing fuselages, it was possible to run the code to estimate the drag of the fuselage, along with the drag of the hub in cruise conditions. Two separate simulations were run with the hub and without the hub to account for the interference drag between these two entities. The Mach number was fixed at 0.37 corresponding to 240 knots at 6,000 ft 95 degrees F. Figure D-2 shows the CFD code running separately. The results are summarized in Table D-2.

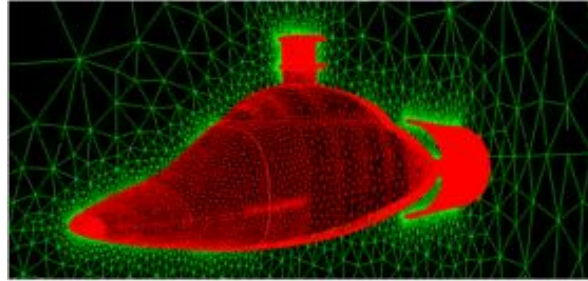


FIGURE D-2: ODYSSEY FUSELAGE AND HUB DRAG EVALUATION WITH CFD CODE

In order to obtain the overall drag of the helicopter at zero angle of attack in cruise conditions, as shown in Figure D-2, the distribution of the coefficient of pressure was computed on the entire vehicle and the correction factor was applied.

TABLE D-2: ASSUMPTIONS, STREAMLINE VISUALIZATION AND DRAG COEFFICIENTS

Assumptions	Grid	Unstructured tetrahedral
	Flow model	Incompressible flow
	Turbulence model	K-ε
	Mach number	0.37
	Freestream velocity	128.42 m/s
Fuselage	Tetrahedral cells	127,711
	Nodes	27,948
	Sref	16m <sup>2</sup>
	C <sub>D</sub>	0.114
Hub	Tetrahedral cells	843,844
	Sref	Cross section area
	C <sub>D</sub>	0.0225

## D.2. Drag Analysis

The critical point to the Odyssey's high speed flight capability was the precise prediction of the fuselage drag. A hybrid method combining CFD drag estimation for the rotor hub, fuselage, and duct and drag buildup method from Prouty's book [38] for other components was used. According to the literature data, this combined CFD and semi-empirical calculation is commonly used for fuselage design in the absence of a wind tunnel model for drag estimation [24]. The Odyssey fuselage contributes 40% to the total flat plate drag area of the vehicle. The drag buildup for the baseline model and Odyssey was conducted based on the CFD result and on the percentage contribution of each component, according to Prouty's representative breakdown of component drag for a conventional single main rotor helicopter [38]. For the final configuration, rotor hub and duct of pusher were included with fuselage in CFD simulation. These components contribute almost 80% to the total flat plate area of the vehicle as shown in Table D-3.

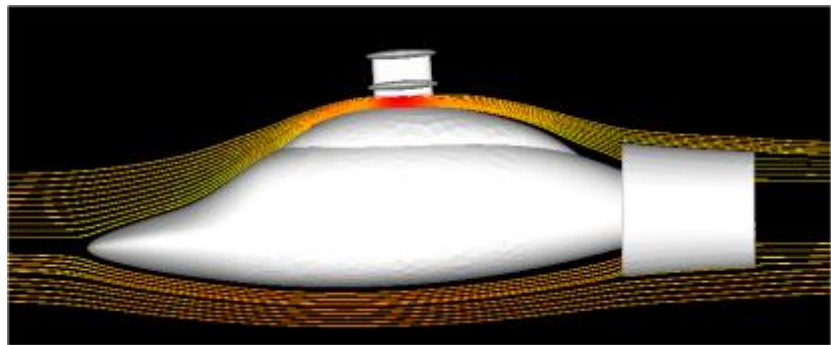


FIGURE D-3: STREAMLINE VELOCITY WITH THE PUSHER PROPELLER DISENGAGED

Airframe of Odyssey contributes most of the vehicle's total drag in forward flight. If this drag can be marginally reduced, an increase of performance could be expected. A study for boundary layer control over the rear portion of the fuselage was conducted in order to reduce the drag. In order to prevent the boundary layer near the ramp of fuselage from separating the flow from the fuselage surface, the shape of the fuselage and propeller duct employ what may be called aerodynamic static pressure thrust or negative form drag. The power

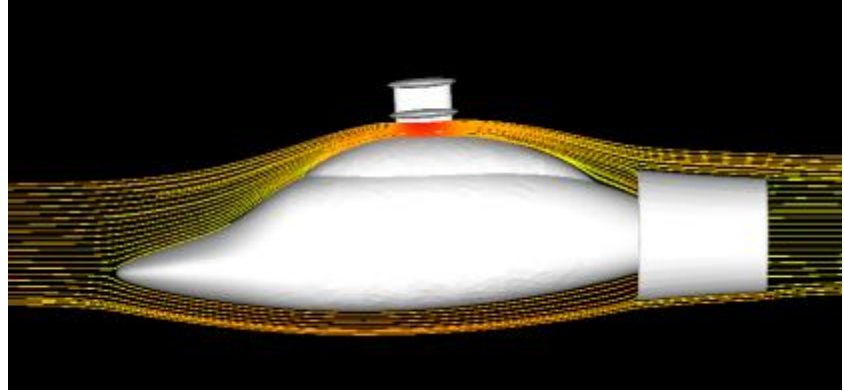


FIGURE D-4: STREAMLINE VELOCITY WITH THE PUSHER PROELLER ENGAGED

provided to the pusher propeller system is thus used not only for thrust, but also for drag reduction. A research for this concept was performed by Goldschmied [19] with specific investigations on the use of ducted fans done by Fanucci [15] and McLemore [36]. The previous experiment showed remarkable results as high as 40 - 50 % propulsive power reduction for axisymmetric bodies. Even a small reduction in flat plate area drag would result in substantial performance improvement at all flight conditions. In this design CFD simulation was performed in order to examine effect of the above concept on our vehicle. In the CFD simulation, an actuator disk was created inside the duct halfway between the axial locations of the counter rotating fans in order to model the propeller. A simulation was conducted at the same flight condition mentioned above while prescribing the pusher propeller system's thrust of 2,313 lb-f using pressure inlet and pressure outlet boundary conditions. The actuator disc was considered separate from the fuselage wall boundaries in Fluent in order to isolate the actual thrust generated by the propeller and determine only the change in axial force due to the change in flow pattern. Table D-3 shows the comparison between fan on and fan off cases.

TABLE D-3: COMPARISON OF FLAT PLATE DRAG AREA WITH AND WITHOUT THE FAN

Component	Fan off		Fan on	
	f (ft <sup>2</sup> )	%	f (ft <sup>2</sup> )	%
Airframe	Fuselage	79.80	11.97	77.43
	Fan Duct			
	Exhaust			
	Pylon			
	Sponsons			
Landing Gear	Wheels	100.00	15.46	100.00
	Struts			
	Total			

Figure D-3 and Figure D-4 show the effect of the propeller suction near the fuselage. The flow is more attached in case of fan on. A 10.3% reduction in fuselage flat plate area was obtained by considering the effect of the pusher as can be seen in Table D-3.

TABLE D-4: DRAG BUILD-UP AND ESTIMATION OF THE FLAT PLATE DRAG AREA

	Component	Drag build-up method		CFD prediction	
		f (ft2)	%	f (ft2)	%
Airframe	Fuselage	7.57	39.05	11.97	77.43
	Fan Duct	1.00	5.16		
	Exhaust				
	Pylon				
	Sponsons				
Landing Gear	Wheels	0.72	3.72		
	Struts	0.39	2.01		
Hub		6.21	32.05		
Rotor-Fuselage Interference		2.89	14.92	2.89	18.69
Exhaust drag		0.10	0.52	0.10	0.65
Miscellaneous drag		0.50	2.58	0.50	3.23
<b>Total</b>		<b>19.38</b>	<b>100.00</b>	<b>15.46</b>	<b>100.00</b>

### D.3. Fuselage aerodynamics and forces

The main goal of the fuselage design was to determine the most favorable geometry that would allow the correct cabin configuration, reduce the overall flat plate drag area and limit the airloads due to side slip angle or angle of attack during cruise. Forces and moments were computed and collected to be used as inputs to the FlightLab model. In the vehicle body frame, shown in Figure D-5, the forces along the X, Y, and Z axis were computed along with the moments L, M, and N.

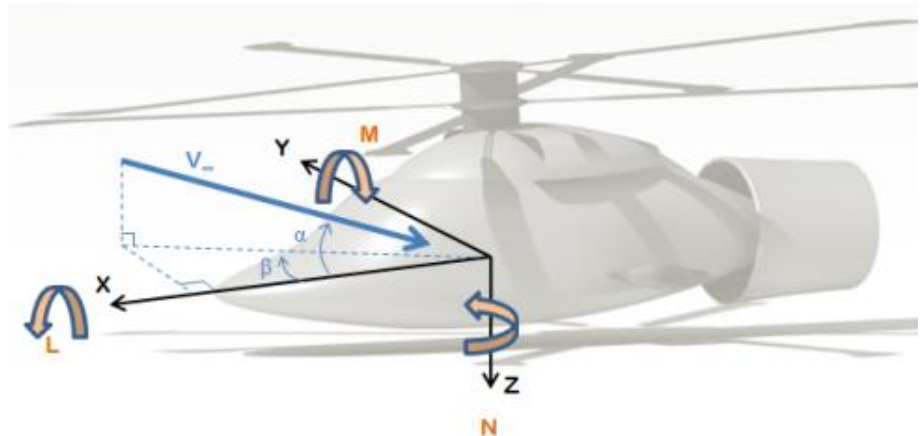


FIGURE D-5: BODYFRAME

The position of the center of gravity was identified by the CATIA model of Odyssey. Table D-5 summarizes the inputs to calculate the airloads on the body.

TABLE D-5: CG POSITION OF ODYSSEY

Body frame axis	Dimension (mm)
X	4,175.07
Y	-36.703
Z	1,914.39
Fuselage length	8,646
Origin X	721.25
Origin Z	789.22

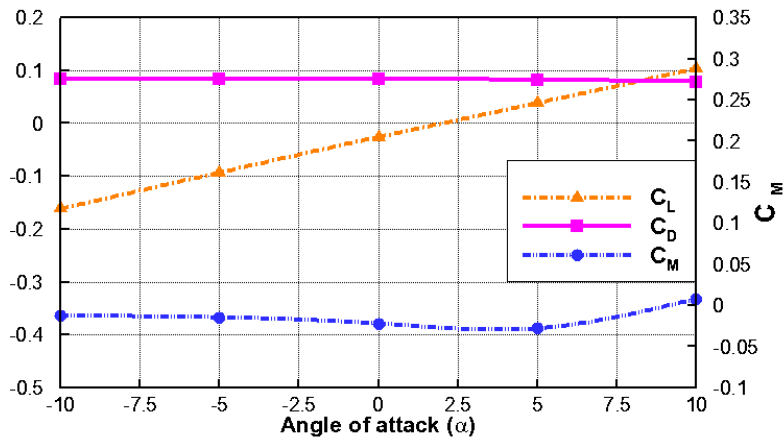


FIGURE D-6: AIRLOADS VS. ANGLE OF ATTACK

Using these parameters, it was possible to calculate the dimensionless parameters corresponding to the airloads such as  $C_L$ ,  $C_D$ , etc... Figure D-6 presents the variation of the lift, drag and pitching moments of the body as a function of the angle of attack  $\alpha$ . The same analysis was conducted with respect to the variation of the sideslip angle  $\beta$  and the results are presented in Figure D-7.

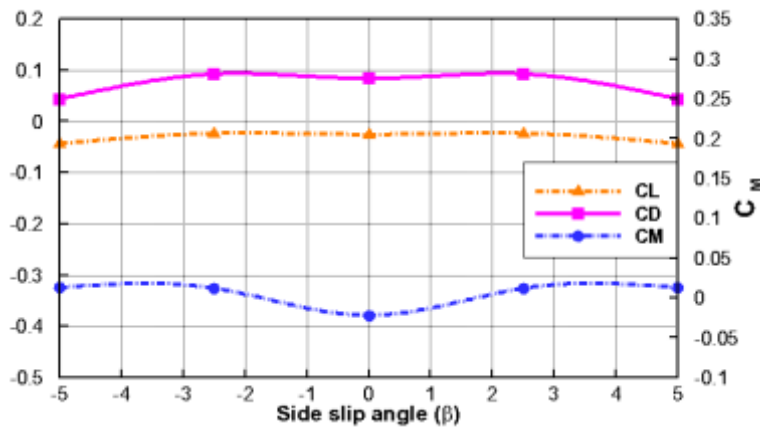


FIGURE D-7: AIRLOADS VS. SIDESLIP ANGLE

The fuselage was designed and optimized to reduce the drag sensitivity to the angle of attack or side slip angle variations. In this case, it was possible to assume that the attitude of Odyssey in cruise did not impact the flat plate drag area. As shown in Figure D-8, the value of the flat plate drag area is very stable and assumed constant on a range of  $\pm 10$  deg AoA. The pitching coefficient is also very stable on this range of AoA and the lift coefficient follows a linear behavior. At zero angle of attack, the fuselage presents a very slight negative lift mainly due to the increased pressure on the windshield of Odyssey.

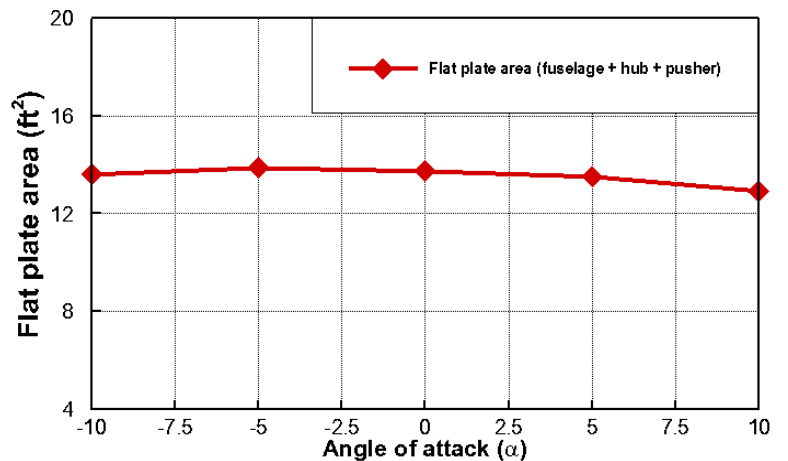


FIGURE D-8: VARIATION OF THE FLAT PLATE DRAG AREA VS. ANGLE OF ATTACK

## Appendix E AUXILIARY PROPULSION DESIGN

The design process for a pusher type propeller on rotorcraft is simplified by the fact that there is no take off thrust requirement, which typically drives the sizing for fixed wing propellers. The design point for sizing an auxiliary propulsor for a high speed rotorcraft like Odyssey is derived from a cruise requirement. For Odyssey to achieve the high speed requirement of the SAR mission, the propeller must be capable of producing on the order of 2,300 lbs of thrust at 230 kts. Propeller performance analysis was conducted using ‘Strip Theory’ [7] to determine the power absorption and efficiency for a given design. A publicly available propeller design tool called Javaprop was used to perform the analysis. Strip Theory uses 2-dimensional airfoil data combined with propeller design variables such as diameter, rotor speed, number of blades, and twist and chord distribution to determine the flow conditions through the propeller. The design process is summarized in Figure E-1.

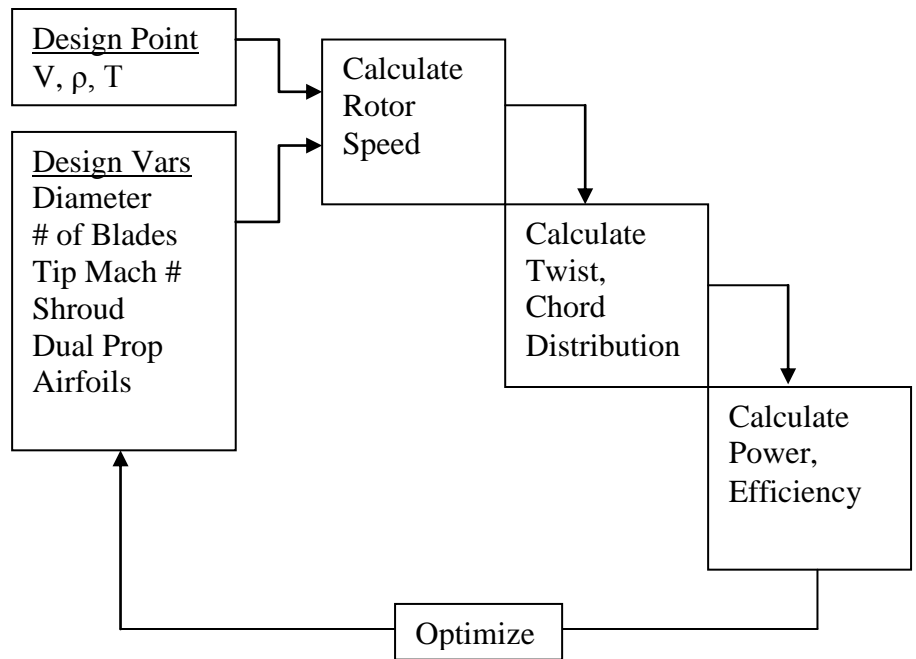


FIGURE E-1: PROPELLER SYSTEM DESIGN PROCESS

Several classic propeller airfoils were evaluated for maximum L/D performance and design Mach number. For the midsection section, the Eppler 193 was chosen for its maximum L/D ratio and historical success in propeller designs. Near the 70% radius, the airfoil shape changes to an MH 116 for better performance in a high Mach environment. This airfoil configuration was found to outperform others tested through trial and error, including the Clark Y, ARA-D propeller airfoils. Since the airfoil selection was not a significant driver to the overall design of the propeller system, this configuration was used to evaluate all propeller designs.

In designing a propeller system for specified condition, the designer is naturally led to choose the largest feasible propeller diameter. As the diameter grows, the required rotor speed goes down, eliminating viscous losses and improving propulsive efficiency. In the case of the Odyssey, the propeller was limited to 5 ft in diameter due to the proximity to the ground. Using momentum theory and assuming no viscous losses, the maximum amount of thrust available from a 5 ft diameter was found as a function of input power and velocity.

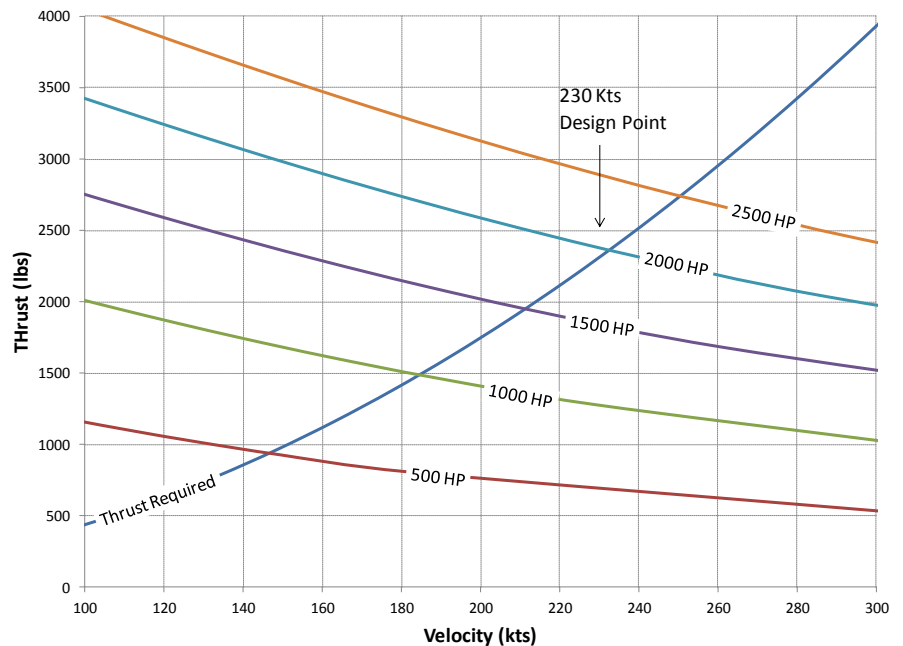


FIGURE E-2: IDEAL THRUST AVAILABLE FROM A 5 FT DIAMETER PROPELLER

Figure E-2 reveals that to achieve speeds in excess of 200 kts, the propeller will need to consume more than 1,000 hp. Since this plot is based on the maximum ideal propulsive efficiency, real world designs will require approximately 10-20% more power to account for viscous losses and 3 dimensional effects. To achieve the design cruise speed of 230 kts, the propeller will need to consume more than 2,000 hp.

The 5 ft diameter propeller producing 2,300 lbs of thrust has a disk loading of 117 lbs/ft<sup>2</sup> for a single rotor design. This was found to be so high that the resulting blade chord needed to meet the thrust requirement was infeasible. Adding more blades helped to reduce the size of an individual blade, but adds to the weight and complexity of the system. Increasing rotor speed was another means to reduce the blade size. However it was found that a tip speed exceeding Mach 1 was required to meet the thrust requirement, which is highly undesirable. To keep the size of the propeller blades within reasonable limits, a constraint was considered called the blade activity factor. The activity factor is a measure of solidity and is found by Equation 20.

EQUATION 20

$$AF = \frac{10^5}{16} \int_0^1 \frac{c}{D} \left( \frac{r}{R} \right)^3 d \left( \frac{r}{R} \right)$$

Typical propeller blades have an activity factor 100 to 150, and an upper limit of 200 was implemented based on historical design practices [7]. A tip speed constraint of Mach 0.8 was added to reduce compressibility effects during cruise. This addition of these constraints led to the implementation of a dual counter-rotating type propeller to share the disk loading between two rotors and reduce the required rotor speed. Figure E-6, Figure E-8, and Figure E-7 page 39 show the Odyssey’s pusher propeller configuration

The merits of a propeller duct were investigated for the Odyssey’s auxiliary propulsion system. Propeller ducts are often considered for two primary reasons: Increased static thrust, and improved blade loading. Additional benefits include improved safety and reduced noise. It is unlikely that a propeller duct will increase thrust at the Odyssey’s high speed cruise condition via pressure differentials on the duct structure, as it will in a static condition. However, the improved blade loading was found to greatly enhance the performance of the propeller at all operating conditions. By improving the blade loading at the tip, the propeller thrust can be distributed across the radius resulting in improved efficiency and reduced power consumption. Figure E-3 demonstrates the improved blade loading for a ducted propeller by showing the thrust distribution across the radius. Both propeller types are producing the same amount of total thrust.

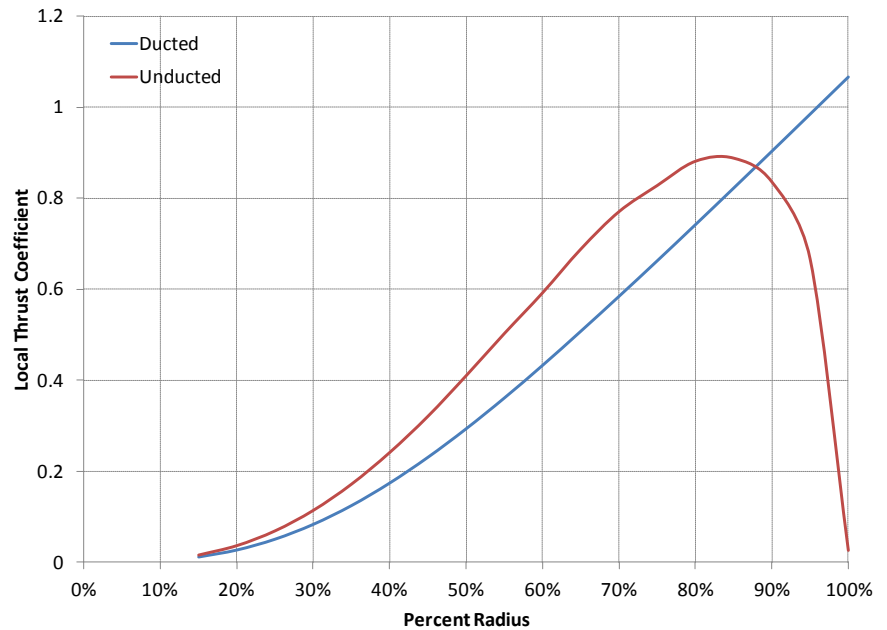


FIGURE E-3: LOCAL THRUST COEFFICIENT FOR A DUCTED AND UNDUCTED PROPELLER BLADE

The ducts effect on total power consumption was evaluated at various forward flight speeds and design configurations. Figure E-4 shows a series of unique, optimum propeller design configurations for both the open propeller and the ducted propeller.

Each point in Figure E-4 represents a unique design in terms of number of blades, twist and chord distribution. The diameter is fixed at 5 ft, and tip speed fixed at Mach 0.8. Because the ducted propeller improves blade loading, fewer blades are required when compared to the open propeller at the same forward velocity design point. A total power savings of about 6% is demonstrated due to the propeller duct. As shown by the Insertion Hover Power reference line at 1,880 hp, the forward flight condition is sizing the transmission and engines. Therefore it was determined that the 6% power savings offered by the duct was significant enough to warrant its use in the Odyssey design.

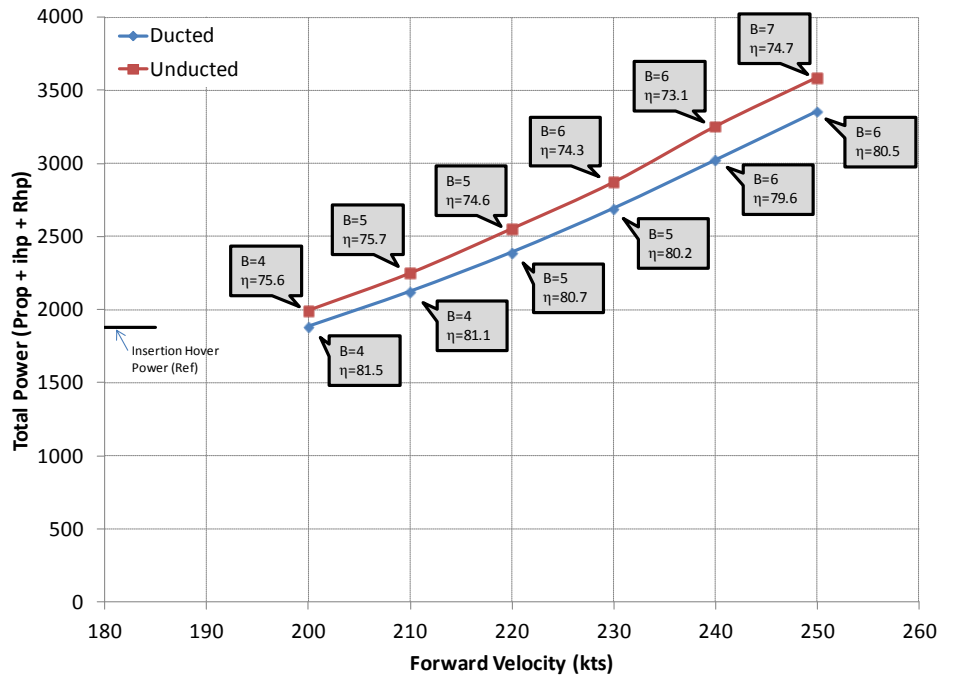


FIGURE E-4: 5 FT DIAMETER PROPELLER DESIGN TRADE STUDY

### E.1. Final Design Configuration

The final propeller system design configuration is shown below in Table E-1.

TABLE E-1: ODYSSEY PROPELLER SYSTEM DESIGN SPECIFICATIONS

Design Point:		
V=	230	kts
T=	2313	lbs
Design Characteristics		
Type:	Ducted Dual Counter-Rotating Propellers	
Dia <sub>prop</sub> =	4.75	ft
Dia <sub>duct</sub> =	5	ft
N=	3365	rpm
M <sub>tip</sub> =	0.8	(a=1154 fps for 6k95)
B=	5	blades per propeller
Twist=	45	degrees
AF=	143	
Design Point Performance:		
P <sub>total</sub> =	2256	hp (at design point)
η=	72.20%	(=propulsive power/power input)

The Odyssey propeller system's off-design performance was determined for a range of pitch settings and forward flight velocities, and is shown in Figure E-5. For all off-design points, propeller speed is held constant at 3,365 RPM.

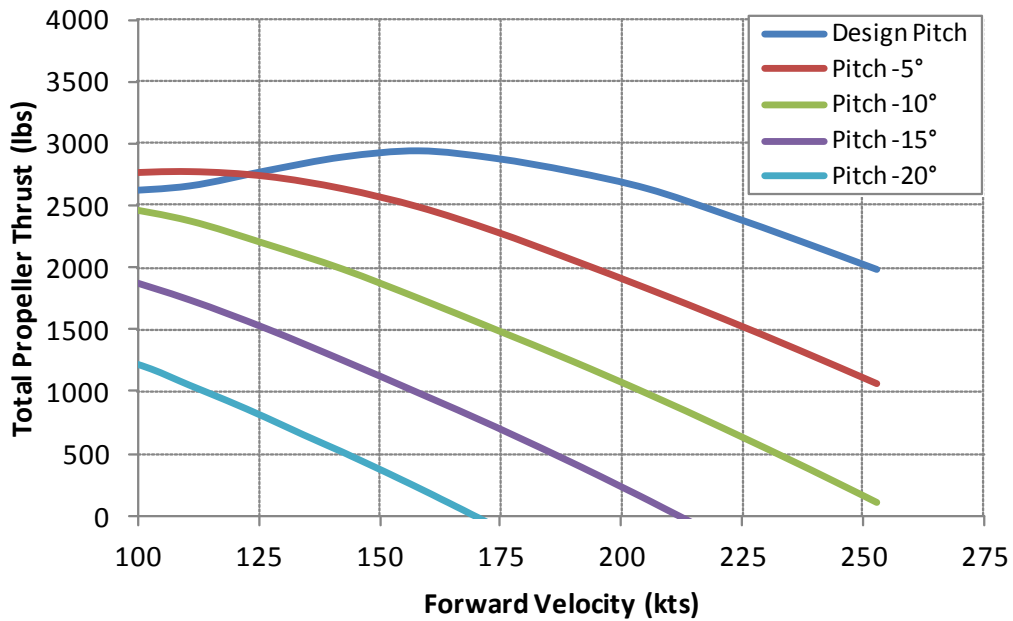


FIGURE E-5: ODYSSEY PROPELLER SYSTEM'S OFF-DESIGN PERFORMANCE

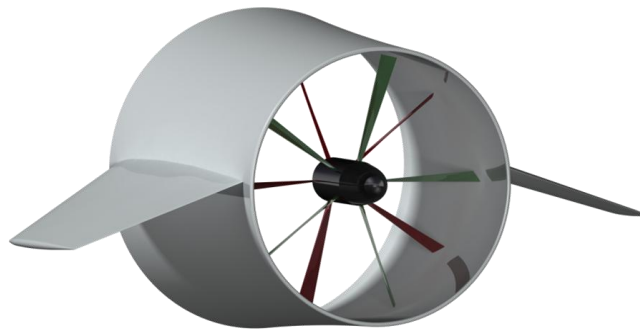


FIGURE E-6: DUCTED CONFIGURATION WITH HORIZONTAL STABILIZER

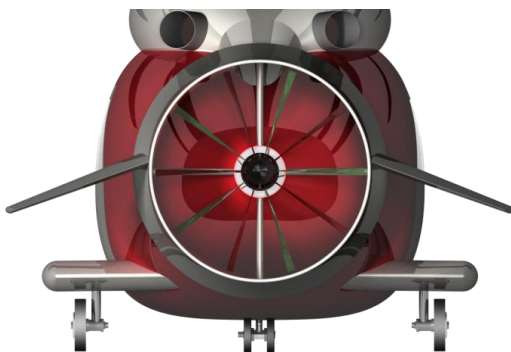


FIGURE E-8: PUSHER PROPELLER CONFIGURATION (REAR VIEW)



FIGURE E-7: DUAL COUNTER-ROTATING BLADES

## Appendix F ENGINE DESIGN

### F.1. Baseline engine GE CT701C

The RFP recommends using the GE CT7-8A engine as the baseline. This engine is a commercial variant of the T700 developed by General Electric. In our case, the HH-60G Pavehawk is equipped with the military version of this engine, the GE 701C.

Based on the preliminary study, it was possible to estimate the power required by the vehicle to hover in military hot day conditions and reach the maximum cruise speed. The baseline engine is the T700 GE 701C which is used by the HH-60G Pavehawk [51]. The fuel capacity of the baseline helicopter is 361.5 gallons with two tanks. The torque transmission limits are 135% OEI and 120% dual engine below 80 knots and 100% dual engine above 80 knots. These limits are fundamental to size the transmission of the vehicle.

### F.2. Rubberized engine

Since the RFP presents this engine as the baseline, it was decided to plot the power graphs with respect to its power limits. However, this engine can be "rubberized" in order to meet a higher power demand. In this case the effects of engine scaling must be addressed on the Specific Fuel Consumption (SFC) and the weight of the engine [40]. The Engine Scaling Factor (ESF) is defined in Equation 21 where MRP stands for Maximum Rating Power.

$$\text{ESF} = \frac{\text{MRP}_{\text{actual}}}{\text{MRP}_{\text{baseline}}}$$

The SFC must be corrected in accordance with the ESF. Based on historical data and trends, the Georgia Tech Center of Excellence in Rotorcraft Technology (CERT) developed a scaling equation for the SFC, presented in Equation 22.

$$\text{SFC}_{\text{cor}} = \text{SFC}_{\text{baseline}} \frac{-0.00932(\text{ESF})^2 + 0.865\text{ESF} + 0.445}{\text{ESF} + 0.301}$$

The weight of the engine group can be estimated using Equation 23.  $N_{\text{eng}}$  is the number of engines and MCP is the Maximum Continuous Power. The weight  $W_{\text{engine}}$  is given in lbs for one engine.

$$W_{\text{engine}} = N_{\text{eng}} \frac{0.1054 \left( \frac{\text{MCP}}{N_{\text{eng}}} \right)^2 + 358 \left( \frac{\text{MCP}}{N_{\text{eng}}} \right) + 2.757 \times 10^4}{\frac{\text{MCP}}{N_{\text{eng}}} + 1180}$$

### F.3. Single Engine Hover Ceiling

Because the power required for high speed cruise is greater than the power required for hover, the engine power is sized by the cruise conditions. A characteristic of turbine engines is that available power drops off with a higher altitude and temperature. This decrease can be approximately estimated to 2% per 1,000 ft and 0.5% per degree F. Sizing an engine for 6K95 Hot Day conditions will provide a large amount of excess power available for hover at standard conditions resulting in that Odyssey has a single engine hover out of ground effect capacity at sea-level, increasing the safety of the vehicle. However, increasing installed power greatly penalizes fuel consumption, maintenance costs, and increases Odyssey empty weight through growth effects as shown in Figure F-1 where a polynomial extrapolation was performed on historical data [25]. The increase of the single engine hover ceiling up to 6,000 ft in military Hot Day would represent a

significant jump in fuel consumption, gross weight and DOC. As a consequence, it was decided to size the engine only on the high speed cruise segment.

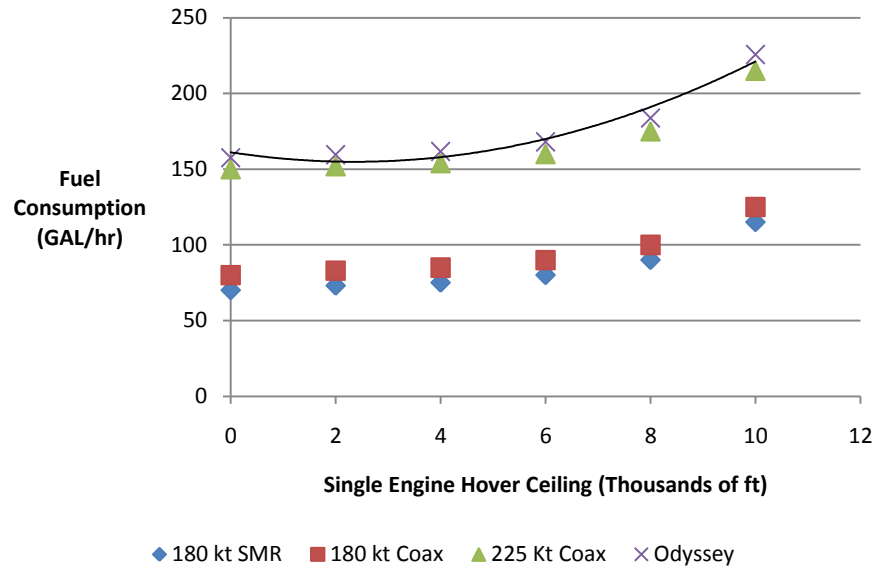


FIGURE F-1: IMPACT OF CEILING ON THE DESIGN GROSS WEIGHT

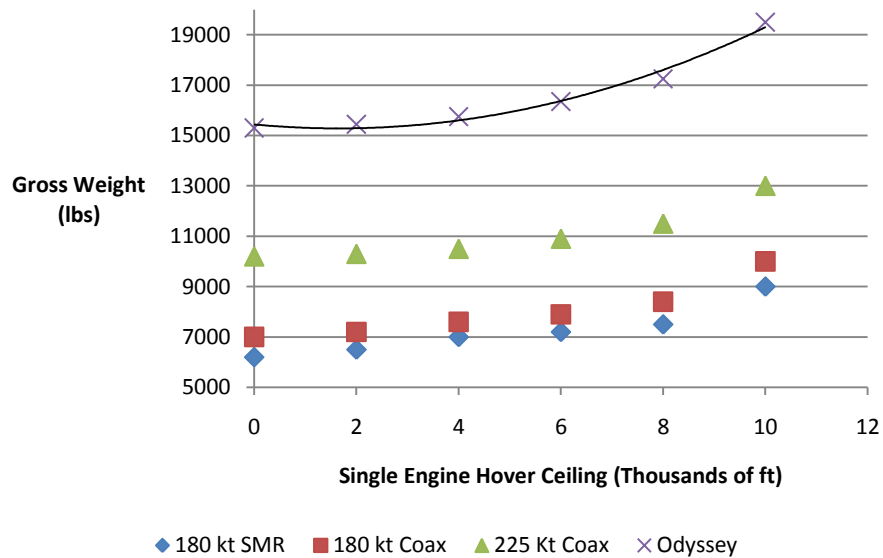


FIGURE F-2: IMPACT OF CEILING ON THE FUEL CONSUMPTION

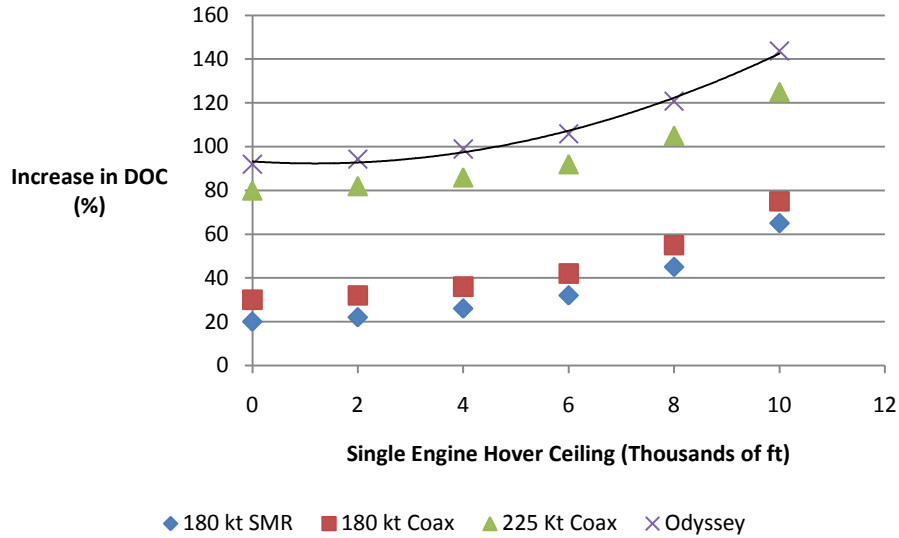


FIGURE F-3: IMPACT OF CEILING ON THE DOC

This trade off analysis is based on historical data for SMR and Advancing Blade Concept™ developed by Sikorsky in 1980. The gross weight impact of increasing the single engine hover ceiling to 10,000 ft was on the order of 16% for Odyssey with auxiliary propulsion. Fuel consumption went up by more than 40% as shown in Figure F-2 and the increase in Direct Operating Cost (DOC) was approximately 50% as shown in Figure F-3.

It was reasonable to assume that the engine would benefit from the research efforts regarding fuel consumption and power to weight ratio in the next couple of years. Based on advanced engine technology levels that are likely to be representative of those improvements in 2025, it was decided to assume a 20% reduction in SFC and weight-to-power ratio.

#### F.4. Final Engine configuration

The final engine selection resulted from a tradeoff analysis to optimize the performance of Odyssey. It would have been possible to opt for a bigger engine than the baseline to provide a large amount of excess power in cruise, with HOGE 6K95 capability with one engine inoperative and an increased maximum cruise speed but this would have required much more fuel, more fuel volume and tanks, along with an increase of the direct operating costs. Instead, we had to size the engine in order to meet both the OEI requirement at sea-level and the minimum cruise speed of 230 knots in case of mission1. Since Odyssey is a lighter than the Pavehawk, it was sensible to look for a smaller engine than the GE CT701C. The rubberized engine is shown in Figure F-4. Hitting 250 knots as max cruise speed at MCP would have reduced the efficiency of the pusher propeller, increased the overall weight and fuel required, the acquisition cost and the direct operating costs.



FIGURE F-4: T700 GE701C

### OEI Contingency Power sizing process

If a pilot encounters the loss of one engine at a higher altitude, the most sensible reasoning leads to an emergency landing. Using the propeller, it is possible to reduce the total power required to reach a landing point. Similarly to an autorotation maneuver, if the loss occurs in hover at 6K95, then the pilot needs to descend and gain some forward flight speed. If the loss of the engine occurs close to the ground, then the ground effect can help the pilot to maintain control of Odyssey. Finally, if the pilot does not have enough altitude to gain forward flight, then an autorotation landing is possible as long as this engine failure does not occur over water.

At sea-level in standard conditions and at maximum takeoff gross weight for Mission 2, the power required to hover out of ground effect is 1,500 hp. Assuming that the behavior of the rubberized engine is similar in OEI and at maximum rated power, it was possible to calculate the ESF by using Equation 21. The resulting ESF was 0.773.

### Maximum cruise speed

The sizing of the engine must account for the maximum cruise speed of Odyssey for Mission 1. The maximum cruise speed at sea-level and at MCP must be greater or equal to 225 knots to take casualties to medical service centers in 60 minutes. As a consequence, the MCP must be sized to meet this requirement. The engine scaling factor to meet this requirement must be calculated and compared to the previous one. The greater value must be kept and this parameter drives the sizing of the engine. At maximum takeoff gross weight, the engine scaling factor to meet this requirement is 0.9326 and is the greater ESF.

### Engine characteristics

This section presents the final scaling characteristics of the engine. The ESF is 0.9626 and the specific fuel consumption corresponding to this rubberized engine is 0.374 lbs/shp-hr. This SFC accounts for the predicted technical improvements by 2025. The dry weight of one engine is given by Equation 23 and corresponds to 376 lbs. The dry weight of the engine accounts for an improvement of 20% of the power-to-weight ratio in the next couple of years. For each rated power, the time limits, the shaft power of the rubberized engine, and the power turbine inlet temperature are presented in Table F-1.

### Hover In-Ground-Effect (HIGE) capability

At maximum takeoff gross weight, Figure G-4 page 47 shows that Odyssey is unable to HOGE at 6K95 with one engine failure. Although this is not a requirement of the RFP, it was reckoned that an emergency engine rating was necessary to provide Odyssey with a HIGE capability at 6K95 with One Engine Inoperative (OEI). In this case, the power rating for 30 s is calculated using Equation 24 where t is expressed in minutes [47]. The maximum OEI power available at 6K95 for 30 seconds is 1,402 hp. It is possible to calculate the corresponding height above the ground where the HIGE power required equals the OEI power available. The In-Ground effect correction factor  $\Lambda$  is calculated by Equation 25 where Z is the height above the ground and R is the rotor radius [46]. This theory has been shown to be accurate for only  $Z/R > 1$ . Using both equations it was possible to compute the height above the ground where hover is possible at 6K95 and at maximum takeoff gross weight with one engine inoperative. This height is 26 ft.

EQUATION 24

$$HP_{30s} = MCP(1 + 0.252e^{-0.0173t})$$

EQUATION 25

$$\Lambda = \left(\frac{Z}{2R}\right)^{1/3}$$

TABLE F-1: CHARACTERISTICS OF ODYSSEY'S ENGINE

Rated Power	Time limit	Odyssey Shaft power per engine (Sea-level Std conditions)	Odyssey Shaft power per engine (Hot Day 6K95)	Power turbine Inlet temperature
Emergency Contingency Rating	30 s OEI	1,937 hp	1,402 hp	911 degC
Contingency Rated Power (CRP)	2 1/2 min OEI	1,809 hp	1,309 hp	903 degC
Maximum Rating	10 min dual	1,762 hp	1,275 hp	878 degC
Intermediate Rated Power (IRP)	30 min dual	1,678 hp	1,215 hp	851 degC
Maximum Continuous Power (MCP)	N/A	1,550 hp	1,122 hp	810 degC

**Power available**

The engine power available as a function of altitude is presented in Figure F-5. It is possible to calculate the power available in the military Hot Day criteria using Equation 26 [24].

EQUATION 26

$$HP_{available} = HP_{sea-level} \left( 1 - 0.195 \times \frac{alt}{10000} \right) (1 - 0.005 \times \Delta T)$$

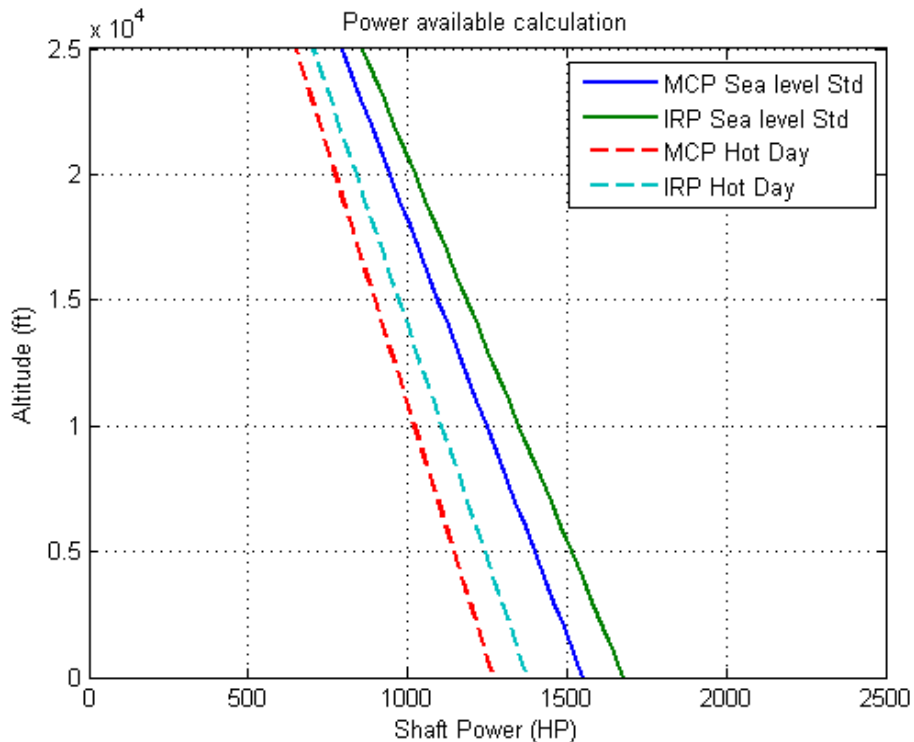


FIGURE F-5: POWER AVAILABLE OF ODYSSEY'S ENGINE VS. ALTITUDE AND ATMOSPHERIC CONDITION

## Appendix G ODYSSEY PERFORMANCE SUMMARY

This chapter presents a summary of the performance of Odyssey as a function of atmospheric conditions and engines operation mode. A time analysis of the three missions is provided along with absolute and maximum ceilings.

### G.1. Power curves

The AEO power available curve is available in Figure F-5 page 44. Using this power available and computing the power required to drive the main rotor, the auxiliary propulsion and the gear boxes, it was possible to draw the final performance curves of Odyssey.

For mission 1 SAR, the maximum takeoff gross weight is 12,656 lbs and the power curve at sea-level is presented in Figure G-1. It can be seen that Odyssey has a large amount of excess power at sea-level, contributing to excellent performance and safety margins. The parasite drag accounts for the majority of the power required at high speed and the main rotor power required is decreasing along with the forward flight velocity. The pilot must engage the pusher prop at the minimum power required around 70 knots.

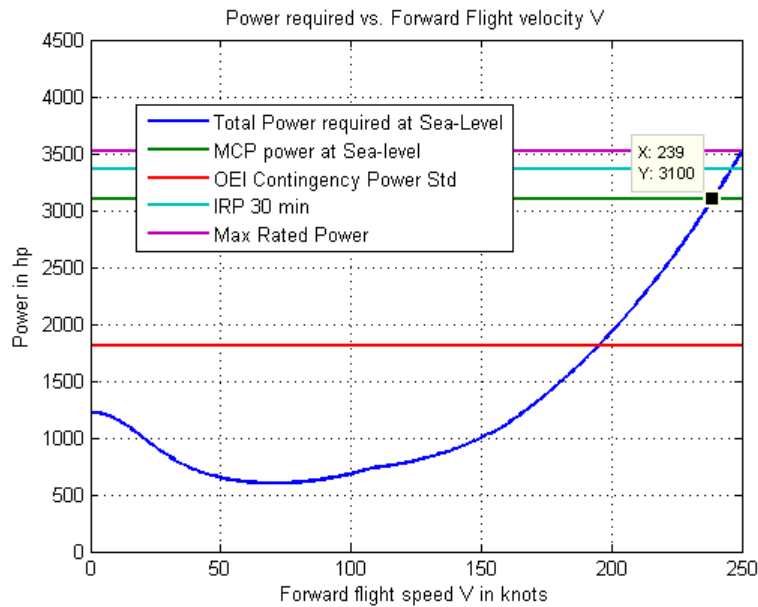


FIGURE G-1: POWER CURVE AT SEA-LEVEL FOR MISSION 1

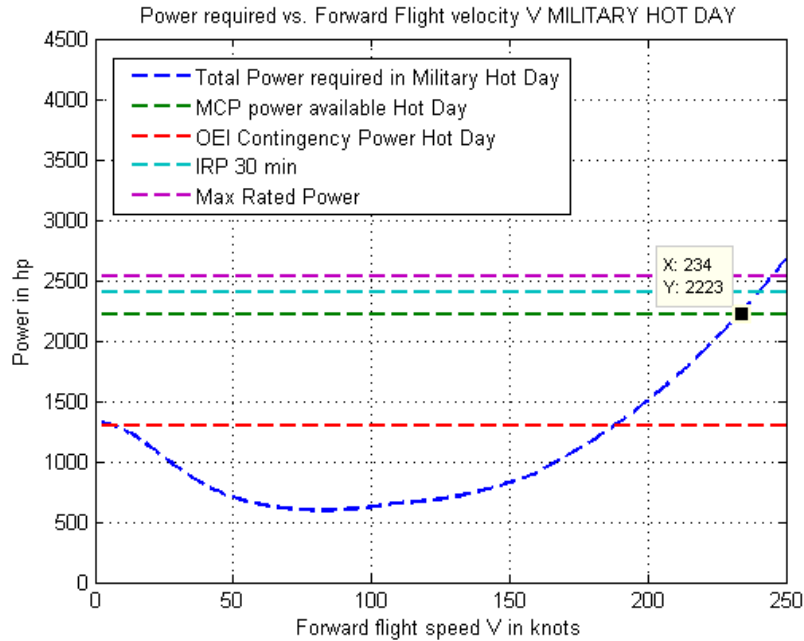


FIGURE G-2: POWER CURVE IN MILITARY HOT DAY CONDITIONS FOR MISSION 1

Figure G-2 shows the same configuration at 6K95 in military Hot Day conditions. The power required for hover is higher than at sea-level mainly due to the rise of the induced power. The power available is reduced because of the altitude and the drop of air density. However, the parasite drag is reduced because the air density is almost 26% lower than at sea-level. The total power required in high forward speed is thus reduced.

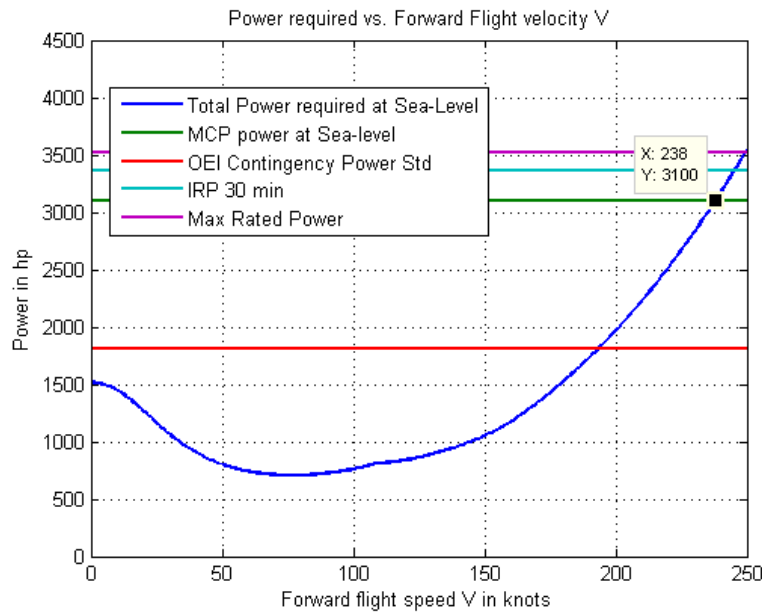


FIGURE G-3: POWER CURVE AT SEA-LEVEL FOR MISSION 2

For mission 2, the maximum takeoff gross weight is 15,020 lbs and the power curve at sea-level is presented in Figure G-3. The amount of power required in hover is greater than mission 1 after takeoff

because the weight of the vehicle is bigger in this case. Since mission 2 represents the maximum takeoff gross weight, it can be seen on this curve that the hover capability is preserved at sea-level when one engine is inoperative (OEI). Figure G-4 shows the same configuration at maximum takeoff gross weight and in military Hot Day conditions. For the same reasons, the induced power in hover is higher than at sea-level but the total power required in forward flight is reduced mainly because the parasite power is proportional to the air density.

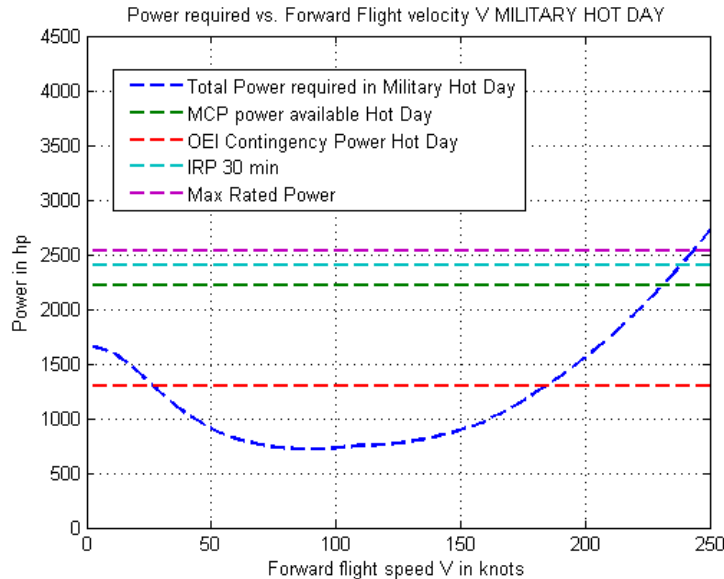


FIGURE G-4: POWER CURVE FOR MISSION 2 IN MILITARY HOT DAY CONDITIONS

## G.2. Speed performance with All Engines On (AEO)

### Maximum cruise speed

The maximum cruise speed is determined by the engines limits at MCP. In Figure G-1, the maximum cruise speed for mission 1 corresponds to the intersection of the MCP available and the power required, leading to a max speed of 239 knots at sea-level. This speed allows Odyssey to perform the inbound leg of 225 nm in less than 56 minutes. It is important to realize that the inbound leg is performed almost at the takeoff gross weight because the fuel consumed to reach the accident area almost corresponds to the extra payload carried by Odyssey during this cruise segment. In military Hot Day conditions, it was necessary to meet the Golden Hour rule as well and the maximum cruise speed at MCP is 234 knots, which approximately corresponds to an hour of flight to perform the inbound leg.

### Dash speed

The dash speed of Odyssey is defined as the maximum speed that the vehicle can reach using IRP for 30 minutes. At sea-level the dash speed is 246 kts at maximum takeoff gross weight.

### Best endurance speed

The best endurance speed is required to optimize Odyssey's performance in loiter during mission 1. A higher endurance corresponds to a larger area of search and rescue. The endurance is defined as the hours of loiter per pound of fuel. Loiter is performed at the forward speed where power consumption is minimum. In case of mission 1,  $V_{be}$  corresponds to 70 knots at sea-level and 82 knots in military Hot Day conditions. For missions 2 and 3,  $V_{be}$  corresponds to 77 knots at sea-level and 89 knots in military Hot Day conditions.

### Best range speed

The best range speed corresponds to the speed maximizing the specific range of the vehicle. The specific range is the distance traveled per unit fuel and is similar to miles per gallon on automobiles. Since the power required by the helicopter as a function of forward speed is known, along with the fuel consumption of the engine as a function of horse power, it was possible to compute the fuel flow rate at any given forward speed. The maximum specific range corresponds to the inverse of the slope of a tangent to the power required curve. Using Figure G-1, Figure G-2, Figure G-3, and Figure G-4, the best range speeds were identified. In case of mission 1,  $V_{br}$  corresponds to 129 knots at sea-level and 137 knots in military Hot Day conditions. For missions 2 and 3,  $V_{br}$  corresponds to 134 knots at sea-level and 144 knots in military Hot Day conditions.

### Absolute ceiling and service ceiling

When the power required equals the power available then the altitude of absolute ceiling is reached. It was possible to iterate on the altitude to find the absolute and service ceiling. The altitude corresponding to a rate of climb of 100 ft per minute corresponds to the service ceiling. Both ceilings can be identified if we plot the rate of climb of the helicopter in hover as a function of the altitude as shown in Equation 27 [41].

EQUATION 27

$$RoC = 60 \times 550 \frac{E_{PW}}{W}$$

The rate of climb in hover at MCP is shown in Figure G-5. The rate of climb was calculated using only the excess power available. This is the vertical rate of climb at zero forward flight speed and AEO. In this case, the maximum vertical rate of climb at sea-level for the maximum takeoff gross weight was found to be 3,479 ft/min and drastically drops to 988 ft/min in military Hot Day conditions.

The excess power calculation gives access to the service ceiling, which corresponds to the altitude where the vertical rate of climb is 100 ft/min. At standard temperature, the service ceiling of Odyssey is 19,500 ft. However, in hot day conditions, the service ceiling is reduced to 11,650 ft.

The absolute ceiling corresponds to the maximum altitude that the vehicle can reach by moving vertically. The absolute ceiling is reached when the vertical rate of climb is equal to zero. At standard temperature, the absolute ceiling of Odyssey at maximum takeoff gross weight is 20,100 ft and this absolute ceiling is reduced to 12,200 ft in Hot Day conditions.

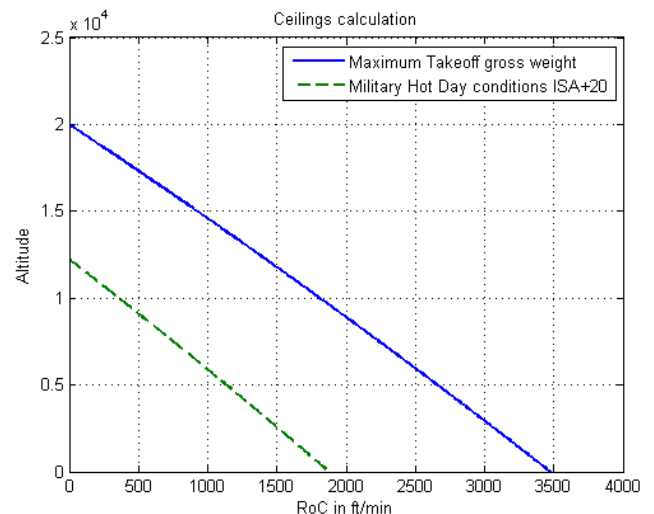


FIGURE G-5: ROC AT MAXIMUM TAKEOFF GROSS WEIGHT

## G.3. Engine failure condition performance

### One Engine Inoperative (OEI) performance

With One Engine Inoperative (OEI), the maximum contingency power of the only operative engine left is required. The 2 ½ min OEI power is 1,809 hp at sea-level. It can be seen in Figure G-1 and in Figure G-3 that Odyssey can hover in OEI at sea-level conditions, which is a critical safety parameter if Odyssey operates from an aircraft carrier for example.

However, the HOG6 6K95 capability is lost when one engine is inoperative, requiring an emergency landing in this case. If hovering in ground effect with the emergency engine rating is not possible, the rate of descent in this case can be evaluated by using Equation 28, leading to a rate of descent of 3,200 ft/min.

This rate of descent is dangerous and an emergency landing might be compromised in this case because the pilot will certainly run out of time to identify a landing area and perform a safe maneuver. In this case an autorotation maneuver is recommended.

EQUATION 28

$$V_d = \frac{33000 \times rhp}{W}$$

**Autorotation maneuver and AI index**

The total kinetic energy stored in the rotor is determined by the moment of inertia of the entire system composed of main rotors, pusher prop, shaft, and so on. The time available before the rotor completely stops is estimated as initial kinetic energy of the entire system divided by the torque times rotational speed. Actually a larger moment of inertia is needed to give the pilot some time to enter into autorotative mode. Since the torque must be as small as possible, the pilot will reduce the collective pitch as much as possible.

Once the autorotative mode is entered, the power is supplied by the air to the main rotors, as in a wind mill. The RPM stabilizes and the rate of descent is roughly given by Equation 28. However, the rate of descent will be minimum around 70 knots since the power required is minimum at this forward flight speed.

Deadman's curve [52] shows that two flight regimes must be avoided. The first one corresponds to a low velocity and a large height. The power consumption is there too high. An emergency landing is possible using vortex ring state but the pilot must carefully trade potential energy with kinetic energy. The second flight regime to avoid corresponds to a high forward flight velocity and a low altitude. In this case, a high speed impact with the ground is very likely and the pilot must pull out first to gain some altitude and trade kinetic energy for potential energy.

The AI is calculated using Equation 3 page 10. In hover, the tip speed is 650 ft/s, the blade moment of inertia is 650 slug/ft<sup>2</sup> and the rotational speed is 32.5 rad/s. In the case of maximum take off gross weight and at sea-level, the AI is evaluated at 183 and Figure G-6 shows the comparison of Odyssey with existing vehicles. The autorotation performance is better than the Blackhawk and bigger helicopter like the CH-53 Stallion. Increasing the AI would require an increase of the kinetic energy of both rotors. This can be achieved through higher tip speed or higher mass distributed at the tip of the blade, but this would increase the overall mass of the rotor system. It is also possible to calculate the time that the stored kinetic energy could supply the power required to hover before stalling. This is the estimated time allowed to the pilot to recognize engine failure and disengage the shaft to enter autorotative maneuver. This parameter is given by Equation 29 and is used by Prouty [38]. Typically, this parameter is supposed to be between 1.5s and 2s and Odyssey meets this requirement.

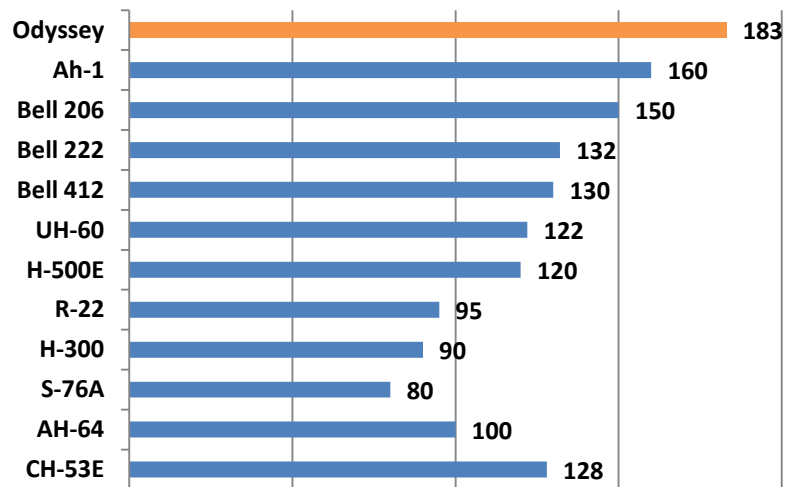


FIGURE G-6: AUTOROTATIVE INDEX DERIVED FOR SEVERAL HELICOPTERS AND ODYSSEY

EQUATION 29

$$t_{k/e} = \frac{I_R \Omega^2}{2(2 \times rhp)} = \frac{AI \times W}{2 \times rhp \times 550} = 1.66 \text{ s}$$

### G.4. Payload Range diagram

The Range and endurance mission can be calculated using the power required chart to determine the maximum range speed in cruise  $V_{br}$  (this is the speed corresponding to the tangent with the power required curve) and the maximum endurance speed  $V_{be}$  (this is the speed corresponding to the maximum excess power). Then using the Breguet's equation we can compute the maximum range of the helicopter using Equation 30 and the maximum endurance using Equation 31.

EQUATION 30

$$Range = \frac{V_{br} T}{rhp \times SFC \times N_{eng}} \ln \left( \frac{1}{1 - \frac{W_f}{W}} \right)$$

The payload range diagram is shown in Figure G-7. It can be seen that the military Hot Day conditions decrease the maximum range of the helicopter at a given payload weight. The limits were drawn at maximum TOGW (=15,020 lbs). It is possible to calculate the maximum range of Odyssey when extra fuel instead of payload is carried in the cabin. This is the range of deployability of the vehicle. The maximum fuel weight in this case corresponds to the maximum fuel tank capacity (2,122 lbs) and an extra fuel weight of 3,600 lbs in the cabin when the weight of the additional fuel tanks is taken into account. In this case the maximum fuel weight available is 5,722 lbs. At the maximum TOGW, the maximum range is 1,552 nm (2,874 km). In other words, Odyssey can be deployed in less than 12 hours anywhere on the US territory after or in prevention of a natural disaster.

The endurance of Odyssey is calculated at max TOGW. At sea-level the endurance is estimated at 4.01 hrs for a best endurance velocity of 77 knots. In military Hot Day conditions, the endurance is estimated at 3.94 hrs for a best endurance velocity of 89 knots. It can be seen that the Hot Day conditions impose a higher speed to maximize the endurance of Odyssey.

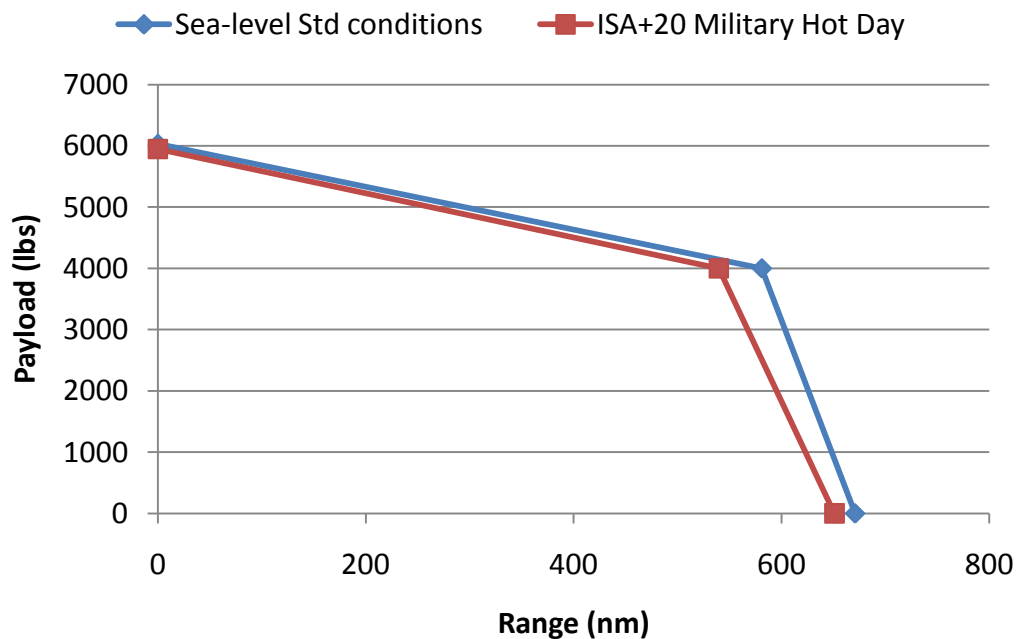


FIGURE G-7: PAYLOAD RANGE DIAGRAM AT MAX TOGW

EQUATION 31

$$SpecificRange = \frac{V_{be}}{SFC \times rhp \times N_{eng}}$$

$$Endurance = \frac{SpecificRange \times W_f}{V_{be}}$$

## G.5. Performance summary

TABLE G-1: ODYSSEY PERFORMANCE SUMMARY

Max TOGW	Mission 2	15,020 lbs
Max Fuel required	Mission 1	2,122 lbs
MCP available	Std	3,100 shp
	ISA+20	2,244 shp
AEO at max TOGW		
Max cruise Speed	Std	239 knots
	ISA+20	234 knots
Dash speed	Std	246 knots
Best endurance Speed	Std	77 knots
	ISA+20	89 knots
Best range Speed	Std	134 knots
	ISA+20	144 knots
Vertical rate of climb	Std	3,479 ft/min
	ISA+20	988 ft/min
OEI at max TOGW		
HOGE	Std	Yes
	ISA+20	No
AI	N/A	15.3
Ceilings at max TOGW		
Service ceiling	Std	19,500 ft
	ISA+20	11,650 ft
Absolute ceiling	Std	20,100 ft
	ISA+20	12,200 ft
Range/endurance at max TOGW		
Max Range	Std	642 nm
	ISA+20	623 nm
Max Endurance	Std	4.0 hrs
	ISA+20	3.94 hrs
Deployability (max fuel)	Std	1,552 nm

## Appendix H WEIGHT BREAKDOWN AND MATERIAL SELECTION

In the Georgia Tech IPPD methodology depicted in Figure 0-1 page 1, the revised vehicle system and detail design is an input to the cost analysis. The empty weight breakdown can be calculated using the CATIA model created and the historical trends for coaxial helicopters. The empty weight breakdown is presented in this chapter and a detailed calculation for the fuel system has been provided as an example.

### H.1. Weight calculation of the fuel system

According to the performance section, mission 1 SAR requires the most fuel available in the internal tanks.

As a consequence, this mission sized the fuel tanks and the fuel pumps. Considering a fuel weight of 2,120 lbs to perform the mission, the JP-5 fuel density is 6.8 lb/gal [28]. The equivalent total volume of the tanks is 311 gallons. It is not expected to see a significant change in the fuel density by 2030. In addition, the JP-5 is the standard fuel used by most civil and military helicopters and this value seems reasonable for our calculations. Historical statistical data have led to an extrapolation of the weight of the fuel system for helicopters. Using Equation 32 it is possible to evaluate the weight of this system, where  $N_t$  is the number of tanks,  $N_{eng}$  is the number of engines,  $V_{fus}$  and  $V_{aux}$  is the mission fuel volume required (in gallons).

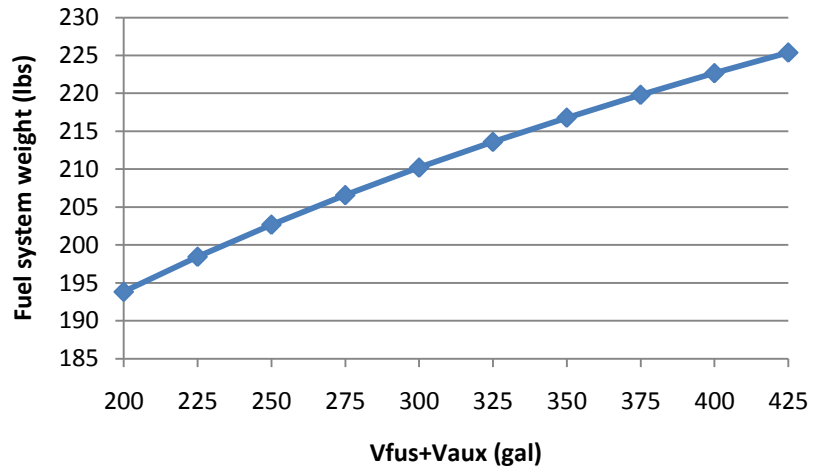


FIGURE H-1: ODYSSEY FUEL SYSTEM WEIGHT CALCULATION

EQUATION 32

$$W_{FuelSystem} = 36(N_t)^{0.5}(N_{eng})^{0.4}(V_{fus} + V_{aux})^{0.2}$$

For our vehicle Figure H-1 shows the calculation of the fuel system, composed of the tanks and the fuel pumps. In this case the fuel system weight was evaluated to 229 lbs.

### H.2. Material selection



FIGURE H-2: ODYSSEY GEAR HOUSING IN GRAPHITE-EPOXY MATERIAL

The goal for the material selection of Odyssey was to exploit advantages of the lightness and strength of composites for structures of priority while maintaining the cost efficiency by using metal alloys when applicable. The empty weight breakdown is presented in this section. After several iterations in the IPPD design loop, CIRADS converged on an estimated empty weight of 8,470 lbs. This value was essentially obtained by using historical trends and data regressions. However, some components were further examined to evaluate with a great level of confidence the weight. The material selection was a fundamental part for the calculation of the empty weight. Composites were extensively used to reduce the overall weight. However, the major weakness of composite materials is their overall

bad behavior in the plastic region. The limit structural load of Odyssey is limited by this extensive use of composite materials. The main rotor blades and the pusher blades are designed in composites. The gear housing, as shown in Figure H-2, has been designed in Graphite-Epoxy for higher strength and weight savings. However, the Graphite-Epoxy is expensive and presents a lower resistance to impacts. The gears are designed in cast iron to reduce vibrations by damping. This solution presents a good wear resistance and a cheap alternative, though low tensile strength and ductility.

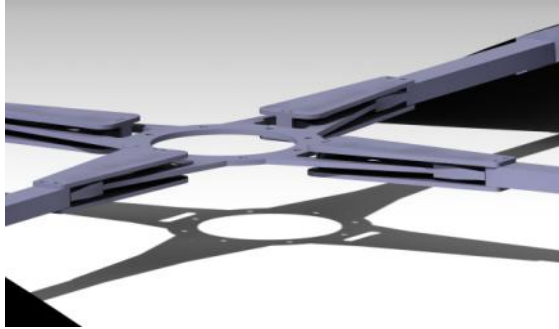


FIGURE H-3: STARFLEX OF ODYSSEY'S MAIN ROTOR

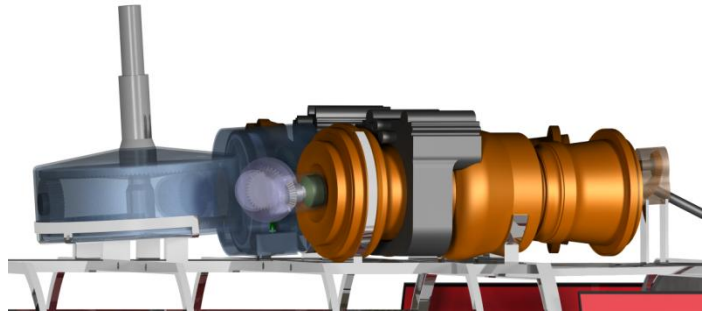


FIGURE H-4: ODYSSEY ENGINE AND TRANSMISSION MOUNTS

The hub and the starflex shown in Figure H-3 are designed in titanium alloys, which are light and resistant to corrosion in parts exposed to humidity and rain. The spars of the starflex are composed of Graphite-Epoxy and the ribs are designed in graphite to save weight. Finally the skin of the blades is composed of fiberglass because this material is light, durable and affordable. The hubs for the main rotors and pusher propeller were made of Nomex Honeycomb which has lower weight, higher strength and corrosion resistance. The main rotor blades and the pusher propeller blades were made of three subparts: spars, ribs, and skins. Spars are made of graphite-epoxy and ribs were made of graphite. Figure H-4 shows the engine and transmission mounts. The primary structure of the landing gears is composed of stainless steel AM-350 to sustain high dynamic and static loads. In addition, the steel presents a high resistance to corrosion and is relatively cheap, though heavier than other materials. For cost effectiveness and strength, the primary cabin structure was designed in aluminum alloys to resist corrosion and protect the pilots in case of a crash. However alloys are generally difficult to weld during the manufacturing process. Graphite-Epoxy composes the majority of the primary structure and the bulkheads. Figure H-5 shows the entire primary structure along with the swivel doors, the fuel tanks, the duct frame and the pusher propeller transmission shaft.

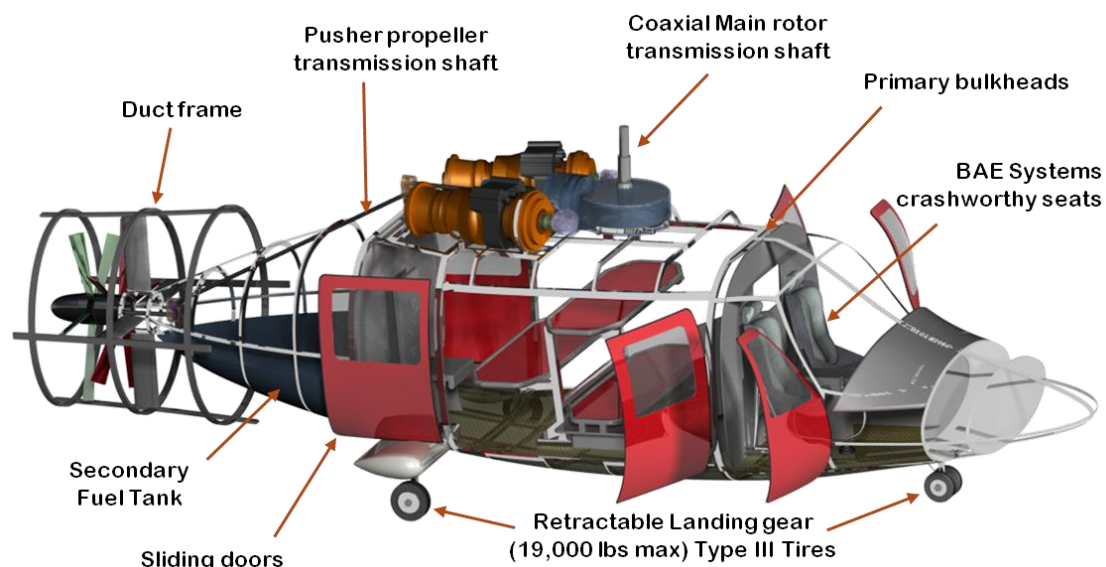


FIGURE H-5: ODYSSEY PRIMARY STRUCTURE

The doors are designed in fiberglass for the same reasons mentioned previously in the blade section. Fiberglass requires a longer manufacturing time and might increase the manufacturing costs. The duct fan is composed of graphite filament-wound and presents strength to support the horizontal stabilizers and transfer the aerodynamic loads to the entire structure as shown in Figure H-6.

The fuselage section of Odyssey extensively utilizes composites because of the need for a crashworthy cabin and safety standards. Table H-1 reports the material selection of the important components of the fuselage and the corresponding material's advantages. The internal structure through the cabin was made of composites to ensure high safety standards and crashworthy index. The rest of internal structure was made of lithium–aluminum alloy to efficiently reduce the manufacturing as well as maintenance costs.

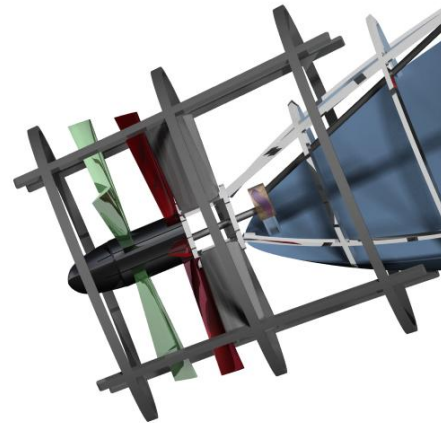


FIGURE H-6: PUSHER STRUCTURE AND DUCT FRAME

The skin of the fuselage was divided into two sections for material selection purposes: 1) before the engine i.e. nose to cabin, and 2) after the engine. A highly corrosion resistant composite was picked for the front to ensure safety. The aft engine part of the fuselage contains a thermally resistant skin so that structural damages due to heat effects of combustion and exhaust are minimized. The rest of the fuselage section uses typical selection of helicopter materials such as graphite filament-wound for the tail cone, fiberglass for doors, and steel alloy for landing gear.

TABLE H-1: MATERIAL SELECTION FOR THE FUSELAGE SECTION

Component	Material	Advantages
Internal Structure (cabin)	Graphite-Epoxy	Corrosion resistant, lighter
Internal Structure (other)	Lithium-Aluminum Alloy	High strength, low weight
Bulkheads	Graphite-Epoxy	High strength, low weight
Skin – Front (nose-cabin)	Carbon fiber and Nomex honeycomb sandwich	Corrosion resistant, lighter, ease of manufacturing
Skin - Aft engine	Kevlar fabric	Thermally stable, abrasion and impact resistant
Tail cone	Graphite filament-wound	High strength, low weight
Doors	Fiberglass	Light, durable and cost-effective
Landing Gear	Steel alloy (4340)	High strength, corrosion resistance, low cost

### H.3. Stealth mode

Although no specific requirements for helicopter's stealth mode were defined in the RFP, some easily employable techniques were investigated to explore the possibilities of developing a military version of Odyssey. The recent success of UH-60's stealth mode operation heavily influenced the development of this optional characteristic of Odyssey.

#### Exhaust IR suppression

The main source of locating and attacking (Ex: missile lock-on) a helicopter is the high temperature engine exhaust. An infrared (IR) suppression system could be integrated into the airframe that would reduce the temperature of exhaust gases and thereby increase the survivability of the helicopter. The suppression systems could be directly connected to the two exhaust nozzles on either side of the tail boom. The exhaust from the twin engines could be supplied to these systems which would efficiently mix the high temperature exhaust gases with atmospheric air and thereby lower the temperature. This low temperature

mixture could be expelled resulting in a lower IR signature for the helicopter. This technique was implemented on RAH-66 Comanche and later versions of UH-60 Blackhawk.

### Radar signal absorption

Another source of locating a helicopter is the radar signal reflection. Typical helicopters reflect a large number of the incoming radar signals resulting in immediate location of the vehicle. Modern stealth implementations use several radar-absorbent materials (RAMs). One of the cost efficient and highly effective techniques is to paint the helicopter with a wave absorbent paint called the “iron ball paint”. The paint consists of tiny spheres coated with ferrite. The cast radar waves cause oscillations in these molecules which results in conversion of the radar energy to heat. This heat is stored and released by the helicopter. Through this method the amount of reflected radar waves is significantly reduced and the helicopter couldn’t be easily located.

### H.4. Empty weight breakdown

Based on the material selection and the historical trends, it was possible to compute the empty weight breakdown of Odyssey. The Rotary Wind Structures Technology (RWST) program [29] can be used to estimate the weight savings due to the utilization of smart materials and more efficient design tools by 2025.

The empty weight breakdown is presented in Figure H-7. It can be seen that the primary structure and the main rotor represent the biggest contributions to the empty weight, followed by the engines and the auxiliary propulsion. The manufacturing variation was estimated at 50 lbs and approximately 140 lbs of extra components were taken into account. The AVC system weight could be estimated at 300 lbs [6]. The AC and anti-ice systems are electrical and hydraulics is significantly reduced to 51 lbs for landing gear electro-hydraulic actuators. The technology of fly-by-wire was selected to increase the weight savings.

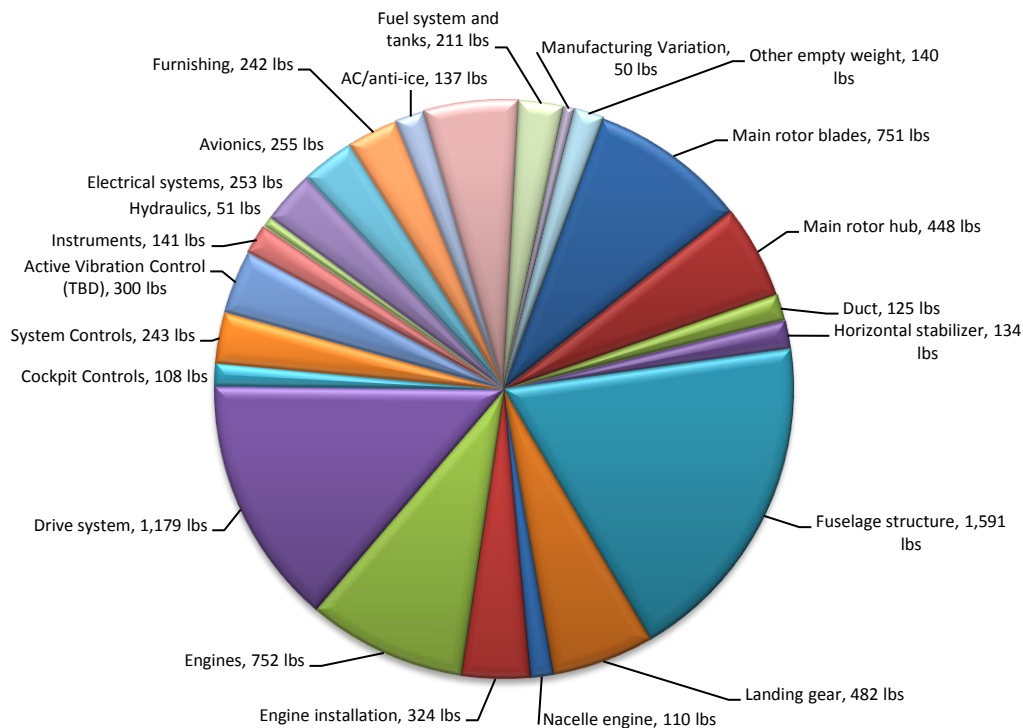


FIGURE H-7: ODYSSEY EMPTY WEIGHT BREAKDOWN

## Appendix I YAW CONTROL AND GURNEY FLAPS

Coaxial helicopters utilizing differential collective for yaw control are known for having poor yaw control characteristics in low power or autorotative conditions. When the rotors are in a zero-lift condition, differential collective increases drag on both the upper and lower rotors, which results in zero net yaw control torque. In the case of autorotation, the main rotors drive the transmission resulting in a torque reversal through the main rotor shafts. Without the use of any special control system rigging, the application of differential collective during an autorotative maneuver results in a reversed control response of the aircraft. To demonstrate this phenomenon, Figure 1 shows the effect of differential collective during a high power condition. The left side of Figure I-1 shows a high power condition with no differential collective. The right side of Figure I-1 shows the same flight condition after the application of differential collective. The result is an unbalanced torque through the main rotor shafts producing yaw acceleration of the aircraft.

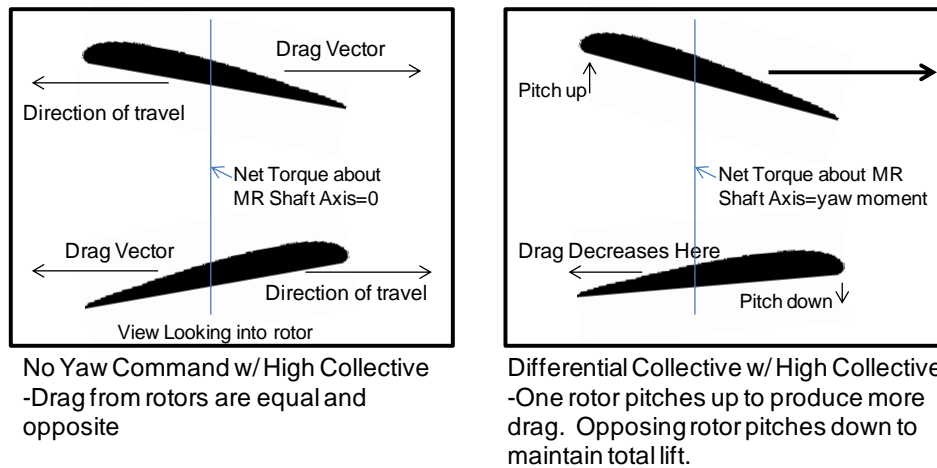


FIGURE I-1: DIFFERENTIAL COLLECTIVE IN HIGH POWER STATE

Figure I-2 shows a flat pitch condition, where the rotors are in a low power state creating zero lift. The application of differential collective in this case results in a mutual increase in torque across both the upper and lower rotors. As both rotors experience an equal and opposite increase in torque, the net result is little or no yaw control torque applied to the aircraft.

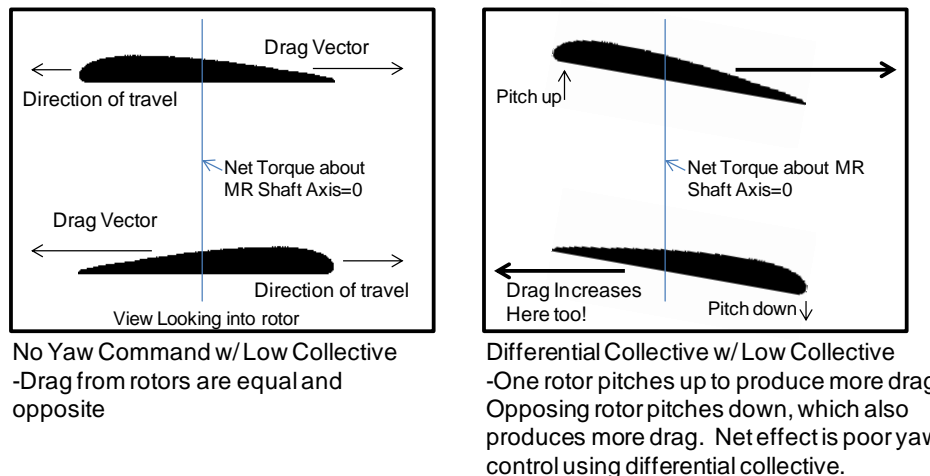


FIGURE I-2: DIFFERENTIAL COLLECTIVE IN LOW POWER STATE

Some coaxial helicopter designs attempt to supplement differential collective as a means for yaw control by adding rudders to the vertical tail sections. The problem with rudders is that they only provide yaw control during forward flight. If a pilot must depend on the rudders to provide yaw control during an autorotative descent, the pilot must also be concerned with maintaining sufficient forward velocity to avoid losing such control. While the combination of differential collective and rudder control is a feasible solution to the coaxial helicopter's inherent yaw control problem, it still leaves open the possibility of entering a zero yaw control state.



FIGURE I-3: VR-7 AIRFOIL WITH DOUBLE GURNEY  
(X/C=0.9, H/C=0.025)

A unique method of yaw control is proposed for the Odyssey that utilizes small actuated gurney flaps near the trailing edge on both the upper and lower surface of the main rotor blades, as shown in Figure I-3.

Gurney flaps have been studied in recent years for their application as an active rotor control mechanism [50]. This unique active control strategy has been shown to be successful in reducing four-per-rev vibratory loads by up to 83% [32]. The benefits of implementing gurney flaps in the Odyssey, as shown in Figure I-4, are twofold. For conditions where differential collective is sufficient for yaw control, the gurneys can be used to reduce noise and vibrations associated with high speed flight. For low power and autorotative conditions where differential collective fails, the double sided gurneys will be used to control yaw by creating differential rotor drag.

Simultaneous actuation of the upper and lower gurney flaps on one of the two main rotors will increase the profile drag of the rotor disk resulting in yaw control torque. This process requires that the precise dimensions of the actuated gurneys are such that the aerodynamic lift and pitching moment coefficients are not significantly disturbed while the drag coefficient is increased with increased actuation. Since the utilization of gurney flaps for yaw control is only required during low power and reversed autorotative states where the rotor lift is less critical, minor disturbances to the lift and pitching moment coefficient may be acceptable. In high power states where rotor lift is critical, yaw control from differential collective is preferred.

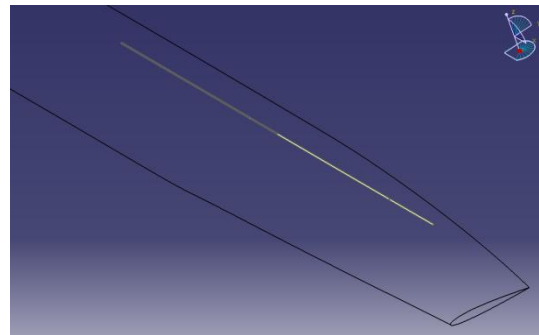


FIGURE I-4: GURNEY FLAPS ON THE MAIN ROTOR BLADE UNDER CATIA

To provide sufficient yaw control, the gurney flaps must increase the profile drag of the main rotor disk. The aerodynamics of actuated flaps is such that an increase in drag is experienced with an associated increase in lift. The primary objective of the double actuated gurney flaps is to increase drag while maintaining lift, rather than improving lift. Based on an aerodynamic study of trailing edge gurney flaps with a height/chord of 2%, the drag coefficient was found to increase by more than a factor of 2 for a constant lift [27]. This study was conducted for a single gurney with the objective of affecting the lift performance of the airfoil. It is assumed that the implementation of a double sided gurney with higher height/chord actuation and the objective of increasing drag can increase the airfoil drag by as much as 5. To demonstrate that double sided gurney flaps can provide sufficient control force for yaw control, a dynamic simulation was performed on a dummy mass with yaw inertia representative of the Odyssey design. First, the baseline profile rotor torque was found to be 1,700 ft-lbs per main rotor using Equation 33 and Equation 34:

EQUATION 33

$$Cp_0 = \frac{\sigma C d_0}{8} (1 + 4.6\mu^2)$$

EQUATION 34

$$T = C_{pp}A\Omega^2R^3$$

To represent the full yaw control torque capability of the double sided gurney on a coaxial helicopter, a maximum control torque of  $5 \times 1,700 - 1,700 = 6,800$  ft-lbs was imposed (subtracting 1,700 ft-lbs for the counter torque of the opposing rotor). This dummy mass was controlled by a dummy control system. Control gains were adjusted so that the dummy mass responds as quickly as possible to a 10 degree yaw heading change with no yaw heading reversal. The results are shown in Figure I-5. Comparing these results to the ADS-33 Moderate Amplitude Heading Change requirements, shown in Figure I-6, reveals that the peak yaw rate of 6.15 over a yaw heading change of 10 deg is sufficient to meet the Level 2 requirement.

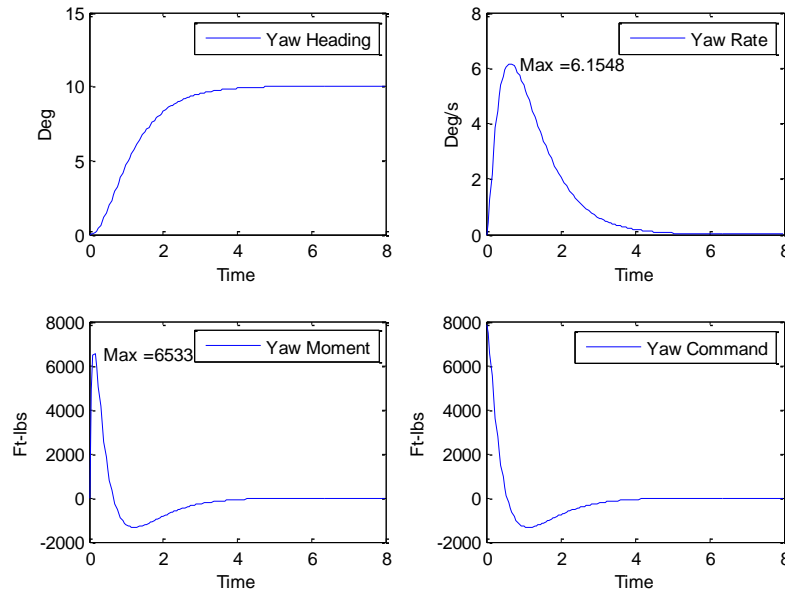


FIGURE I-5: DYNAMIC SIMULATION OF GURNEY FLAPS YAW CONTROL POWER

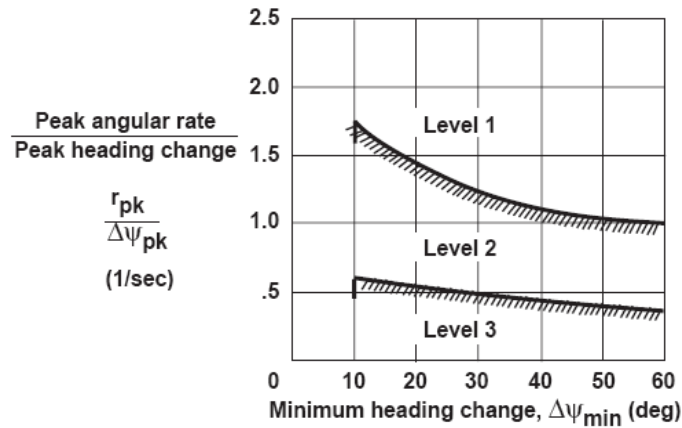


FIGURE I-6: ADS-33 REQUIREMENTS FOR MODERATE AMPLITUDE YAW HEADING CHANGES

## Appendix J DRIVE SYSTEM

### J.1. Requirements

The main requirements of the drive system design was to obtain a optimum design to slow down the coaxial main rotors and also produce power to a translation thrust pusher propeller. The drive system is required to step down the shaft speed from the two engines through different stages while changing the axis of rotation.

### J.2. Conceptual Design

To accomplish these requirements, a few concepts were analyzed, mainly to identify the best option for speed shift. Two-speed designs are less complex compared to variable speed designs but possess inherent power interruptions during speed ratio transition. Rotorcraft application requires positive and continuous power transfer & variable speed. The major portion of a flight mission is hover and cruise. Transition between the above operation points is a minor portion of the flight mission. Two-speed designs can be adaptable to be quasi- variable through variable transition assist, which may be either external powered (controller) or internally take-off driven (variator - traction drive or power electronics motor-generator system). Speed range changes for CVTs need to be computer controlled sensing both transmission and engine speed/power.

For this design a planetary CVT was selected. The Differential Planetary Drive, shown below in figure, capitalizes on the output variability of a dual-input to single-output planetary differential using one input to serve as a controller.

Primary power is input to the sun gear, output power is transferred through the carrier, and speed variation is achieved by varying the speed of a special ring gear from zero speed to required speed with a variable speed controller device/system. The ring gear is special in that it has both an internal and external teeth contained within an integral ring. As depicted, ring gear speed is varied from zero to the required speed by a speed controller driving the external teeth. The controller ratio may be varied in design permitting selection of the optimal power and speed range. As depicted, the controller rotates in the opposite direction of the primary input but may be the same if an idler is employed. The speed controller may be a variety of possible devices either externally powered and controlled or take-off driven from the transmission power input shaft. The power take-off may be a continuously variable speed device as suggested elsewhere for the other configurations. The main disadvantage is the power loss to spin/control the ring speed. This loss is overcome by using a motor to add-in power to the pusher propeller module. This hybrid system works in the following manner. The ring gear is held stationary and the pusher propeller is declutched for hover and low speed flight. The propeller clutch is engaged as speed increases and the propeller supplements the main rotors in forward thrust. After a certain forward speed, the main rotors are almost completely offloaded of forward thrust and slowed down to sustain high forward speed flight without reaching critical tip speeds. The main rotors are slowed down by disengaging the ring gear clutch and using an electric variator. This variator works as an electric generator or motor based on ring gear speed variation from its ideal operating rpm. The generator supplies power to a storage system, the power from which can be reused by the motor in the propeller module.

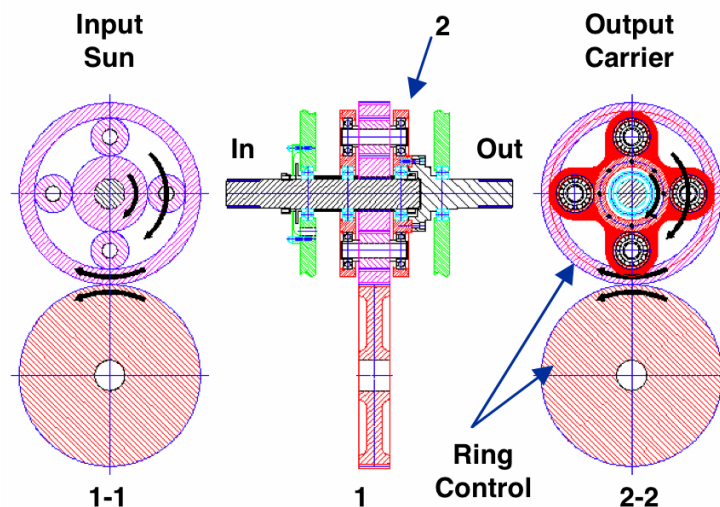


FIGURE J-1: CONCEPT OF PLANETARY CVT [3]

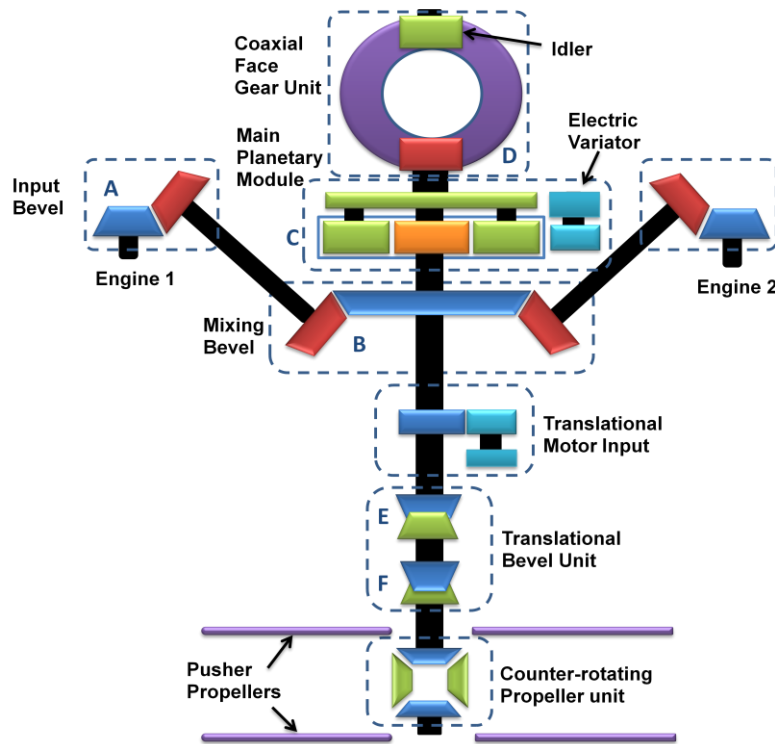


FIGURE J-2: TRANSMISSION SCHEMATIC

### J.3. Gear Train Sizing

The Gear train is sized for bending stress, contact stress and durability. The loading at each stage is calculated based on stage torque. Table J-1 shows the parameters that were used for the design.

TABLE J-1: TRANSMISSION DESIGN INPUTS

Engine Limits T700 GE 701C	SHAFT HP	POWER TURBINE RPM / %
Contingency Rated Power (CRP) (2.5 min. OEI)	1940	20,900/100
Maximum Rating (10 Min. dual)	1890	20,900/101
Intermediate Rated Power (IRP) (30 min dual)	1800	20,900/102
Maximum Continuous Power (MCP)	1662	20,900/103
<b>Odyssey Limits</b>		
Transmission Limits:	135% Single Engine (No time Limit)	
	120% Dual Engine, at or below KIAS (No time limit)	
	100% Dual Engine, above 80 KIAS (No time limit)	
Rotor Limits:	Max 310 RPM	
	Min 214 RPM	
Propeller Limits:	Max 3350 RPM	
	Min 3000 RPM	Clutched: 0 RRPMP

The gear stresses are calculated analytically using Lewis Bending-Stress formula and Hertz Contact-Stress formula. Appropriate AGMA correction factors are applied to account for reliability, safety and operability. The following integrated design methodology was used to design the drive system.

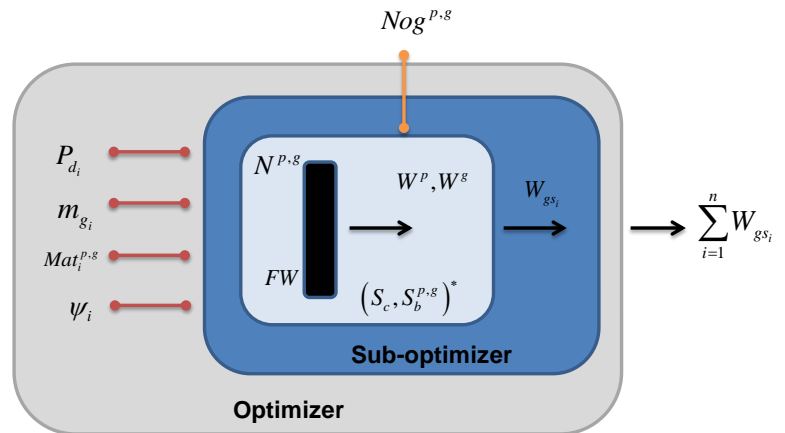
AGMA correction factors:

- 5000 flight hour TBO
- 75% application factor (included to account for typical mission power variation)
- 50% reliability factor (corresponding to 99.99% reliability rating)
- 42% reverse bending factor for planet gears

### J.4. Optimization Setup

A Genetic Algorithm (GA) was used to optimize the overall drive system. GAs are highly precise and efficient when working with discrete variables and their stochastic nature improve the possibility of a global optimum. Gear parameters are mostly discrete in nature making GA ideal for this design. ModelCenter (Phoenix Integration) was used to automate the genetic algorithm and the sizing program. A multiple elitist strategy with tournament selection was used in the GA to ensure the appropriate amount of exploration while improving convergence. The GA setup for the split torque and planetary designs are given in Table J-4. The other parameters that are of importance are those of the individual gearsets (P2). The gearset has to be optimized for number of teeth and face width. Number of teeth is discrete integer and face width is continuous but limited to  $12/P_d \leq FW \leq 16/P_d$

for spur gears and  $ocd/5 \leq FW \leq ocd/3$  by AGMA standard. A Full Factorial Sub-Optimizer (FFSO) is used for the P2 parameters. Full-factorial sweep is computationally expensive but guarantees a global optimum. The total combinations for FFSSO are reduced by discretizing the face width factor to 12 (10 for bevel) divisions (the 12 /10 divisions was a choice made using a convergence criteria of ~ 1%) and using a hunting ratio algorithm. The hunting ratio criterion eliminates the chance of any pair of gear teeth from coming into contact more or less frequently than the other pairs by eliminating  $N^{p,g}$  combinations with common factor. A penalty function was introduced to the objective function for a violation of allowable stresses. This is done because the FFSSO handles the stress constraints instead of the GA. The weight penalty term for exceeding bending stress limitations is given in Equation 35 and a similar formulation was used for contact stress. After run of a few experiments with different values of penalty parameter  $r_p$  values with P1 parameters that make the constraints active,  $r_p$  is empirically approximated to 5,000 and is applied only when a violation takes place. The penalty function enables the GA to search close to the constraint boundaries and obtain valid results from the sub-optimizer. The design is therefore hardly ever over-designed.



$$W_{g^{s_i}} = (Nog^p \times W^p) + (Nog^g \times W^g)$$

FIGURE J-3: OPTIMIZATION SETUP

EQUATION 35

$$w_p = r_p \times \frac{S_b - S_{ba}}{S_{ba}}$$

Table J-2 presents the optimization parameters for the design of the transmission. P1 parameters are handled by main optimizer and P2 parameters are handled by sub-optimizer. FFSSO stands for Full Factorial Sub-Optimizer and Nog is the number of similar gears in gear train.

TABLE J-2: OPTIMIZATION PARAMETERS

Parameter	Symbol	Type	Range	Optimizer	Rules
Diametral Pitch	$P_d$	$P_1$	1, 1.25, 1.5, 1.75, 2, 2.5, 3, 4, 5, 6, 8, 10, 12, 14, 16, 18	GA	High $P_d$ for initial stages and low $P_d$ for final stages
Helical Angle	$\psi$	$P_1$	0, 10,20,30	GA	0 for Bevel
Gear Ratio	$m_g$	$P_1$	(discretization tolerance of 0.01)	GA	Bevel: 2 - 6 Spur: 2 - 10, Planetary: 2- 10
Gear Material	$M$	$P_1$	AISI 9310, VASCO X2M, PYROWEAR 53	GA	
Number of Teeth	$N$	$P_2$	(range varies with $\psi$ )	FFSO	Hunting Ratio
Face Width	$FW$	$P_2$	Spur - $12/P_d \leq FW \leq 16/P_d$ Bevel - $ocd/5 \leq FW \leq ocd/3$	FFSO	

The individual parameters are broken down for the gearset and the GA in ModelCenter parses the  $P_1$  parameters ( $P_d$ ,  $m_g$ ,  $M$ ,  $\psi$  and dimensional constraints) of each stage to the overall sizing Matlab (Mathworks) program. Each concept has an overall sizing program which accesses generic sizing codes with the gearset information –  $P_3$  parameters (number of gears, pinion torque, bevel gear offset angle) in addition to  $P_1$  information.  $P_3$  parameters are dependent only on  $P_1$  and the transmission layout. Four generic codes that form the FFSSO were written for spur gears (with helix angle), bevel gears, face gears and planetary gears (with helix angle). These codes access material libraries, geometry factor tables and hunting ratio algorithms. The FFSSO performs a full factorial sweep of the number of teeth and face width through nested loops and returns the optimum combination of  $P_2$  given  $P_1$  and  $P_3$  parameters. The program returns the objective value with the addition of a penalty function if no feasible design space was provided by  $P_1$ .

TABLE J-3: GEAR MATERIAL PROPERTIES

Description	Units	AISI 9310	VASCO X2M	PYRO WEAR 53
AMS Spec		6265/6260		6308
Heat Treatment		C-H	C-H	C-H
Main Drive Application		Y	Y	Y
Accessory Application		Y		
High Temp. Application			Y	Y
Case Hardness	HRC	61	62	62
Core Hardness	HRC	37	40	40
Brinell Hardness	BH	632	647	647
Allowable Contact Stress	psi	244,897	250,145	250,145
Allowable Bending Stress	psi	52,102	51,990	51,990
Poisson's Ratio		0.292	0.3	0.292
Modulus of Elasticity		2.90E+7	2.964E+7	3.00E+6
Density	lb/in <sup>3</sup>	0.283	0.3	0.282

Since the design involves a planetary gear system, number of planets was included as a design variable. The maximum number of planets that can be accommodated in a design depends on the planetary gear ratio. An equation for calculating number of allowable planets was developed and is shown in Equation 36, where k is a correction factor for gear interference approximated to 0.95.

EQUATION 36

$$Nog_{pl} = \frac{k * \pi}{\sin^{-1} \left( \frac{(m_g - 2)}{m_g} \right)}$$

TABLE J-4: GENETIC ALGORITHM SETUP

Odyssey GA parameters			
Population Size	110	Convergence	
Selection Scheme	Multiple Elitist	Max generations	1000
Preserved Designs	12	Generations w/o improvement	20
	Discrete Variables	Continuous Variables	
Crossover Probability	1	1	
Mutation Probability	0.05	0.1	

### J.5. Optimization results

Table J-5 shows the drive system weight breakdown. The results of the optimizer are presented in Table J-6.

TABLE J-5: DRIVE SYSTEM WEIGHT BREAKDOWN

Drive System Weight	in lbs
Engine and Common Gearing	87.264
Main Rotor Gearing	222.0551
Propeller Gearing	25.44596
Controller and Motor	140
Battery	25
Housing	178.64
Shaft	349.5
Bearings and Sleeves	53.9
Lubrication Systems	21.12
Clutches	49.28
Miscellaneous	27.28
<b>Total</b>	<b>1179.5</b>

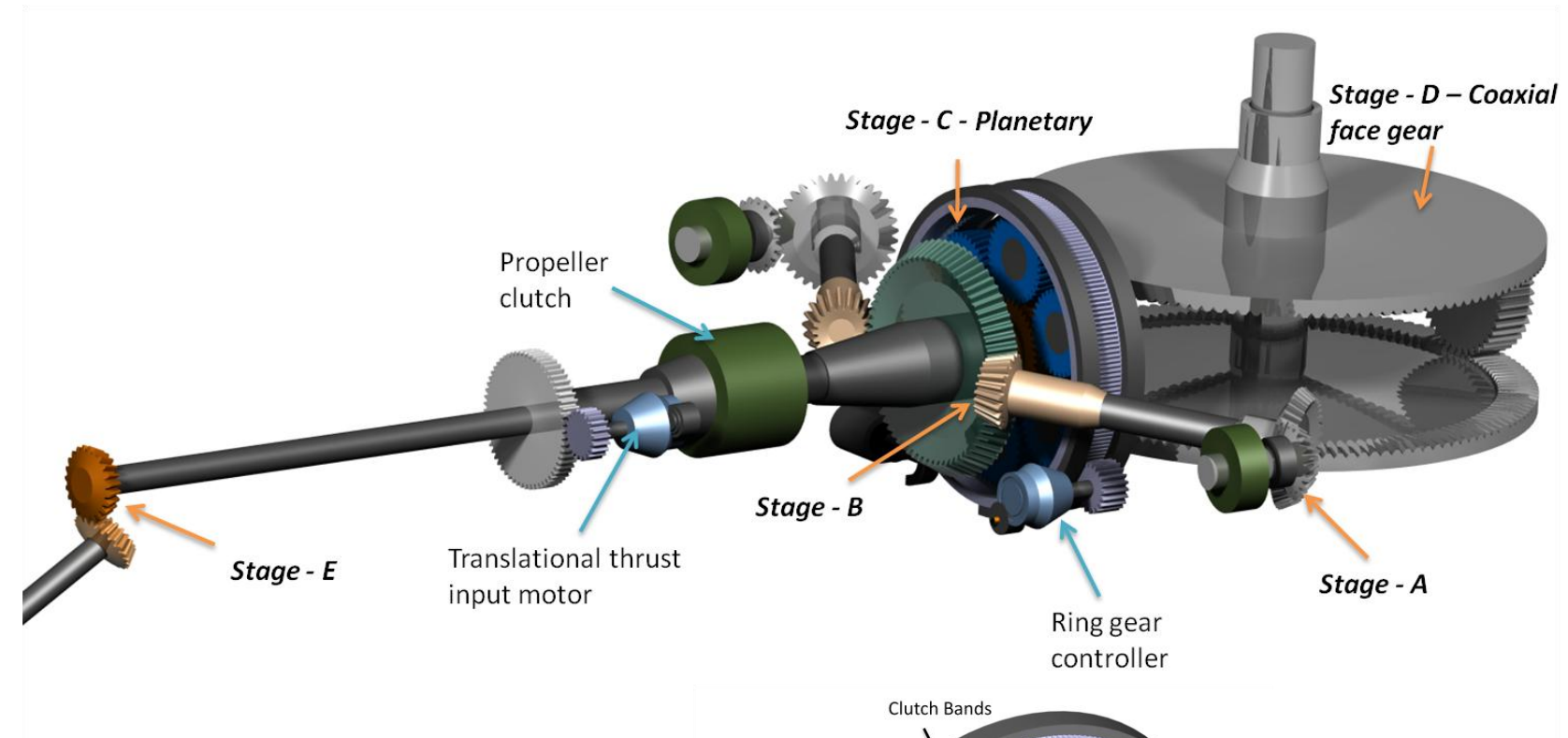
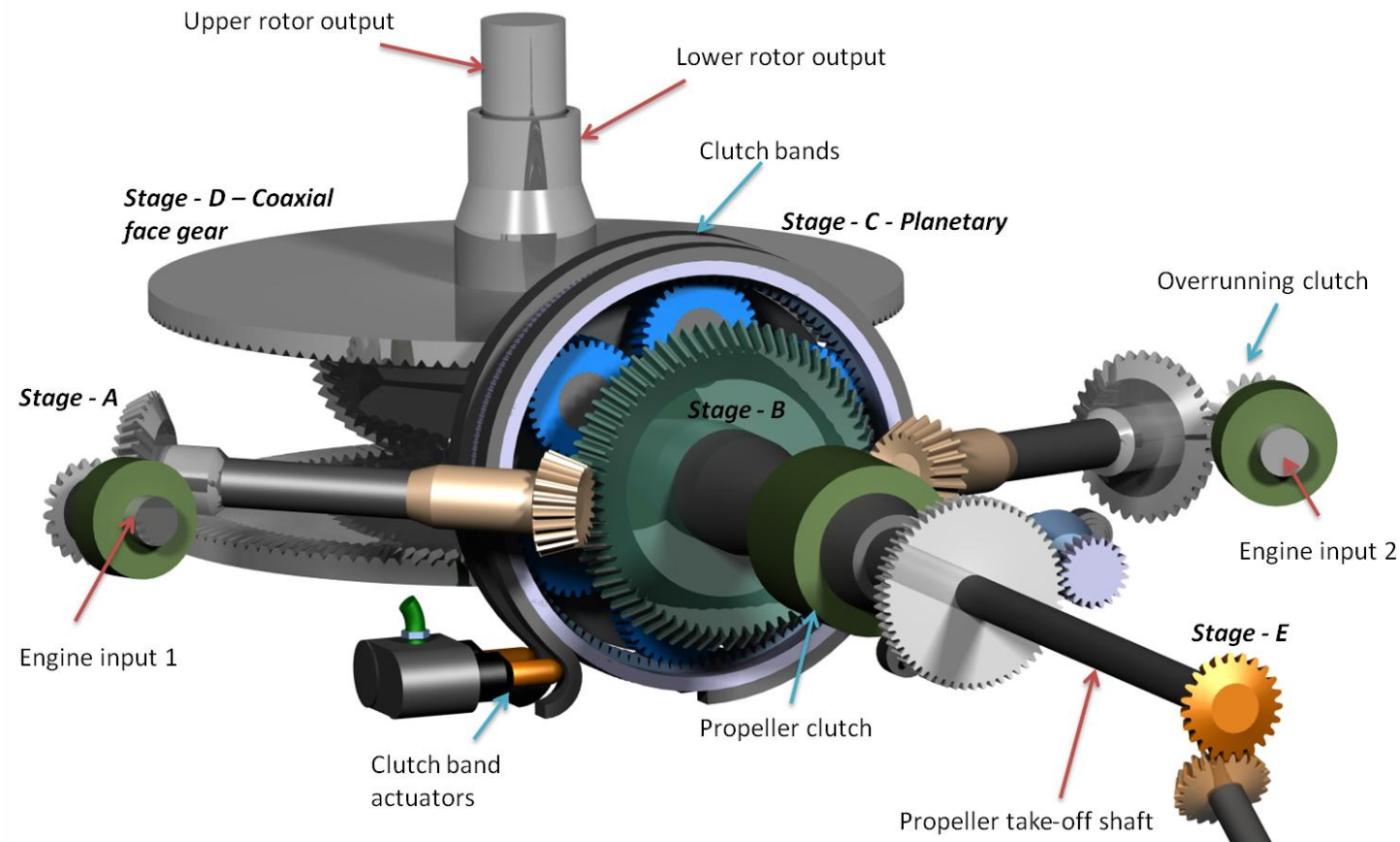


TABLE J-6: ODYSSEY TRANSMISSION RESULTS

Odyssey Transmission																		
Stage	Type	Pd	mg	F	$\phi$	$\psi$	weight		N	rpm	No.	weight	Material	Bending Stress (ksi)		Contact Stress (ksi)		
		$\text{in}^{-1}$		in	deg	deg	lbs					lbs		$S_b$	$S_{ab}$	$S_c$	$S_{ac}$	
A	Bevel	5	2.17	1.29	20	0	29.554	Pinion	23	20900	2	2.23	VASCOX2M	40.680	51.990	157.141	203.754	
								Gear	50		2	12.54	VASCOX2M	51.752	51.990			
B	Bevel	4	2.76	1.577	20	0	57.710	Pinion	21	9614	2	5.32	AISI9310	39.512	52.102	187.995	211.59	
								Gear	58		2	47.08	VASCOX2M	50.762	51.990			
C	Planetary	6	4	2.121	20	10	54.834	Sun	21	3480.9	1	7.97	Pyrowear53	45.896	51.990	181.478	206.621	
								Planet	21		1740	4	7.91	VASCOX2M	50.597			51.990
								Ring	63		0	1	7.36	VASCOX2M	33.089	51.990	130.756	208.694
								Carrier	-		870.2	-	7.84	AISI4340	-	-		
D	Face	5	2.81	2.4	25	0	167.221	Pinion	26	1 + 1 idler	13.6	VASCOX2M	41.394	51.990	175.383	207.545		
								Gear	73		309.9	2	69.99	VASCOX2M			37.843	51.990
E	Bevel	6	0.96	0.95	20	0	4.019	Pinion	23	3480.9	1	2.252	AISI9310	43.155	51.102	176.243	206.754	
								Gear	22		3639.2	1	1.766	VASCOX2M	43.282			51.990
F	Bevel	6	1.09	0.9	20	0	10.287	Pinion	23	3348	1	4.9	AISI9310	48.578	52.102	172.214	204.866	
								Gear	25		1	5.38	VASCOX2M	49.024	51.990			
G	Bevel	7	-	0.75	20	0	11.140	Pinion/Gear		6696.05	2	3.68	AISI9310	41.201	52.102	161.462	206.561	
								Idler			2	1.89	VASCOX2M	50.220	51.990			
Total							309.32											

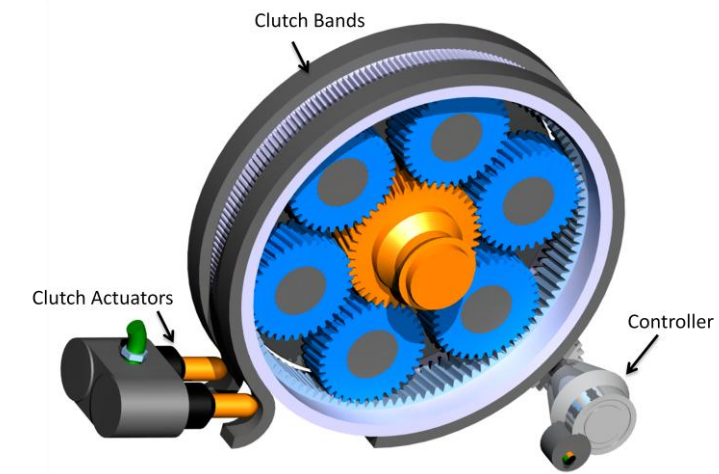


FIGURE J-5: RING GEAR AND CLUTCH BANDS ACTUATORS

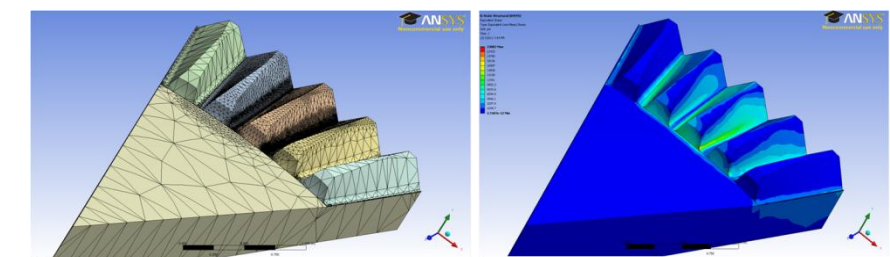


FIGURE J-4: FACE GEAR FINITE ELEMENT ANALYSIS IN ANSYS

## J.6. Controller design

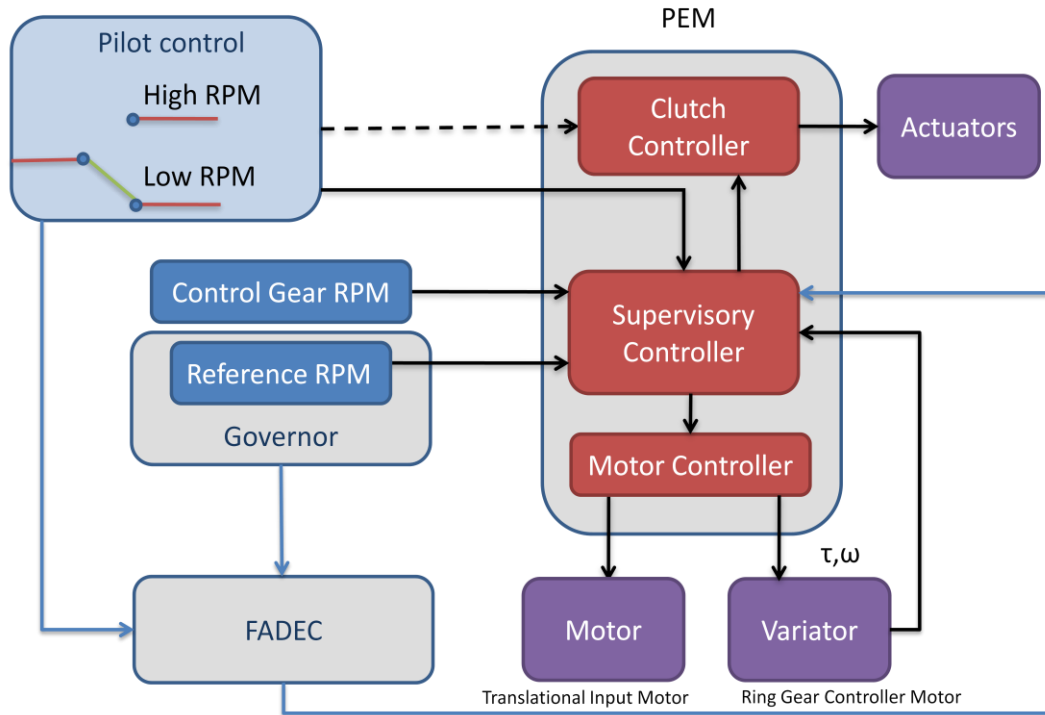
A Power Electronics Module (PEM) was designed to control the variable speed planetary transmission. This system is shown in Figure J-6. The Pilot has control over the selection between high and low speed transitions in this initial concept. At hover and low speed operation, the PEM is set for high rotor rpm, meaning the ring gear clutch bands are engaged. For high-speed flight, the PEM is set for low rotor rpm. The PEM is made up of a Supervisory Controller (SC), Motor Controller (MC) and Clutch Controller (CC). SC monitors controller gear speed and rotor rpm (from the speed governor). The governor works as a primary input to both the engine control system (FADEC – Full Authority Digital Engine Control) and the PEM. The speed switch should have an input to the FADEC system as well to ensure that the engine does not try to reset the speed of the rotor. SC monitors motor torque, to enable accurate inputs to the MC. The MC powers the motors and supplies precise voltages to ultimately keep the reference rpm stable. The CC controls the engagement and disengagement of the clutches. This system should have a provision for manual override from the pilot to be able to engage the clutches for flight safety purposes. This is indicated by the dashed line in Figure J-6. The PEM should also receive an input from the vehicle electrical system. The ring gear and the clutch bands actuators are shown in Figure J-5 page 64. Figure J-4 shows the finite element analysis in ANSYS.

The High rpm to low rpm transition PEM sequence is as follows:

1. Disengage clutch. Power disengagement involves retracting actuators simultaneously.
2. Power motor to maintain controller and ring gear somewhere between 0 rpm and an upper limit. The upper limit depends on the dimensions of the system and the sensitivity that this upper limit might have on the rotors performance.
3. Increase controller rpm to slow planetary carrier according to a predetermined optimum speed change rate (approximately 5-10 rpm per second main rotor equivalent)
4. The PEM will now seek to keep the rotor rpm stable by controlling the motor torque and speed.

The low rpm to high rpm transition PEM sequence is as follows:

1. Slow the ring gear at a predetermined optimum slowing rate (approximately 5-10 rpm per second main rotor equivalent) by powering the motor.
2. Once ring gear has been brought to a slow speed below 100 rpm (motor torque limit), the clutches can be engaged. Below 100 rpm, frictional force to slow the ring gear can be developed by the clutches without considerable wear.
3. Power to the clutch actuators is discontinued and the clutches engage. The ring gear is now held stationary and the drive system returns to normal operating mode



High RPM: 310 Main Rotor  
Low RPM: 214 Main Rotor

FIGURE J-6: POWER ELECTRONIC MODULE ARCHITECTURE

Motor:

- 3 phase, 4 pole, 375 volt
- AC induction air cooled type
- Variable frequency drive
- Max power of 124 hp
- Max RPM of 14,000
- Weight 70 lbs

## Appendix K STRUCTURAL ANALYSIS AND ROTOR DYNAMICS

### K.1. V-n Diagram

The requirement for the flight envelope is dictated by FAR part 29 Section 29.337: limit maneuvering load factor. As per this regulation, the helicopter must be designed for:

- (a) A limit maneuvering load factor ranging from a positive limit of 3.5 to a negative limit of -1.0; or
- (b) Any positive limit maneuvering load factor not less than 2.0 and any negative limit maneuvering load factor of not less than -0.5 for which--]
  - (1) The probability of being exceeded is shown by analysis and flight tests to be extremely remote; and
  - (2) The selected values are appropriate to each weight condition between the design maximum and design minimum weights.

The flight envelope (velocity-load factor diagram) for odyssey, which is shown in Figure K-1, shows a clear satisfaction of the requirements. However, there is always ambiguity with the flight envelope in the preliminary design phase. Therefore, accurate analysis could only be obtained through flight testing.

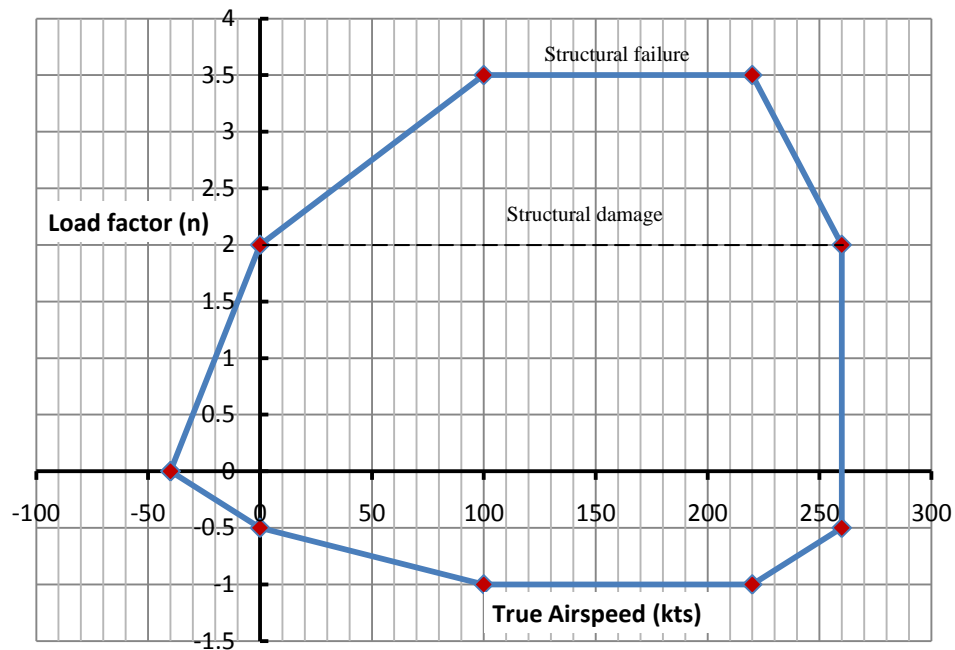


FIGURE K-1: VN DIAGRAM

### K.2. Rotor Structural Dynamics

On a working helicopter, the rotor spins at a certain frequency, causing the blades to vibrate at some other frequencies. If the frequencies collide, then the amplitudes of vibrations will grow, causing what previously could be minor vibrations to become major changes in the structure, possibly producing structure failure. For all operational modes this resonance should be avoided. The best way to recognize this phenomenon is through the use of a fanplot which overlays the blade frequencies with that of the spinning rotor.

Resonance is a structural phenomenon that happens during dynamic operations. Because of that, the layout of the blade becomes extremely important to determine what the blade natural frequencies are. For simplicity, if the blade can be pictured as a hanging beam connected to the rotor, then the frequencies will be affected by both the type and strength of the connection between the beam and the rotor and the by the beam structural properties.

### Blade Properties

The beam properties are determined from the shape of the cross-sectional blade at  $r/R$  sections. Some of the properties were estimated from previous blade designs. However, the main blade properties are presented below. The material used is Tungsten Carbide for its high young's modulus values; its properties were already given in Table C-3 page 30.

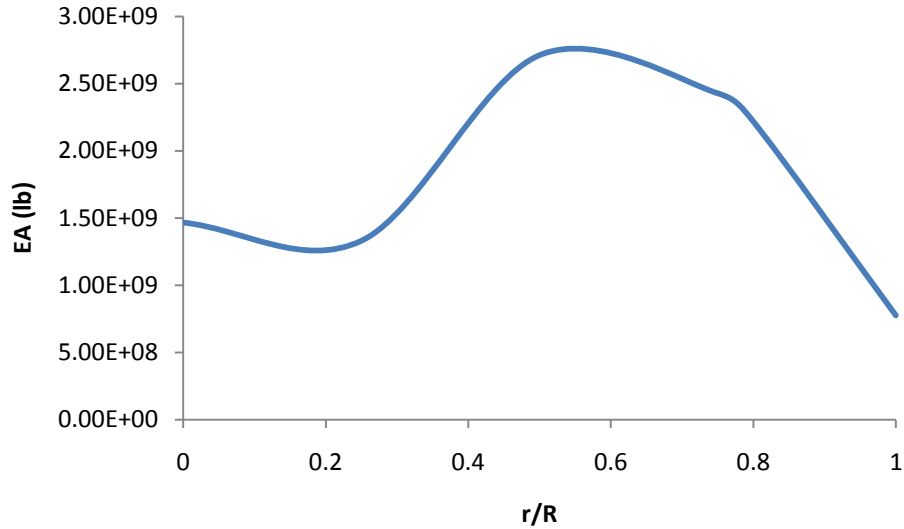


FIGURE K-2: AXIAL STRENGTH OF BLADES

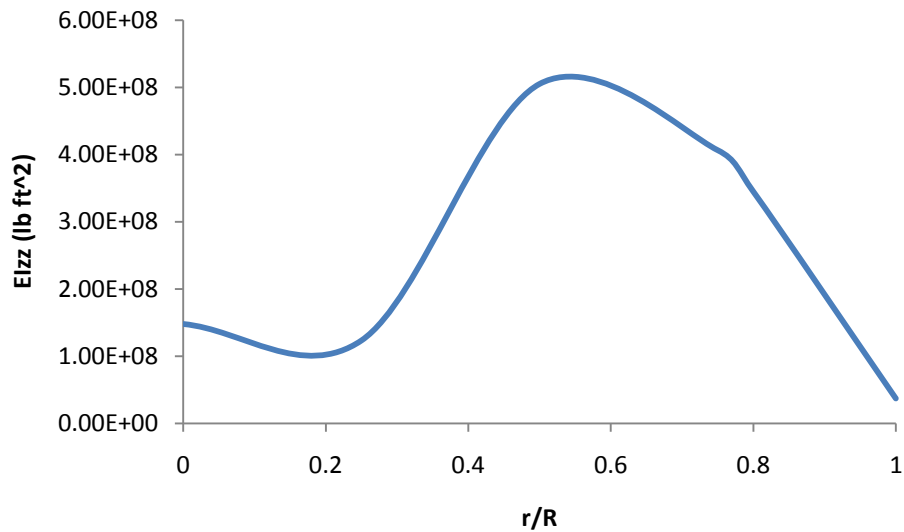


FIGURE K-3: LAG STIFFNESS OF MAIN ROTOR BLADES

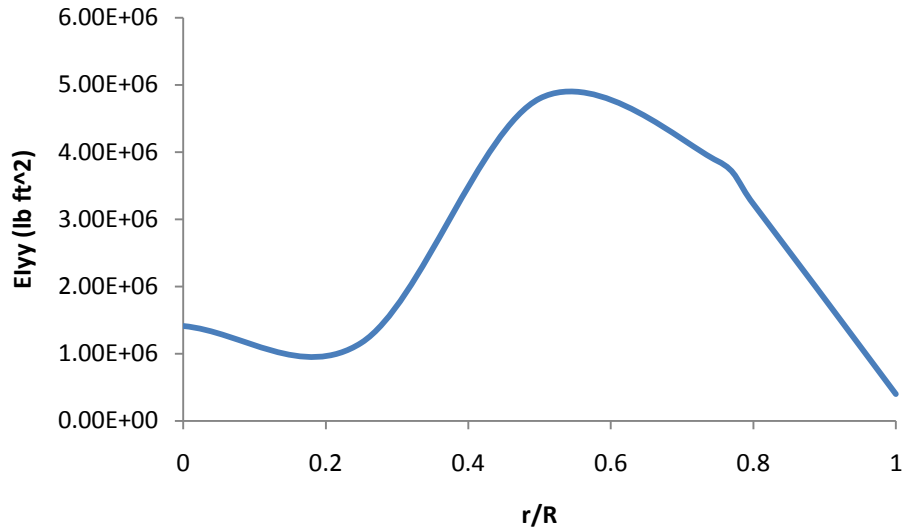


FIGURE K-4: FLAP STIFFNESS OF MAIN ROTOR BLADES

As the design is still in the first stages, and a detailed composite layup was not done, a black box composite structure with isotropic properties was assumed. This effect is captured in the elevated material strength at the widest elliptical area. The extra stiffness should be helpful if auxiliary structures for example, active flaps or individual blade control were to be added to the blade at a later stage. Figure K 2, Figure K 3, and Figure K 4 above show the main rotor blade stiffness in flapping and lead-lag motion, along with the axial strength.

### Fan Plot

The structural dynamics were performed in the Rotorcraft Comprehensive Analysis System (RCAS). A bearingless single main rotor model was made using the structural properties presented above. Because Odyssey has two identically structured rotors, the structural dynamics of one should be the same as the other. As RCAS is a simulation tool, the bearingless model was simulated with a black box torque tube with some stiffness and snubber with stiffness and damping that were set to be reasonable values. In this model then, the blades would have a pitchlink connected to the hub for pitch control and will get the other controls from the torque tube interaction, as shown in Figure K-5.

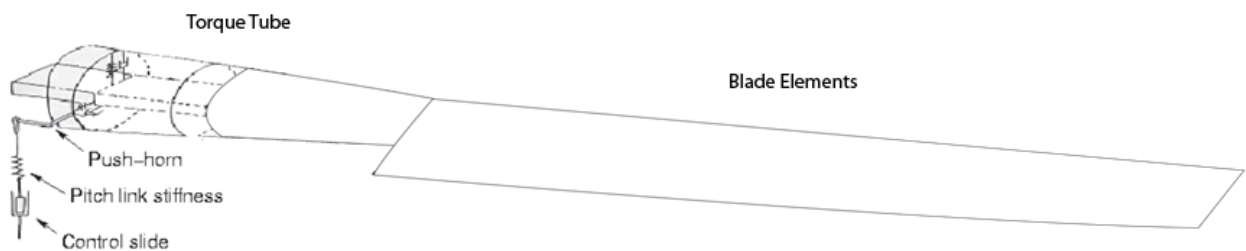


FIGURE K-5: RCAS BLADE MODEL

As odyssey is a variable speed rotor, the rotor blade interaction then will have to be free from resonance at a few points as well, mainly the hover rpm and the forward flight rpm. Hover is at 310 RPM and for forward flight, the rotation is further reduced down to 215 rpm. The fan plots for the rotations are presented below.

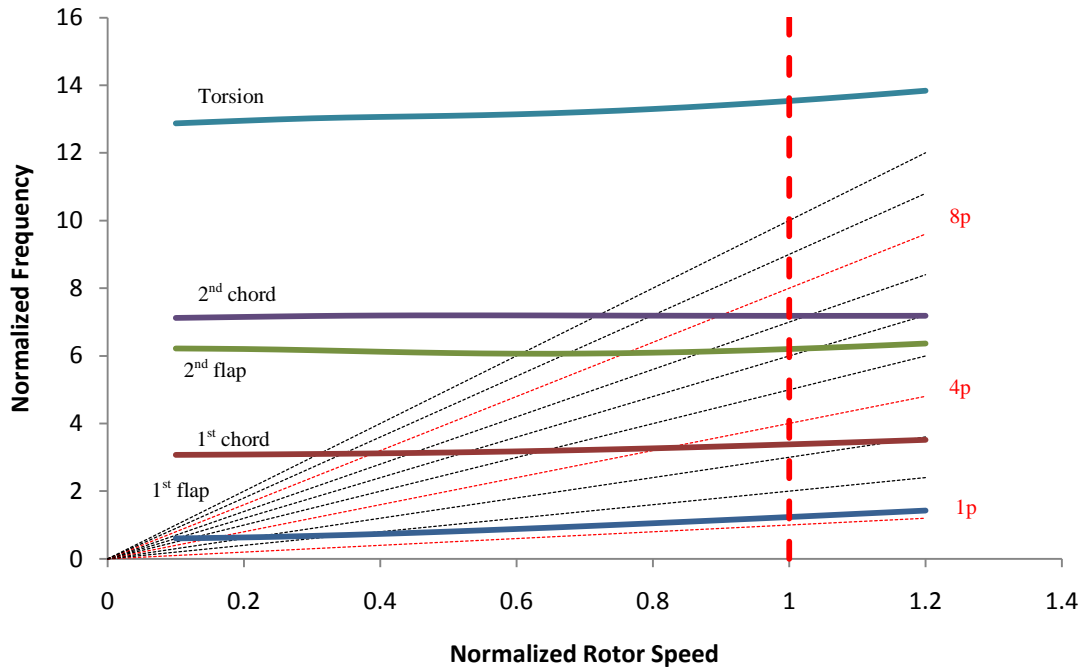


FIGURE K-6: HOVER FANPLOT AT 310 RPM (TIP SPEED: 650 FT/S)

Figure K-6 shows the fanplot of the main rotor in hover and Figure K-7 shows the fanplot in forward flight. The vertical red line represents the nominal frequency, and the main thing is to have no intersections between the red lines, representing the main rotor rotating frequencies (1p, 4p and 8p because we have a 4-blade rotor) and the color lines. The diagrams show that at the specific rpms, there will be no resonance issues. However, there are crossings pretty close to the nominal, and as long as the rotorcraft doesn't stay in those conditions too long, then there should be no structural issues during flight. Odyssey has no rotor stability issues or significant coupling between modes of the rotor and fuselage. The use of stiff-inplane rotor blades enabled to eliminate the ground and air resonance. In Figure K-6 the blade stiffness required to carry the lift on the advancing blades led to a very high torsional stiffness such as the first torsional mode was well above 12p. This high stiffness is very helpful to minimize coupling between flap and torsion degrees of freedom [6]. Because the rotor does not have lag dampers, the only damping present in the first chord wise mode arose from the structural aerodynamic damping.

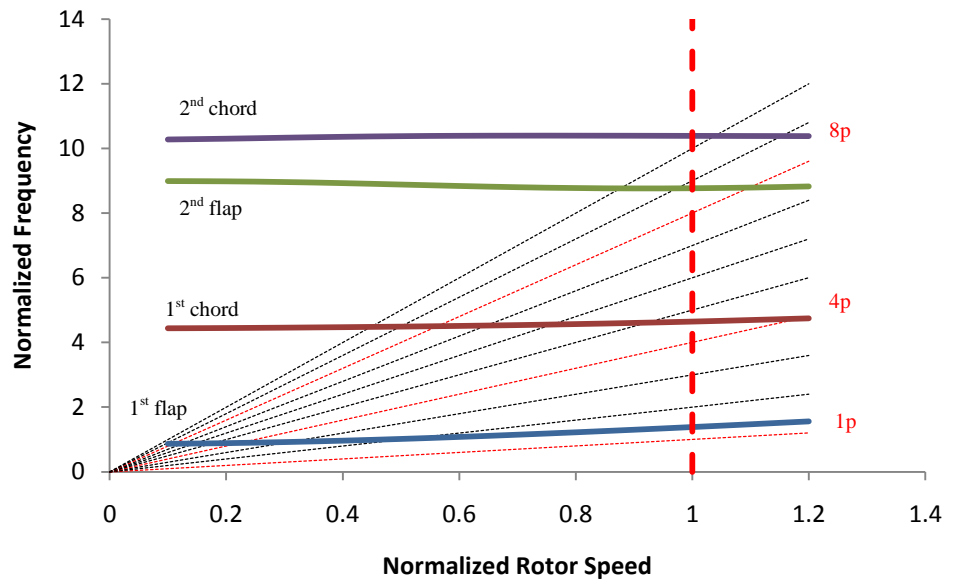


FIGURE K-7: FORWARD FLIGHT FANPLOT AT 215 RPM (TIP SPEED: 450 FT/S)

### K.3. Active Vibration Control

Experience on the Sikorsky XH-59A showed that adequate control of the  $4n$ /rev vibrations may be an undeniable requirement to achieve high speed forward flight [6]. The Odyssey design team recommends the installation of an Active Vibration Control (AVC) system similar to the one implemented on the XH-59A. The efficient weight of this system was taken into account in the empty weight breakdown shown in Figure H-7 page 55. It is necessary to design a system that can track the evolution of the rotor speed when Odyssey flies from 0 to 239 kts. The AVC system was based on the existing off-the-shelf system currently incorporated on the S-92A [20] and the UH-60M BlackHawk [31]. The AVC achieves vibration attenuation by applying  $4$ /rev vibratory forces to the airframe to counteract the vibrations created by the main rotor. Feedback sensors are required and actuators incorporated in the airframe create the vibratory forces. The actuators are placed close to the locations at which the struts that support the transmission connect to the fuselage. In this case, it is easier to cancel the rotor forces before they enter the fuselage primary structure. The positive results obtained on the X2TD are shown in Figure K-8. Similar positive results may be obtained on Odyssey. Because this analysis requires a lot of time and flight test, we can only assume the positive impact of such a device on our vehicle and flight test on prototypes may be necessary to size the actuators.

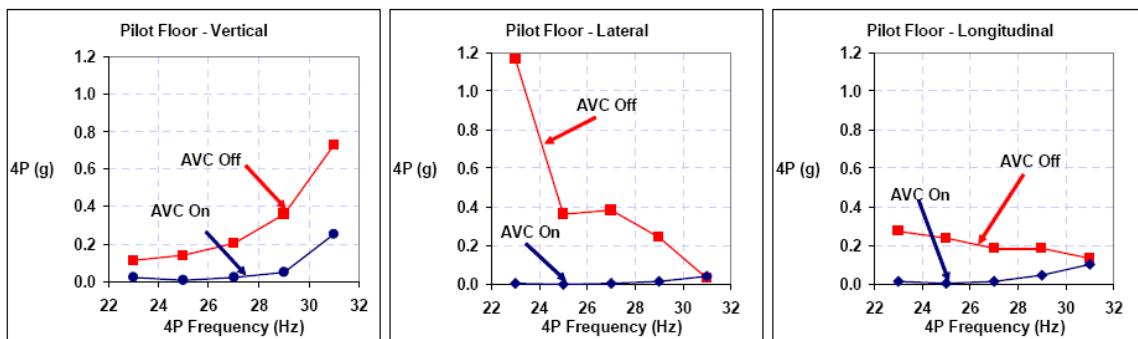


FIGURE K-8: PREDICTED PILOT 4/REV VIBRATION [49]

### K.4. Airframe Structural Integrity

The airframe has to be able to support sufficient loading in flight and more importantly in maneuver conditions without plastic deformation. The loading can be determined from the V-n diagram shown in Figure K-1. The main support rings and the floor spar use ‘I’ beam cross sections for its good bending stiffness and decent torsional and twist properties. The rest of the support is made from rectangular beams, for the simplicity of construction. However, for the final design, it might be wise to do a trade study between hollowed tubes and the current selection of beam cross sections. It’s known that rectangular beams aren’t the best in terms of maximizing support and weight, and I beams do not maintain symmetry and that’s especially problematic when the aircraft is going through maneuvers and induces loads that’s not along the strong axis of the beam.

Initial design had the airframe completely in aluminum, but due to the forces on the airframe, the material was reinforced with a stronger material. Instead, Tungsten Carbide is added with the aluminum to produce a hybrid structure with the properties below. Another trade study will have to be done on the amount of each in the structural combination. Indeed we want to minimize the Tungsten Carbide used as it is a much heavier material than aluminum. Again, like the rotorcraft blades, the material has isotropy for simplicity.

It was determined in the V-n diagram that the most loading the airframe will have to support is 3.5G. Therefore a gravitational load of 3.5G was applied in all directions to ensure that the airframe can support any kind of maneuvers.

The most serious loading comes from side loading at  $3.57 \times 10^7$  lb/ft<sup>2</sup>. This lies outside the aluminum yielding strength, but lies within the Tungsten Carbide yield strength, and since the material is a combined material, it lies within the hybrid material yield strength either. But the hybrid material might be over-designed with having too much Tungsten Carbide as there’s possibly too much safety factor right now.

The weight then calculated from the CAD model is 283lbs. This seems to be heavy for just support structure. In the actual airframe, the skin of the rotorcraft will be able to support some loading too, reducing the needed mass in the airframe even more.

Since the rotorcraft is a system with almost infinite degrees of freedom, the forces at the hub are taken as an overall indication of vibrations. This is good point to pick as the rotor is main force generator and therefore vibration inducer on the rotorcraft. To get the hub forces, the airframe along with the coaxial rotors was assumed as a rigid body in RCAS. The RCAS model consisted of 2 of the rotor structures made for the fan plots and additionally, for each structural element aerodynamic panels were added to incorporate the air loading. For simplicity and trim problems, the blade structure was back-scaled to rigid blades. The wake model used a dynamic inflow, which should do a decent job capturing basic wake interactions. Then a speed sweep was done with the model to reach the designed forward flight speed. The hub forces generated are summarized in Table K-1.

TABLE K-1: MAIN ROTOR VIBRATIONS

	<b>Rotor1 Harmonic Cos</b>	<b>Rotor1 Harmonic Sin</b>	<b>Rotor2 Harmonic Cos</b>	<b>Rotor2 Harmonic Sin</b>
Xf (lbs)	1.89E+02	5.27E+02	4.41E+02	7.14E+01
Yf (lbs)	-1.98E+02	-1.02E+02	5.26E+01	-2.06E+02
Zf (lbs)	-2.11E+02	-5.27E+02	-4.07E+02	-8.94E+02

## Appendix L NOISE EMISSION

### L.1. Applicability of ICAO Stage 4 Noise emission

The RFP states that the vehicle must be compliant with the ICAO Level 4 standards in noise emission. FAA Part 36 explains: “For any Stage 4 airplane, the flyover, lateral, and approach maximum noise levels are prescribed in Chapter 4, Paragraph 4.4, Maximum Noise Levels, and Chapter 3, Paragraph 3.4, Maximum Noise Levels, of the International Civil Aviation Organization (ICAO) Annex 16, Environmental Protection, Volume I, Aircraft Noise, Third Edition, July 1993, Amendment 7, effective March 21, 2002” [17]. Since Odyssey is a compound helicopter, it does not meet the description of a tilt rotor or a propeller-driven aircraft. Chapter 8 of the Annex 16, Volume 1, deals with the noise of helicopters.

Three conditions must be tested to show compliance with the Level 4 standards. The description of each condition, as stated in the Annex 16, is provided below:

- *Take-off*: a flight path reference point located on the ground vertically below the flight path defined in the take-off reference procedure and 500 m horizontally in the direction of flight from the point at which transition to climbing flight is initiated in the reference procedure
- *Overflight*: a flight path reference point located on the ground vertically below the flight path defined in the take-off reference procedure and 500 m horizontally in the direction of flight from the point at which transition to climbing flight is initiated in the reference procedure
- *Approach*: a flight path reference point located on the ground 120 m (394 ft) vertically below the flight path defined in the approach reference procedure. On level ground, this corresponds to a position 1 140 m from the intersection of the 6.0° approach path with the ground plane

### L.2. Noise level requirements

For all helicopters, including their derived versions, for which the application for the Type Certificate was submitted, or another equivalent prescribed procedure was carried out by the certifying authority, on or after 21 March 2002, the following noise levels shall apply:

- *Take-off*: 106 EPNdB for helicopters with maximum certificated take-off mass, at which the noise certification is requested, of 80 000 kg and over and decreasing linearly with the logarithm of the helicopter mass at a rate of 3 EPNdB per halving of mass down to 86 EPNdB after which the limit is constant
- *Over-flight*: 104 EPNdB for helicopters with maximum certificated take-off mass, at which the noise certification is requested, of 80 000 kg and over and decreasing linearly with the logarithm of the helicopter mass at a rate of 3 EPNdB per halving of mass down to 84 EPNdB after which the limit is constant
- *Approach*: 104 EPNdB for helicopters with maximum certificated take-off mass, at which the noise certification is requested, of 80 000 kg and over and decreasing linearly with the logarithm of the helicopter mass at a rate of 3 EPNdB per halving of mass down to 84 EPNdB after which the limit is constant

In order to obtain the noise level requirements for Odyssey, it is necessary to calculate the limits using Equation 37.  $TOGW_{kg}$  is the maximum take-off gross weight expressed in thousands of kilograms ( $TOGW_{kg}=6.812$ ).

EQUATION 37

$$N_{TO} = 87.03 + 9.97 \log_{10}(TOGW_{kg}) = 95.33 \text{ EPNdB}$$

$$N_{Approach} = 90.03 + 9.97 \log_{10}(TOGW_{kg}) = 98.33 \text{ EPNdB}$$

$$N_{Overflight} = 85.03 + 9.97 \log_{10}(TOGW_{kg}) = 93.33 \text{ EPNdB}$$

### L.3. Aeroacoustics code WOPWOP

PSU-WOPWOP is based on the original WOPWOP code utilizing object-oriented design principles and focusing on the prediction of the noise of maneuvering rotorcraft or any other moving body. PSU-WOPWOP calculates the noise at specified observer locations with the aeromechanical data of the simulated aircraft or any other simulated object (i.e. the aircraft and blade motion and blade airloads or fluctuating forces on an arbitrary body such as landing gear). Using the input data, it solves the Ffowcs William Hawkins Equations using Farassats formulations. A Fast Fourier Transform is applied to post process the data. The noise produced by the main rotors and propellers of pusher of the Odyssey is analyzed using PSU-WOPWOP. Like any other computational analysis software, it can be divided into 3 stages:

- Pre-processing: creation of rotor geometry and observer grid
- Processing: actual computational analysis of Odyssey
- Post-processing: presentation of results in a form that can be easily analyzed

#### Pre-processing

PSU-WOPWOP is an object oriented analysis code. Certain features of FORTRAN 95 are used to define an object hierarchy that helps to build large, complex objects. An object called a “patch” is the core of PSU-WOPWOP. This patch stores the surface geometry and flow data for a single surface. Any surface which generates noise is modeled by a discrete number of panels over which the integration quantities are assumed constant. At their most basic, each patch stores a grid representing the integration surface and the necessary data at each of the grid points. The grid on the patch can either be structured (from CFD calculations) or unstructured mesh. In order to make complex objects which are again combined to form even more complex objects several patches are combined. For example a main rotor blade is composed of at least 4 patches as shown in Figure L-1. Different numbers of blades are used to create a rotor which in turn constitutes an aircraft.

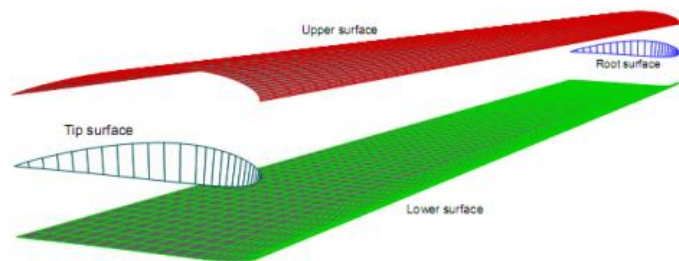


FIGURE L-1: ROTOR BLADE FORMED BY A SERIES OF FOUR STRUCTURED PATCHES [22]

Observers are the microphones or the listening positions and are separated from the aircraft hierarchy. It defines the positions at which the acoustic pressure is calculated. A single observer point or multiple observer grid points can be used in PSU-WOPWOP.

The input file for PSU-WOPWOP contained all basic parameters which described the main rotor blade configuration and flight conditions. The rotor blade was modeled as a grid depending on the accuracy. Airloads obtained from Blade Element Analysis Code or higher fidelity CFD analysis codes are applied to each surface or node of the grid generated. Input files are used to define each object in the object hierarchy. Case files contain the path and filename of the particular case that is to be analyzed. The Namelist file contains the main definitions of the objects mentioned above that are to be used. Change of base files defines the motion of various objects. Patch files are used to create surface patches.

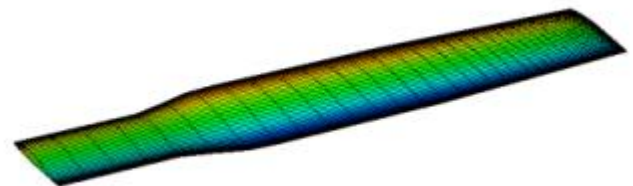


FIGURE L-2: ODYSSEY'S MAIN ROTOR BLADE

For Odyssey, simple patch files using an impermeable surface are used for the co-axial main rotor blades and propellers of pusher. The initial mesh for rotor blades and propellers are generated by GT-Hybrid Grid GENERATOR which creates 3D structured multiblock mesh for blade or propeller automatically. And the surface mesh data of the 3D block mesh is converted to a geometry file created in FORTRAN 95. The blade is divided span-wise into 50 sections. Figure L-2 and Figure L-3 show surface of the main rotor blade and propeller modeled in PSU-WOPWOP.

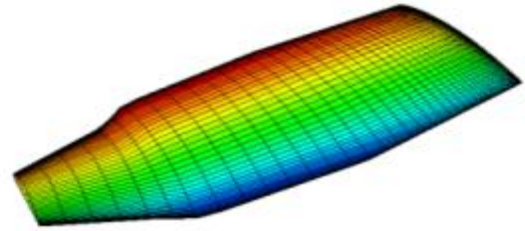


FIGURE L-3: ODYSSEY'S PUSHER PROPELLER BLADE

The flight conditions and rotor blade assumptions are summarized in Table L-1.

TABLE L-1: PSU WOPWOP ASSUMPTIONS

Main Rotor	
Rotor radius	20 ft
Tip Speed	650 ft/s in hover 450 ft/s at max cruise speed
Number of rotors	2 (coaxial)
Number of blades	4 per rotor
Blade airfoils	VR7/VR8
Twist	-10 deg
Pusher	
Diameter	5ft
Number of propellers	2 (counter-rotating)
Number of blades	5 per propeller
Pusher airfoils	E 193/MH 116 9.8%
Pusher RPM	3,365
Twist	-45 deg

### Processing

In order to get the acoustic pressure or the sound level at the observer grid points, the Ffowcs Williams-Hawkings Equation is solved. This is done by using a time-domain integral formulation developed by Farassat using a Retarded Time Algorithm or the Source Time Algorithm. Farassat's Formulation 1A using a Source Time Algorithm is implemented. In this algorithm, the source time or the time at which the noise is produced at the blades is used as a starting point and observer time is calculated from this. The main advantage of this algorithm is that it is computationally less intensive.

### Post-processing

A single observer point is used in front of the helicopter as shown in Figure L-4. In hover, the observer is located 60 ft away from rotor hub. The noise levels are calculated at a point 500 ft away from the helicopter at a point 60 deg below the hub plane for forward flight. Below figure shows observer location from rotor. The Fast Fourier Transform is used to

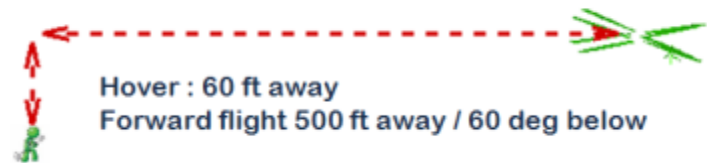


FIGURE L-4: SINGLE OBSERVER POINT DURING PSU WOPWOP PROCESSING

transform data from the time domain to the frequency domain. The FFT library that Wop-Wop uses is a package called Fast Fourier Transform in the West.

The outputs are the acoustic pressure or the sound level in decibels calculated at the observer grid points. The output files are Plot 3D structured binary format and can be processed by using Fieldview or Tecplot. In this aeroacoustic analysis, the thickness noise is only calculated. The noise levels are calculated at a point 500 ft away from the helicopter at a 60 deg below the hub plane. Figure L-5 and Figure L-6 show separately the thickness noise level for the main rotor and for the pusher propeller. Because of the shroud, the noise level of the pusher propeller should be lower. However, the absence of the loading noise makes it impossible to conclude on the overall noise emission of Odyssey.

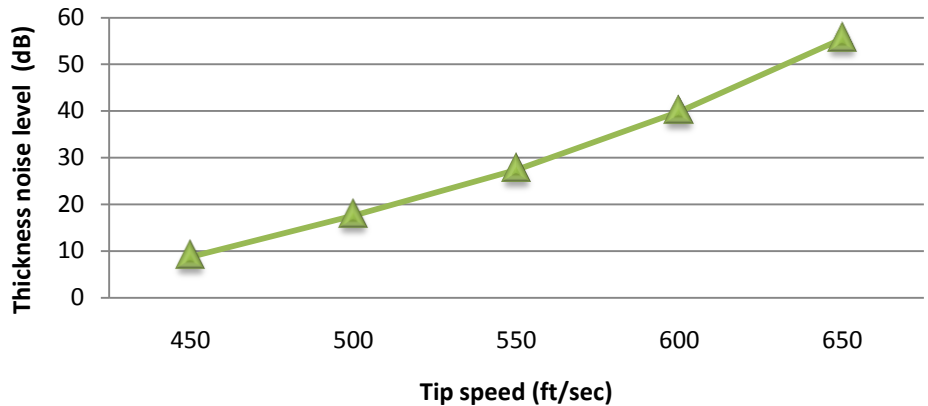


FIGURE L-5: THICKNESS NOISE LEVEL FOR THE MAIN ROTOR ONLY

Figure L-5 and Figure L-6 show separately the thickness noise level for the main rotor and for the pusher propeller. Because of the shroud, the noise level of the pusher propeller should be lower. However, the absence of the loading noise makes it impossible to conclude on the overall noise emission of Odyssey.

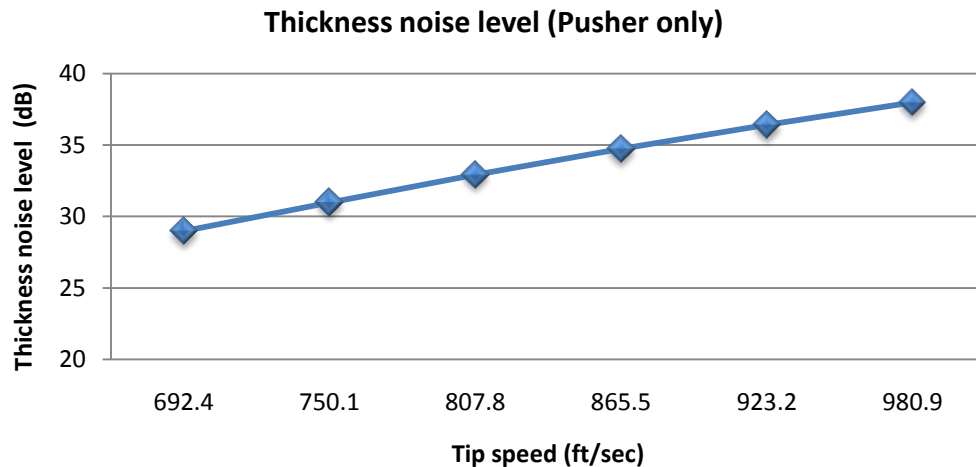


FIGURE L-6: THICKNESS NOISE LEVEL FOR THE PUSHER PROPELLER

Table L-2 shows noise level for different flight conditions. The noise level at hover is calculated about 60 ft. away and the target noise level at this distance is nearly matched. It can be seen that there is a large margin for the loading noise.

TABLE L-2: NOISE LEVEL CALCULATION FOR ODYSSEY

Cases	Target Noise level (EPNdB)	Thickness Noise level	Margin for Loading noise	Target met
Hover	Less than 85 EPNdB	55 EPNdB	30 dB	<input checked="" type="checkbox"/>
Take-off	Less than 95.33 EPNdB	61.49 EPNdB	33.84 dB	<input checked="" type="checkbox"/>
Overflight	Less than 98.33 EPNdB	72.78 EPNdB	25.55 dB	<input checked="" type="checkbox"/>
Approach	Less than 93.33 EPNdB	66.25 EPNdB	27.08 dB	<input checked="" type="checkbox"/>

## Appendix M HANDLING QUALITIES AND FLIGHT CONTROLS

### M.1. FLIGHTLAB Model

The handling qualities analysis of Odyssey was performed using FLIGHTLAB which is widely used in both industry and academia. A detailed simulation model was built and tested against several ADS-33E-PRF requirements and Mission-Task-Elements (MTEs) to accurately examine the most critical stages of the three missions stated in the RFP. The analysis was undertaken as a collaborative effort between Georgia Institute of Technology and the University of Liverpool. The following appendix describes the FLIGHTLAB model of Odyssey.

#### Introduction to FLIGHTLAB

FLIGHTLAB is a comprehensive rotorcraft modeling, simulation, and analysis program created by Advanced Research Technologies (ART). Odyssey was modeled using the FLIGHTLAB Model Editor (FLME) and Control Systems Graphical Editor (CSGE). The simulation model of Odyssey was heavily modified from a generic template for a conventional rotorcraft in FLME. Similarly, the controls were created from a generic control system in CSGE. Once the model was successfully created, Xanalysis was used for simulation and analysis.

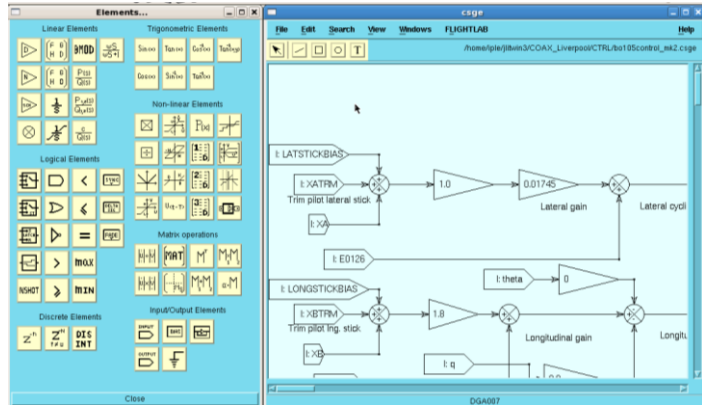


FIGURE M-1: CSGE SCREEN

#### Rotor Model

Odyssey was modeled with a coaxial rotor in FLIGHTLAB with the configuration data provided in Table M-1. The rotor type of Odyssey was represented by an articulated rotor with a stiff hub spring to simplify the model because the detailed blade properties required for a hingeless rotor were not available. Since this was a first order representation and more fidelity for flight dynamics and performance calculations was not needed the articulated rotor should provide an acceptable alternative for the handling qualities analysis of Odyssey. It should also be noted that Micro flaps were not incorporated into the FLIGHTLAB model due to time constrictions, but were analyzed independently (see Appendix I page 56). However, a future analysis and simulation should be performed to test their effect on yaw control. Because Gurney flaps are very small the structural model can be neglected. Modifications to the airfoil data to include aerodynamic variation due to the Gurney flaps should be sufficient. In addition, the application of micro flaps to reduce noise and vibration appears promising and should also be explored.

TABLE M-1: ROTOR CONFIGURATION

Rotor Type	Articulated
Rotational direction	Upper rotor: counter-clockwise Lower rotor: clockwise
Rotational Speed (nominal)	32.5 rad/sec
Rotor radius	20 ft
Number of blades per rotor	4
Number of segments per blade	6
Airload	Quasi-steady model
Airfoil	SC1095
Inflow	Peters-He three state model
Interference	Three state interference model

### Pusher Propeller Model

Because FLIGHTLAB only contained two rotor inputs, which were used for the upper and lower main rotors, an airload table was created to represent the pusher propeller. The table outputted the thrust provided by the pusher propeller as a function of forward velocity and altitude. The table was linked to the total flight speed of Odyssey so that the pusher propeller would produce an additional amount of thrust at the particular flight condition.

### Airframe and Fuselage

A rigid fuselage model was used for Odyssey. FLIGHTLAB provided the option of entering the total mass and inertias of the aircraft using either the fuselage or entire vehicle. The design group decided to obtain these values using the total vehicle in CATIA; the mass and inertia values are presented in Table M-2. FLIGHTLAB uses the fuselage, butline, waterline convention with the origin located at the front of the nose and bottom of the landing gear. A positive fuselage measurement is defined towards the tail, a positive butline measurement is defined out of the left wing, and a positive waterline measurement is defined as up.

TABLE M-2: TOTAL VEHICLE MASS AND INERTIA VALUES

Vehicle c.g.	Fuselage: 12 ft Butline: 0 ft Waterline: 5 ft
Total vehicle mass	8,879 lb <sub>m</sub>
Total roll moment of vehicle inertia	5,061.45 slug-ft <sup>2</sup>
Total pitch moment of vehicle inertia	15,173.55 slug-ft <sup>2</sup>
Total yaw moment of vehicle inertia	15,754.16 slug-ft <sup>2</sup>
Total X-Y product of vehicle inertia	0 slug-ft <sup>2</sup>
Total X-Z product of vehicle inertia	-1,474 slug-ft <sup>2</sup>
Total Y-Z product of vehicle inertia	0 slug-ft <sup>2</sup>

In addition to the total vehicle mass and inertia inputs, a non-uniform airload table was created using an existing FLIGHTLAB table that had numbers similar to that of a generic Black Hawk. The table contained the X, Y, and Z forces and moments of the fuselage as a function of angle of attack and sideslip angle. In order to determine reasonable values for the airload table the ratio of the Black Hawk and Odyssey equivalent flat plate drag areas were used to scale down the forces and moments.

### Horizontal Stabilizer

A horizontal stabilizer was located on the ducted fan in FLIGHTLAB to help account for the pitch-down moment of the aircraft. The horizontal stabilizer was modeled using the CATIA model.

## M.2. Handling Qualities and Piloted Simulation

The handling qualities of Odyssey were determined using ADS-33E-PRF. Both offline prediction tools and online piloted assessment were used to determine the overall handling. Analysis was designed as to cover the wide range of tasks that the aircraft would be expected to perform, and both low speed and forward speed assessment was conducted. As only ADS-33E was used, the aircraft handling qualities have only been evaluated against traditional rotorcraft requirements. As Odyssey has been designed to push the boundaries of traditional helicopters, it is recommended that further handling qualities analysis is conducted for the high speed flight, where the rotorcraft forward thrust in the same way as a fixed wing aircraft (possibly using MIL-STD-1797 or similar specifications).

### Stability of Odyssey

The stability of Odyssey was determined by linearizing the nonlinear FLIGHTLAB model. The linearized model contained 6 body states (p, q, r, u, v, w) and 3 Euler angles (phi, theta, psi). This allowed 8 stability modes of motion to be determined, to address the small amplitude/low frequency handling qualities of the aircraft. Based upon the frequency and the damping of the aircraft 'modes of motion', ADS-33 defines stability boundaries for rotorcraft. These boundaries are independent on airspeed, but have dependency on the aircraft task requirements. For the purposes of this investigation, where applicable, the aircraft was assessed against requirements for 'Target Tracking and Acquisition. This is due to the difficulty of the tasks that would be performed

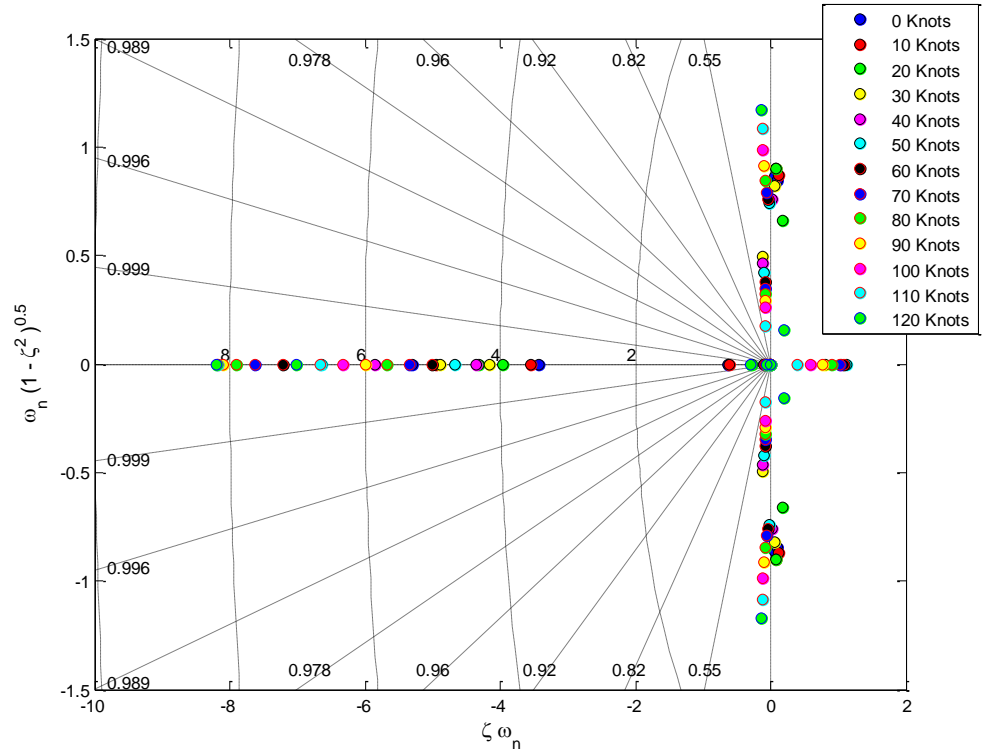


FIGURE M-2: BARE AIRFRAME POLES OF ODYSSEY

by Odyssey. With no augmentation system, the aircraft is unstable throughout its traditional rotorcraft flight envelope. In hover, the aircraft behaves similarly to a traditional helicopter, with two unstable poles, representing longitudinal pitching oscillation and Dutch roll modes. Both have similar frequencies and damping ratios. Both have a time to double amplitude of approximately 7 seconds, representing significant pilot workload to stabilize the motion in both lateral and longitudinal axis. The trend continues within the low speed regime until 30 knots, where a dramatic change in lateral stability occurs. The Dutch roll poles shift to damped oscillations whilst the aircraft begins to suffer from significant yaw instability. As this was not experienced at hover and very low speed flight, it is thought to be due to the airflow over the main rotors with the combination of low airframe damping. This trend then continues throughout the 'rotorcraft' flight regime. The longitudinal pitching oscillation becomes neutrally stable at 50 knots and remains until 120 knots. The unstable yawing mode of the aircraft remains throughout and, at 120 knots is joined by a heavily unstable Dutch Roll mode. Figure M-2 shows a plot of the 'eigenvalues' through the speed range, at intervals from 0 to 120 knots.

### Feedback Control Systems

In order to improve the vehicles handling qualities and control responses, feedback control has been applied in cyclic control and in the rotor collective channels. Figure M-3 shows the cyclic control system of Odyssey and the feedback applied. The cyclic controls of the aircraft are defined in %, with 100% representing full aft longitudinal control stick and full right lateral control stick. Angular feedback is applied in radians and angular rate feedback is applied in radians per second. The trimmed control position settings are contained within XA/XBTRM blocks, whereas pilot control is applied directly in XA/XB (giving perturbation from trim position). Figure M-4 shows the collective, pedal and throttle control channels of the aircraft. The controls are defined in %, with 100% relating to maximum collective, maximum right pedal displacement and maximum Throttle. As shown, no feedback is applied within the collective channel. However, yaw rate feedback is applied through the pedal channel.

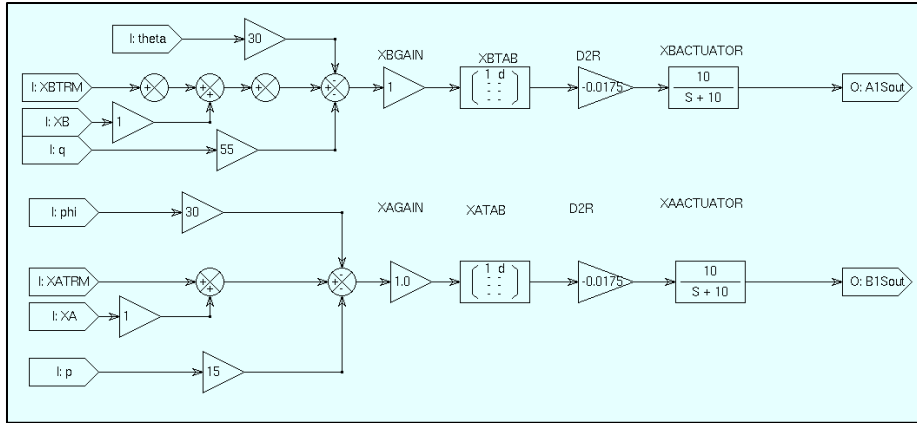


FIGURE M-3: CYCLIC CONTROL CHANNELS OF ODYSSEY

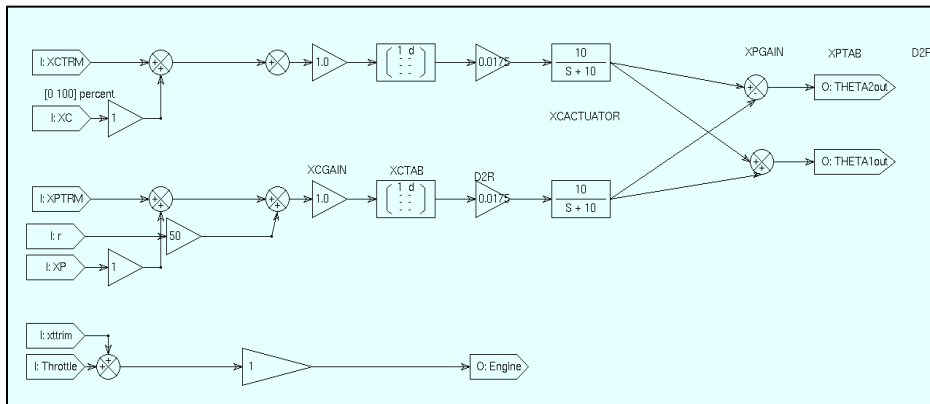


FIGURE M-4: COLLECTIVE, PEDAL AND THROTTLE CONTROL CHANNELS OF ODYSSEY

The control feedback values were chosen to give the best combination of stability, agility and control response. It was desired for Odyssey to function primarily with rate controls. The feedback was used to shape the control response to give good rate authority to the pilot. With the bare airframe model, holding the control stick did not ensure that rate would remain constant, and would cause an out-of-phase response when the control was removed. Figure M-5 shows a response to a longitudinal doublet input of 10%, and how the augmented system improves the controllability, whilst decreasing maneuverability.

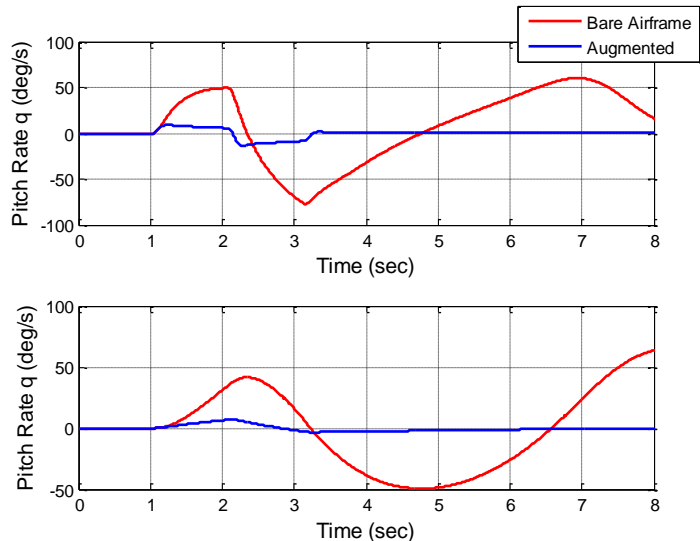


FIGURE M-5: AIRCRAFT RESPONSE TO LONGITUDINAL DOUBLET CONTROL INPUT

Figure M-6 shows the trimmed control positions of Odyssey from 0 to 120 knots following the addition of feedback control.

The additions of feedback control allowed for the stabilization of the aircraft, in all axes. As shown in Figure M-2, the longitudinal pitching oscillation was found to be unstable between 0 Knots and 50 Knots. Based on ADS-33 guidelines, the pitching oscillations would give Level 2 HQ throughout the speed range. Figure M-8 shows the roots of the longitudinal pitching oscillation following stabilization. As shown, the oscillation is within HQ Level 1 throughout. Unlike the bare-airframe, the oscillations are suppressed at 90 knots. This should not cause any problems regarding the handling qualities.

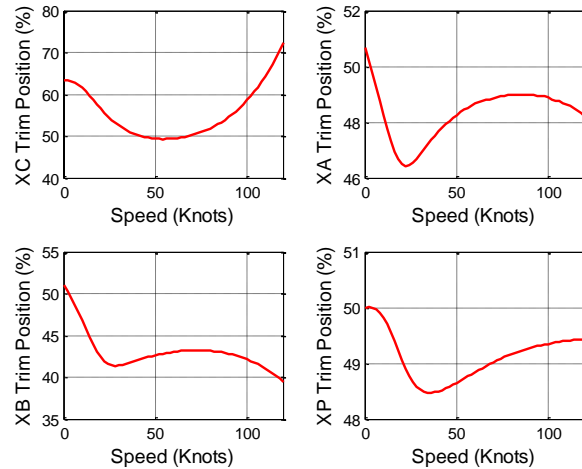


FIGURE M-6: TRIMMED FLIGHT CONTROL POSITIONS

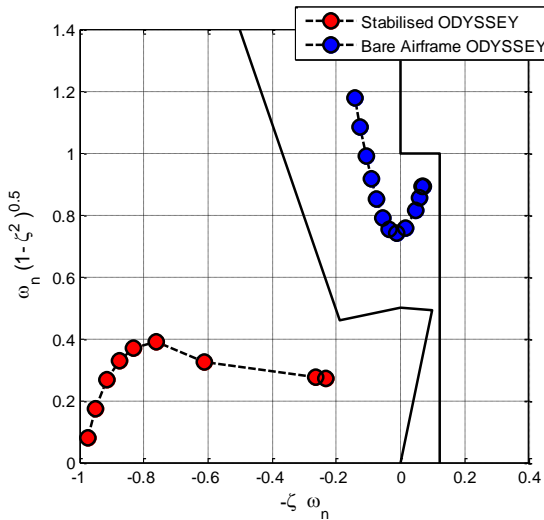


FIGURE M-8: POLES OF LONGITUDINAL PITCHING OSCILLATION

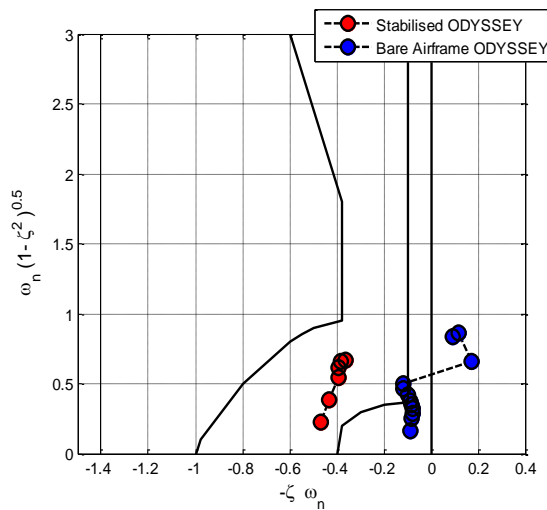


FIGURE M-7: POLES OF DUTCH ROLL OSCILLATION

Figure M-7 shows the improvements made through the use of feedback on the Dutch Roll mode of Odyssey. The bare airframe exhibits instability until 20 knots, at which point the Dutch roll mode becomes lightly damped and low frequency. As shown, this gives predicted Handling Qualities Level 3 based on ADS-33 boundaries. Feedback added to the lateral channel has improved the response, ensuring that it is damped and stable throughout. All oscillatory poles are within HQL 2. Like the pitch oscillations, the motion is damped above 80 knots. As shown in Figure M-2, the bare airframe vehicle exhibits divergent yaw motion for a large proportion of the flight envelope. This was stabilized with yaw rate feedback.

### Quickness of Odyssey

Due to the control response for the Bare Airframe, it was found very difficult to obtain reliable quickness responses. Therefore, only results for the stabilized aircraft are presented. Figure M-9 shows the maximum achievable roll quickness of the aircraft, plotted against ADS-33 roll quickness boundaries. As shown, for all data points, the quickness is within Level 1 requirements. Figure M-10 shows the maximum achievable pitch quickness plotted against ADS-33 requirements. Again, for all data points, the quickness is within Level 1 requirements. This shows that the augmented aircraft should be suitable for high workload missions, including target tracking and acquisition missions.

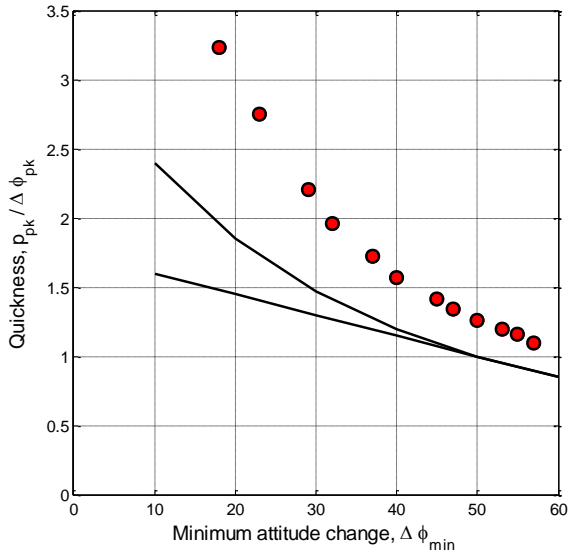


FIGURE M-9: MAXIMUM ACHIEVABLE ROLL QUICKNESS

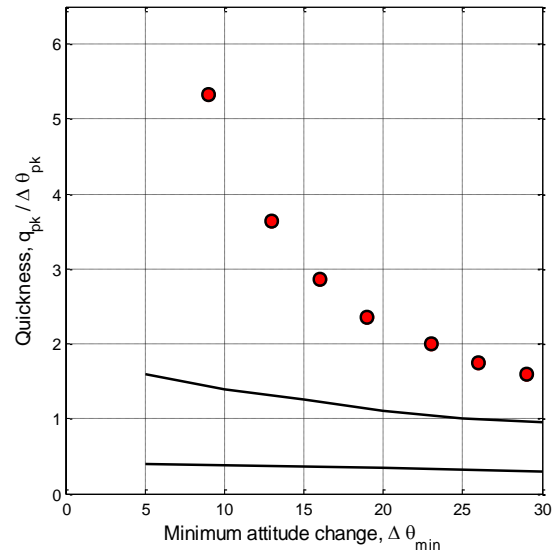


FIGURE M-10: MAXIMUM ACHIEVABLE PITCH QUICKNESS

**Control Power**

The control power of the aircraft was studied against ADS-33 recommendations. Due to instabilities and the control responsiveness of the bare airframe, all ADS-33 control power targets were met for roll, pitch and yaw responses. Once stability augmentation was added to Odyssey, the control power was substantially reduced. Table 4 shows the control power for each axis between 0 and 100 knots in intervals of 10 knots. Results are presented in radians/sec in Table M-3, showing the maximum steady state rate that can be achieved with the control systems.

TABLE M-3: ODYSSEY CONTROL POWER

	0	10	20	30	40	50	60	70	80	90	100
Roll control power	1.10	1.00	0.85	0.80	0.90	1.00	1.00	1.00	1.05	1.05	1.05
Pitch control power	0.80	0.80	0.78	0.81	0.85	0.90	0.91	0.93	0.95	0.95	0.95
Yaw control power	1.00	0.95	0.92	0.90	0.88	0.88	0.88	0.91	0.91	0.91	0.91

TABLE M-4: ODYSSEY CONTROL POWER PREDICTED HANDLING QUALITIES LEVELS

		Speed (Knots)										
		0	10	20	30	40	50	60	70	80	90	100
Roll control power	Agility											
	Limited	L1	L1	L1	L1	L1	L1	L1	L1	L1	L1	L1
	Moderate	L1	L1	L1	L1/2	L1						
	Aggressive	L1	L1	L1/2	L1/2	L1						
	Target Acquisition						L2	L2	L2	L2	L2	L2
Pitch control power	Limited	L1	L1	L1	L1	L1	L1	L1	L1	L1	L1	L1
	Moderate	L1	L1	L1	L1	L1	L1	L1	L1	L1	L1	L1
	Aggressive	L1	L1	L1	L1	L1	L1	L1	L1	L1	L1	L1
Yaw control power	Limited	L1	L1	L1	L1	L1	L1					
	Moderate	L1	L1	L1	L1	L1	L1					
	Aggressive	L1	L1	L1	L1	L2	L2					

Table M-4 shows the predicted handling qualities levels corresponding to different ADS-33 requirements based on the values displayed in Table M-3. As shown, for the vast majority of speeds and aggressiveness, Odyssey meets the requirements set for HQL 1. In terms of roll control power for moderate and aggressive

criteria, the achievable rate is marginally less than the requirement. In terms of roll control power for target acquisition, the aircraft only achieves Level 2 performance. At 40 and 50 knots, the yaw control power is also below Level 1 performance for aggressive tasks.

### M.3. Mission Task Elements

To assess the initial handling qualities of Odyssey, a number of Mission Task Elements (MTEs) were developed, for use in a simulated test trial. A number of these MTEs were taken from ADS-33E-PRF, the current design standard for rotorcraft. In order for a test pilot to identify deficiencies in the aircraft and assign handling qualities ratings, specific measures of performance were required for each task. These were set to give desired performance and adequate performance. The following section outlines the Mission Task Elements that were performed by the test pilot, and the performance standards used.

#### Precision Hover

The Precision Hover task definition was extracted from ADS-33E in order to test the aircraft's capabilities to maintain a precise station hold. To assist the pilot with regards to the set tolerances a 'hover board' device was used which was similar to that defined in ADS-33E. The pilot was asked to translate at a speed between 6 and 10 knots to a location determined by a series of cones and attain a stabilized hover. The task, depicted in Figure M-11, began with the aircraft located at a specified point located at 45 degrees from the target. Following the aircraft translation to the designated hover point the aircraft was required to maintain a stabilized hover for a period of 30 seconds with tolerances also relating to the time to attain the stabilized hover from the initiation of the deceleration. Once in hover mode the tolerances for the aircraft were with respect to the longitudinal and lateral position of the aircraft with respect to the ground as well as altitude and heading deviations.

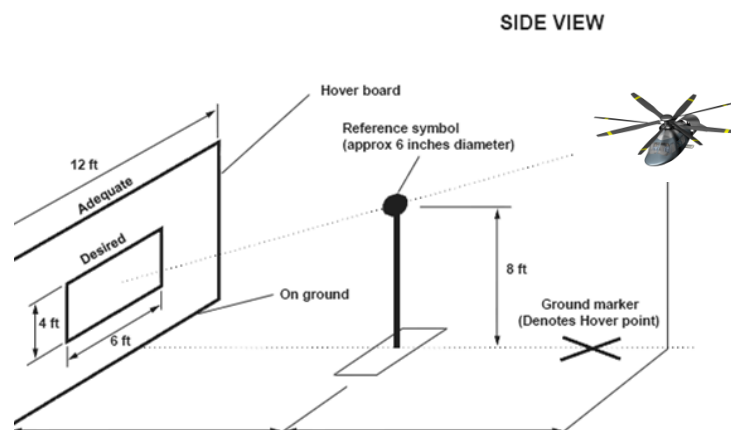


FIGURE M-11: ARRANGEMENT FOR HOVER MTE

TABLE M-5: PRECISION HOVER MTE TOLERANCES

Performance Standards	Desired Performance	Adequate Performance
Attain a stabilized hover within X seconds of initiation of deceleration	13 seconds	18 seconds
Maintain Stabilized Hover for X seconds	30 seconds	30 seconds
Maintain longitudinal position within $\pm X$ ft of a point on the ground	3 ft	6 ft
Maintain Altitude within $\pm X$ ft	5 ft	10 ft
Maintain Heading within $\pm X$ degrees	4 deg	6 deg
Maintain Lateral position within $\pm X$ ft of a point on the board	9 ft	15 ft

#### Pull-Up and Push-Down (Vertical Maneuver)

The Pull-Up maneuver is based on the ADS-33E MTE for the bob-up maneuver utilizing the same 'hover board' set up. The maneuver was initiated from a stabilized hover within sight of the lower hover board.

The pilot was then requested to perform a step collective input in order to increase the torque of the main rotor. Once obtained the pilot was required to reduce the collective and climb the aircraft up to the height of the upper hover board within a given time constraint. Once at the top of the climb the pilot was required to stabilize the aircraft, and during both stabilized hover flight regimes the pilot was required to maintain altitude within given tolerances. Other tolerances for the task were given with respect to the longitudinal and lateral position of the aircraft throughout the maneuver in addition to heading deviations experienced.

TABLE M-6: EMERGENCY PULL-UP MTE TOLERANCES

Performance Standard	Desired	Adequate
Maintain longitudinal and lateral position within $\pm X$ ft of a point on the ground	10 ft	20 ft
Maintain start /finish altitude within $\pm X$ ft	5 ft	10 ft
Maintain Heading within $\pm X$ degrees	10 deg	20 deg
Complete the maneuver within X seconds	20 seconds (low agg.) 10 seconds (med. agg.) 5 seconds (high agg.)	20 seconds (low agg.) 10 seconds (med. agg.) 5 seconds (high agg.)

### Hover Turn

The Hover Turn MTE was designed to simulate low, medium, and high aggression turns during low altitude hovering flight. From a starting position in a stabilized hover the pilot was required to initiate a yaw rate and complete a turn through 90 degrees and stabilize on the new heading with given heading deviation limitations. The entire maneuver was required to be completed with a three given times, which gave desired aggression levels. The MTE was performed at a runway intersection, allowing the pilot to judge his performance and to give a visual indication of the desired heading. Tolerances for the duration of the maneuver were given with respect to the longitudinal and lateral position of the aircraft with respect to the ground as well as altitude deviations during the task.

TABLE M-7: HOVER TURN MTE TOLERANCES

Performance Standards	Desired	Adequate
Maintain longitudinal and lateral position of a point on the ground within $\pm X$ ft	6 ft	12 ft
Maintain Altitude within $\pm X$ ft	3 ft	6 ft
Stabilize final heading within $\pm X$ degrees	3 deg	6 deg
Complete the turn so that a firing solution has been found within X seconds from initiation of the maneuver	20 seconds (Low Agg.) 10 seconds (Med. Agg.) 5 seconds (High Agg.)	20 seconds (Low Agg.) 10 seconds (Med. Agg.) 5 seconds (High Agg.)

### Speed Conversion

The Speed conversion task was designed to expose any undesirable couplings occurring during translation from hover to 250 knots. The task was completed at two levels of aggressiveness; slow transition and maximum achievable aggressiveness. The slow transition test was conducted with a constant acceleration of 1 knot/second. This tested controllability of the aircraft throughout. The second test was completed by adding full power and controlling the aircraft motions. Through the task, the pilot was required to maintain altitude, at 1,000 ft, and heading.

TABLE M-8: SPEED CONVERSION MTE TOLERANCES

Performance Standards	Desired	Adequate
Maintain Altitude within $\pm X$ ft	100 ft	200 ft
Stabilize final heading within $\pm X$ degrees	10 deg	20 deg
Constant Acceleration	1 knot/sec	N/A

### Roll Step

The roll step MTE was selected in order to simulate maneuverability in forward flight at low altitude. The simulation was set to start at the end of a runway, trimmed in a hover condition. The pilot was then required to accelerate to 50, 80, or 100 kts depending on the desired flight condition. The pilot was then required to fly down the runway, passing through numbered gates. The pilot was required to make two crosses of the runway during a test run; at gate 4/12 and gate 8/12. The airspeed controlled the aggression of the task, due to the constant distance between the gates and the size of the runway. Throughout the MTE, the pilot was required to maintain altitude at 50 ft. Originally the test was to be performed using throttle control. However, problems found with low-speed throttle/collective mix gave reason to perform the final tests with collective only.

TABLE M-9: SPEED CONVERSION MTE TOLERANCES

Performance Standards	Desired	Adequate
Maintain airspeed	50 knots ( $\pm 5$ knots) [low agg.] 80 knots ( $\pm 5$ knots) [med. agg.] 100 knots ( $\pm 5$ knots) [high agg.]	50 knots ( $\pm 10$ knots) [low agg.] 80 knots ( $\pm 10$ knots) [med. agg.] 100 knots ( $\pm 10$ knots) [high agg.]
Lateral Deviation	$\pm 15$ ft	$\pm 30$ ft
Heading Deviation	$\pm 10$ deg	$\pm 20$ deg
Height Deviation	$\pm 10$ ft	$\pm 15$ ft

### Piloted Simulation

Piloted simulation of the above MTEs was conducted on the 6th day of May 2011, by former Military test pilot Wg. Cmdr. Martin Mayer. The tests were conducted using facilities at the University of Liverpool Bibby simulation facility, using the Heliflight motion based simulator. All tests were conducted using Odyssey with the stability control system selected. Results from the tests are displayed in the sections below.

### Precision Hover

The aircraft was shown capable of performing the Precision Hover MTE. Due to the control systems, the pilot found the workload low during the stabilization period, making constant low amplitude inputs that allowed him to complete other tasks (divided attention). The main difficulty he found was during the translational phase. The pilot found it difficult to control the movement of the aircraft, sighting the slightly uncharacteristic response to inputs. However, the task was achieved within the desired performance boundaries and, as the problems he felt did not impact heavily on task completion, the pilot awarded a **HQR 3**, within Level 1.

### Pull-up and Push-down

Both pull-up and push-down maneuvers were completed at low, medium and high aggression. At low and medium aggression (20 seconds and 10 seconds respectively), the pilot achieved desired performance and sited no large problems causing him difficulty in the task. One of the reasons that the pilot found the task low workload was the lack of collective-yaw couple. This is due to the coaxial rotor arrangement and an advantage the aircraft has over those of a similar weight class. For both the low and the medium aggression maneuvers, for both pull-up and push-down tests, the pilot awarded **HQR 2**, within Level 1 performance.

For the high aggression task, completion in 5 seconds, the pilot found that the aircraft required considerable compensation. This was required when re-stabilizing the aircraft in a hover condition. Despite the aggression of the control inputs, the pilot found that there was no significant coupling, and that the 'climb/descent' periods did not require significant compensation. However, the pilot felt that performance was difficult to achieve and awarded Level 2 ratings. The high aggression Pull-up received a **HQR 5**, whilst the push-down maneuver received a **HQR 4**. All results are shown Figure M-12.

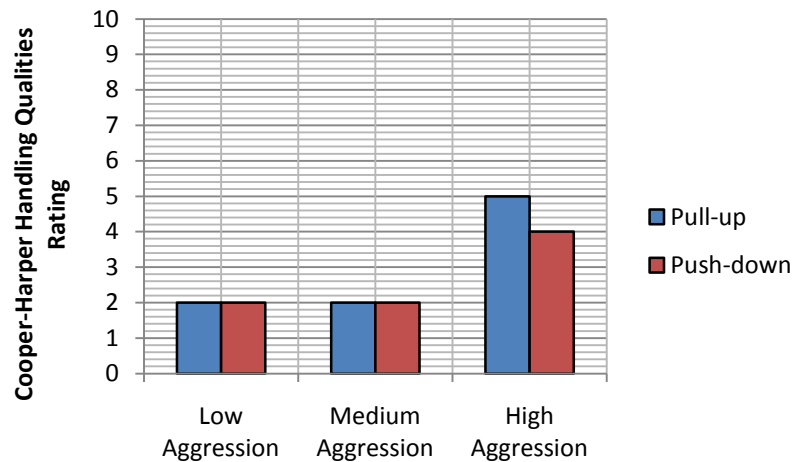


FIGURE M-12: COMPARISON OF CHR FOR SEVERAL AGGRESSION PULL MANEUVERS

### Hover Turn

The hover turn maneuver was completed at all desired levels of aggression; in 20 seconds, 10 seconds and 5 seconds. The main challenge that the pilot faced during completion of the task was yaw overshoot at the end of the maneuver. At low aggression, the pilot felt that he had no trouble in maintaining a stable hover condition but found difficulty yawing out of the maneuver and maintaining desired heading. He commented that it was within the boundaries of desired performance, and awarded **HQR 3**, within Level 1.

When performing the medium aggression turn, with completion in 10 seconds, the pilot felt that the yawing motion was slightly more damped than for the 20 seconds case. However, he suggested that more compensation had to be applied to stabilize the aircraft, and that the rate of yaw had to be controlled carefully in order to not overshoot and maintain desired performance. For these reasons, he awarded a **HQR 4** (Level 2).

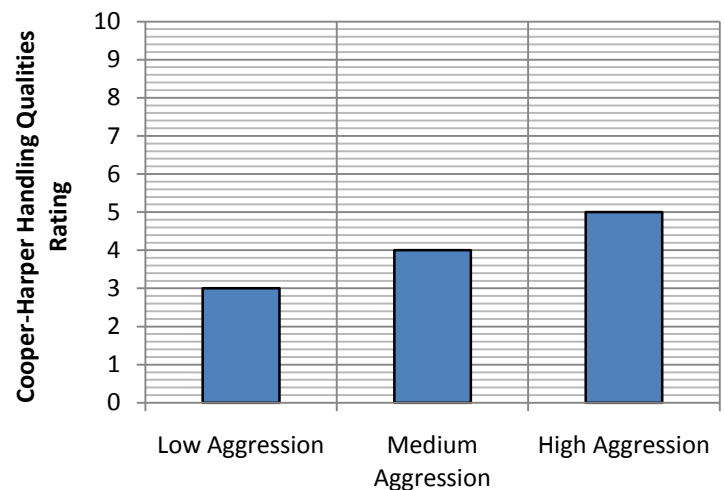


FIGURE M-13: COMPARISON OF CHR FOR SEVERAL AGGRESSION HOVER TURN MANEUVERS

The high aggression task required additional workload, and the pilot commented that to achieve the desired performance, the workload was high. The pilot managed to complete the maneuver in the desired 5 seconds, but said that it would be a significant risk to perform the task in real operation. Although he managed to reach all performance requirements, he felt that the amount of compensation did not reflect Level 1 HQs, and awarded a **HQR 5**. Figure M-13 shows the awarded handling qualities for the MTEs.

As shown, for each level of aggression, the HQR degrades by one rating. This pushes the medium and high aggression tasks within Level 2 performance. However, there is no significant degradation of rating, showing that the vehicle is achieving a high level of performance, even for the most challenging of tasks.

### Speed Conversion

Both speed conversions at low controlled aggression and high aggressions were completed, with the pilot achieving desired performance. For both tests, the pilot engaged the throttle control when at 100 knots. For the low aggression test, the pilot increased airspeed at 1 knot/sec, through the application of control and the manipulation of aircraft pitch attitude. When above 100 knots, the pilot used a combination of throttle and collective to offload the rotor. By doing this, he managed to achieve full autorotation (no power to main rotors) and trimmed flight at 250 knots. In this condition, the aircraft was still controllable and the pilot felt that the aircraft had good handling qualities. Through this test, the aircraft was demonstrated to be a working autogyro. The pilot awarded a **HQR 4** for the low aggression test and a **HQR 5** for the high aggression test. The increase in handling qualities rating was due to the high and uncomfortable pitch attitudes that had to be kept at the start of the maneuver, and the difficulty controlling the height of the aircraft.

### Roll Step

Roll step maneuvers were performed at 3 levels of aggressiveness, achieved by defining the desired task airspeed. The original task was designed to be completed using the throttle control and reducing collective control to offload the main rotors. However, significant handling deficiencies were found during test runs for the task.

The pilot would successfully trim the aircraft using collective control. Following the trim at the correct airspeed, the pilot simultaneously decreased collective whilst increasing throttle. Problems occurred when trying to find this suitable trim condition. Between 60 and 100 Knots, the aircraft was seen to display divergent lateral oscillations. These oscillations were found to be sudden and represent a handling qualities 'cliff'. The pilot made every effort to stabilize oscillation but, the divergent nature combined with the low altitude (50 ft) to make the task almost impossible. It was shown that, at all speeds above 100 knots, no such divergent oscillations occurred. This was due in part to an oversight during offline handling investigations and stabilization of the aircraft. Although the Dutch roll lateral oscillations were stabilized in trim throughout the normal operational rotorcraft speed range, the stability and handling qualities were not observed with the throttle engaged. With the throttle engaged, the collective is reduced to account for the increase in lift provided by the aft propeller. Two specific changes to the dynamics occurred:

- The airframe experiences an increase in aft force, now pushing it through the air
- The rotor dynamics change regarding torque, rpm and cyclic flapping.

Due to these problems, the roll step test points were completed by using collective control only to control both forward airspeed and height throughout. For tests completed at 50 knots and 80 knots, the pilot found the workload similar. The main problem that the pilot experienced was a cross-couple between yaw and roll. Due to the control of yaw using differential cyclic, a large amount of roll coupling is experienced

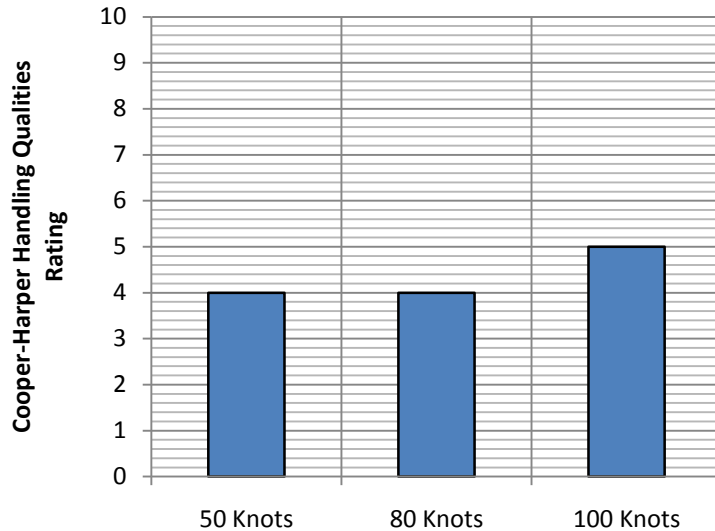


FIGURE M-14: COMPARISON OF CHR SEVERAL AGGRESSION ROLL STEP MANEUVERS

when travelling above the low airspeed regime. The reason for this is likely to be the change in the rotor dynamics, regarding the drag changes and interference effects, all present within the simulation model. The pilot found that desired performance was achievable but the task was involved high workload throughout. As a result, the pilot awarded HQR 4 for both the 50 knot and 80 knot runs.

At the 100 knot run, the task was found to induce higher workload. In preliminary runs, it was found that the amount of roll due to pedal control was too much for the pilot to control. The motions were too violent and, at the low altitudes, caused uncontrollable motion. Therefore, for the task to be flown a 100 knots, the pedals had to be locked in position above 90 knots. This stopped the coupling, at the expense of an easily controllable yaw channel. Due to the difficulty in controlling yaw, the pilot found the 100 knot run more challenging. His performance slipped out of adequate and, due to this he awarded a HQR 5 (Level 2). Figure M-14 shows a comparison of the HQR for all roll step rated runs.

#### M.4. Overall Pilot Assessment

Overall, the test pilot communicated that he thought that Odyssey was a good aircraft and a very good solution to meet the future market place. Overall, he felt that the elements required for a good operational aircraft were present in the simulation model. The pilot particularly liked the way that the aircraft performed like both a traditional rotorcraft and fixed wing aircraft. With this in mind, he liked the independent control of throttle and collective, as shown in Figure M-15. Having the control channels independent gave him more of a sense of the mode in which the aircraft was flying. In this respect, when flying at 200 knots, control felt like it was a traditional fixed wing aircraft. However, the pilot did recommend that an automated system was in place at least for the transition phase, as he found it difficult to control both systems with his left arm.

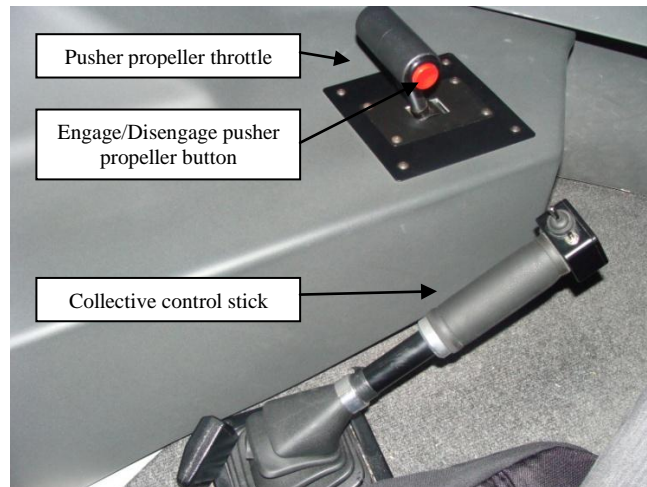


FIGURE M-15: ARRANGEMENT OF THROTTLE AND COLLECTIVE CONTROLS

As discussed, the main handling deficiencies were found at low speed with a combination of both throttle and collective control. The main oversight during the handling qualities investigation was not to assess the characteristics of the vehicle during combination of throttle and collective. It was during this combination that the pilot unveiled a divergent lateral oscillation. This was found when trying to maintain straight and level flight whilst operating between 60-80 knots. The other problem encountered during the testing was the insufficient yaw control at high speed. During the flight trial, the only method to control the yaw was through differential collective. However, at high speed, this created a considerable pedal-roll couple. Therefore, the pedal control power had to be severely reduced. This meant that the control was not sufficient to perform maneuvers, such as coordinated turns. From this it was recommended that, for high speed flight, a rudder device is installed on the aircraft. This could be implemented behind the propeller, in order to deflect the airflow. The inclusion of another method of yaw control would need to be accounted for through control systems but, could be triggered at a certain forward airspeed.

Overall, the aircraft was capable of performing all MTEs presented with Handling Qualities Ratings within Level 1 and Level 2. The tasks selected represented a number of different aggression levels, and performance targets were deliberately set above the desired operational standards. Even without recommended modifications, the aircraft was shown capable and is suitable as a next generation air vehicle. Table M-10 gives a complete breakdown of the handling qualities ratings awarded by the visiting test pilot.

TABLE M-10: SUMMARY OF COOPER-HARPER RATINGS AWARDED

Mission Task Element	Aggression	Cooper-Harper Handling Qualities Rating
Precision Hover	-	3
Pull-up	Low	2
	Medium	2
	High	5
Push-down	Low	2
	Medium	2
	High	4
Hover Turn	Low	3
	Medium	4
	High	5
Speed Conversion	Low	4
	High	5
Roll Step	Low (50 Knots)	4
	Medium (80 Knots)	4
	High (100 Knots)	5

#### M.5. Recommendations for future design iteration

- Method of control between throttle and collective, whilst maintaining their independence as controls
- Fuller investigation in the effects on the 'offline' vehicle handling qualities with a combination of both collective and throttle controls
- Implementation of aft rudder control for use during high speed flight
- Upgrades to simulation model including more advanced control systems, instruments and sounds

## Appendix N AVIONICS

In order to design a more efficient and affordable concept, the optimization of the energy onboard was part of the effort to reduce peak of non propulsive power usage, fuel consumption and equipment weight. The definition of the energy optimized rotorcraft varies depending on the disciplines and the persons involved [36]. Nonpropulsive power is the power not used to move the rotorcraft and includes any power used in the cabin, such as lighting or medical equipment requiring electricity, and in the cockpit, such as avionics and other electrical systems. The increase in electrical power demand also leads to greater system and architecture complexity. However, the reduction in fuel consumption, along with a reduction in the number of maintenance operations, is especially important in a context where the fuel cost and the labor are rising. Maturity is required in power electronics, thermal management and cooling systems while wiring installation can remain an issue at the detailed design stage.

### N.1. Generation and distribution architecture

Odyssey is an energy-managed and fault-tolerant aircraft equipped with a health monitoring system. The engine nacelles are electric and the generation of electricity is achieved through an Integrated Drive Generator (IDG) placed on each engine. The IDG is in charge of the main circuit generation and auxiliary generation. In case of emergency, one IDG can be used for emergency generation in OEI. Control circuits for galley supply are also required. Monitoring and indicating circuits for the cockpit are present to inform the pilots on the subsystems status. Since the system is equally loaded by all active generators under normal operating conditions, the parallel distribution is adopted. The AC/DC energy is distributed towards main and essential busbars before being redistributed to sub-busbars linked to main consumers.

### N.2. Avionics and cockpit features

Pilots are seated next to each other and four Multi-Function Displays are available on the cockpit. These MFDS provide health monitoring of aircraft systems and subsystems, situational awareness along with flight director and anti ground collision system. Two other control displays can be accessed by both pilots in the middle of the cockpit. The flight plans are available, along with data inputs, airport database, and map control. Odyssey is also equipped with a high transmission data link capability to assure permanent communication with the advanced center of control or the hospital. The cockpit of Odyssey is shown in Figure N-1.

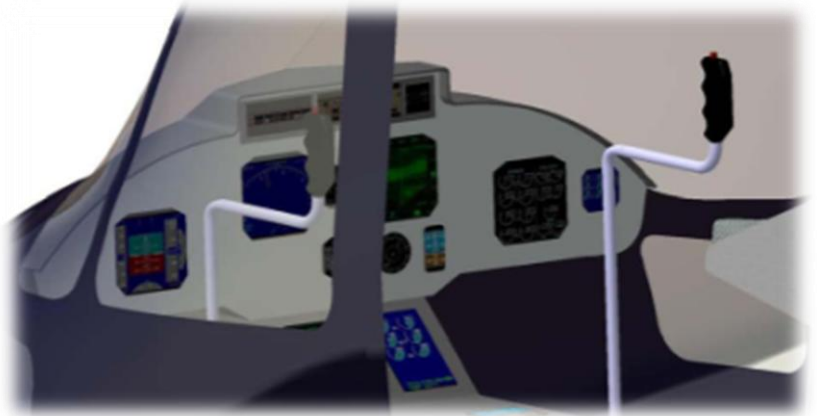


FIGURE N-1: ODYSSEY'S COCKPIT AND AVIONICS

## Appendix O COST ANALYSIS

The cost estimation is a critical aspect of the preliminary design loop. Since Odyssey is based on a 100% new design, costs are examined as a function of technologies implemented and operating conditions. These values can then be used to calculate the OEC and the Cost Index in A.3. . The evaluation of cost must take into account the overall life-cycle cost and is the total cost of ownership of Odyssey. These costs include acquisition cost, operation cost, maintenance cost, and development cost. The objective of this analysis was to provide the reader with an extensive comprehension of the costs involved in this project and give a realistic estimation of Odyssey’s price compared to the other concepts in this competition. In addition, the life-cycle cost analysis identified the sensitivity of Odyssey to some parameters and helped to pick the most cost effective development approach in order to reduce the long-term cost of ownership. The life-cycle cost can be decomposed in three distinct types, as shown in Table O-1.

TABLE O-1: LIFE-CYCLE COST DECOMPOSITION

Life Cycle Cost		
RDTE Cost	Acquisition Cost	Operating Cost
Design phase	Manufacturing Phase	Flight crew cost
Flight test	Dynamic system	Fuel and oil
Systems Management	Engines	Airframe Maintenance
Certification	Avionics	Engines Maintenance

The development cost should take into account the conceptual, preliminary, and detailed design phases, flight testing, systems management, and the cost associated with the certification process. The manufacturing phase along with the dynamic system, the engines integration, and avionics are considered part of the recurring production cost, and are generally associated with the acquisition cost or the price of the vehicle. Last but not least, the operating cost consists of but is not limited to the flight crew salary, the fuel/oil price, the airframe maintenance, and the engines maintenance.

TABLE O-2: EXISTING AIRCRAFT USED FOR THE VALIDATION OF THE BELL PC MODEL

Aircraft	Empty Weight (lbs)	Payload Weight (lbs)	Occupants	Max. Cont. Cruise (kts)	Max. Range (naut. mi.)
Bell 429	4245	2755	8	150	390
Bell 430	5305	3975	10	143	324
S-70	11790	8000	19	149	250
EC145	3951	3776	11	133	370
AW139	8000	4400	17	165	550



Bell 429

Bell 430

S-70

EC145

AW139

Since the RFP focuses on the reduction of inventory and operating cost, it was necessary to build a Bell PC Model adapted to Odyssey and validated on existing vehicles shown in Table O-2. The Bell PC model, whose primary inputs are shown in Table O-3, was the primary tool to estimate the cost in this section. Some assumptions were made to simplify the study and a penalty of 25% on the development cost was assumed to account for the compound configuration, the Gurney flaps and the revolutionary transmission systems. The values generated by the program, in 2001 dollars, were readjusted to 2011 dollars by using an inflation factor of 29.8%. The transmission system was examined closely to develop a more accurate recurring cost model.

TABLE O-3: BELL PC MODEL GENERAL INPUTS

	A	B	C	D	E	F	G	H
1	DEVELOPMENT PROGRAM GROUND RULES AND AIRCRAFT CONFIGURATION							
2	PROJECT TITLE:	GaTech AHS 2010						
3								
4	PROGRAM INPUTS:	Previous	Return to Rate Inputs					Next
5		Engineering Design Man-hour Source:						Parametric
6		System Weight Source:						Allocated
7		Number of Prototypes						3
8		Will there be a ground test vehicle (GTV), static test article (STA),						
9		and/or fatigue test article (FTA)?						Yes
10		Will a wind tunnel test be required?						Yes
11		Aircraft Application						Military
12		Attack Aircraft or Transport						Transport
13								
14		Will kit development be included in the program cost?						No
15		Rough Order of Magnitude (ROM) adjustment						10.0%
16		General & Administrative (G&A) adjustment						10.0%
17		Percent profit for military development programs						12.0%
18								
19	AIRCRAFT CONFIGURATION:							
20		Aircraft Type						Helicopter
21		APU Installation?						No
22		Landing Gear Type						Retractable
23		Number of engines						2
24		Aircraft Weight Empty						8,429
25								

### O.1. Development cost

The Research, Development, Testing and Evaluation (RDTE) cost was computed by the Bell PC model. A few assumptions had to be made in order to run the model for a non conventional compound configuration. Figure O-1 shows that engineering will be the most costly development factor, followed by manufacturing, planning, tooling and logistics. Three prototypes are needed to conduct testing and the certification campaign. One vehicle will be needed for ground testing; another for static test and the last one will be used for fatigue test. The total RDTE cost equals \$369 million (in 2011\$).

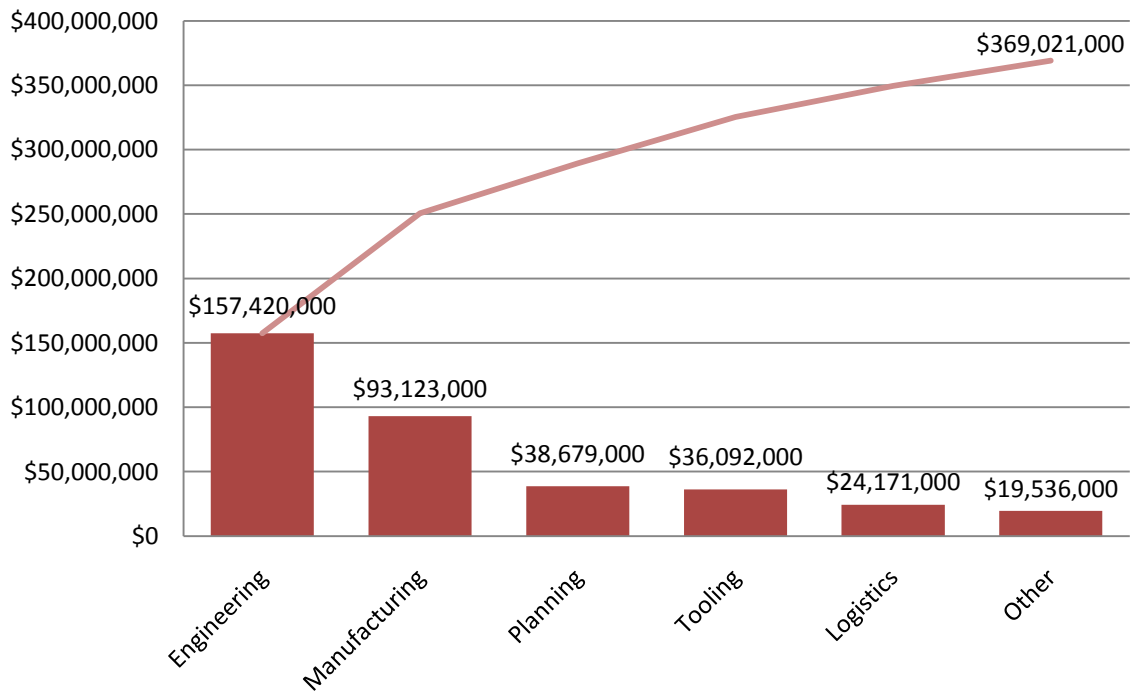


FIGURE O-1: ODYSSEY'S DEVELOPMENT COST (IN 2011 USD)

However this study only shows an evaluation of the RDTE cost based on many assumptions. It was decided to run later a statistical analysis to highlight the probability of hitting this value. 10,000 cases were run in a trial version of @RISK, which is an add-in to Microsoft Excel® using Monte Carlo simulation to show the possible outcomes of a scenario. One can judge which risk to take and which one to avoid, allowing for the best decision making process under uncertainty. Using a uniform distribution on the inputs variables (engineering, manufacturing, planning, tooling, logistics, and empty weight breakdown) it was possible to compute the final distribution of the RDTE cost, shown in Figure O-2. The left hand side shows the probability density function which follows a normal distribution and the right hand side shows the cumulative distribution function. There is a 90% chances to hit \$359 million for the RDTE cost and more than 98% chances to hit \$369 million.

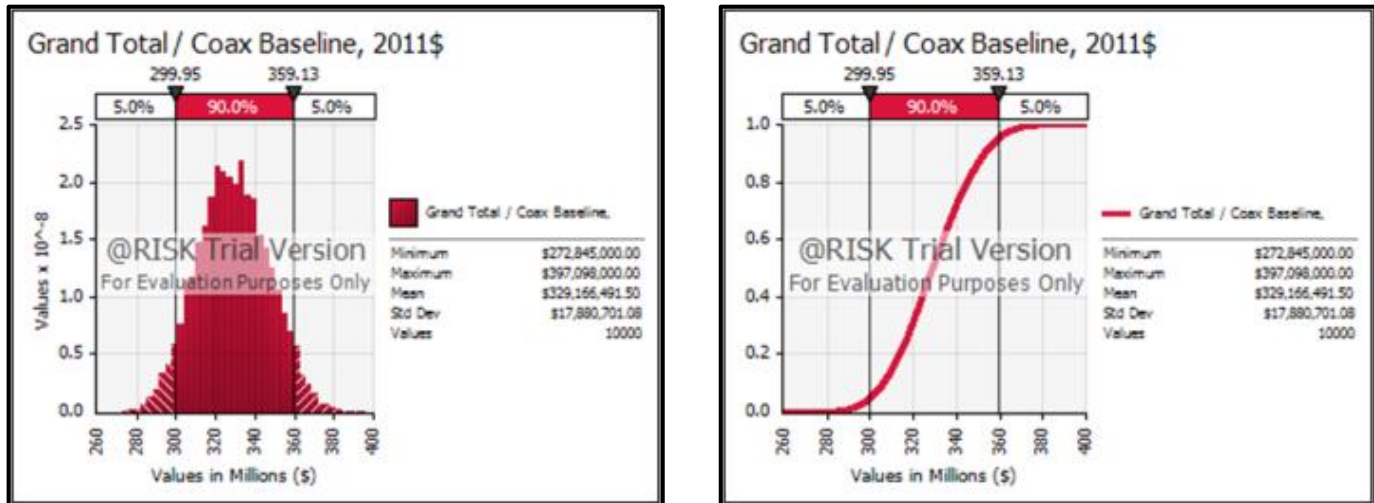


FIGURE O-2: MONTE CARLO SIMULATION OF THE RDTE COST

### Odyssey's transmission cost model

The Bell PC model was used to create an independent cost evaluation of Odyssey's transmission. The material selection and identification was a key step to calculate costs on the distinct stages of the transmission. The next move consisted in searching what components needed to be taken into consideration when calculating the different assembly types within each material. Production and tooling cost were necessary for each material. Production costs consist of all costs incurred in respect to the material characteristics. These characteristics range from physical aspects to handling difficulty. We obtained a specific production cost for each material-assembly type pair. The subcomponents necessary in finding production costs are material weight, material cost, and manufacturing complexity. Tooling costs refer to the actual assembly of the material. The subcomponents necessary in coming up with an accurate overall tooling cost for each material-assembly type pair involved the material weight, the tooling factor and the quantity of subparts made from each material.

At each Stage of the transmission, different parts such as gear(s) and ring(s) were analyzed. In order to compute costs for each part, we added up the costs of the materials and of the parts. The result was a distinct Production and Tooling cost for each stage for each manufacturing method (forging, sandcasting, machining, etc).

The results for the overall transmission are presented in Figure O-3. Based on the material used at each stage, we determined the possible manufacturing process for each of the particular parts. Table O-4 below shows the available assembly types for each of the parts in the transmission. Table O-5 shows the final configuration to reduce the cost of production of the first unit. The first unit of the transmission will cost \$1,167,700 in 2011\$. Applying a learning curve on this production might help to reduce the average cost of the unit. Assuming 200 units, the average production unit cost would drop to \$801,500 and would take approximately 1660 man-hours to complete.

TABLE O-4: POSSIBLE MANUFACTURING PROCESS FOR EACH PART

Alloy (Part)	Possible Methods
VASCOX2M (Sun)	Forging, Castings, Machining
VASCOX2M (Ring)	Forging, Castings, Machining
VASCOX2M (Planet)	Forging, Castings, Machining
AISI4340 (Carrier)	Forging, Castings
Pyrowear53 (Pinon)	Forging, Castings
VASCOMX2M (Gear)	Forging, Castings, Machining

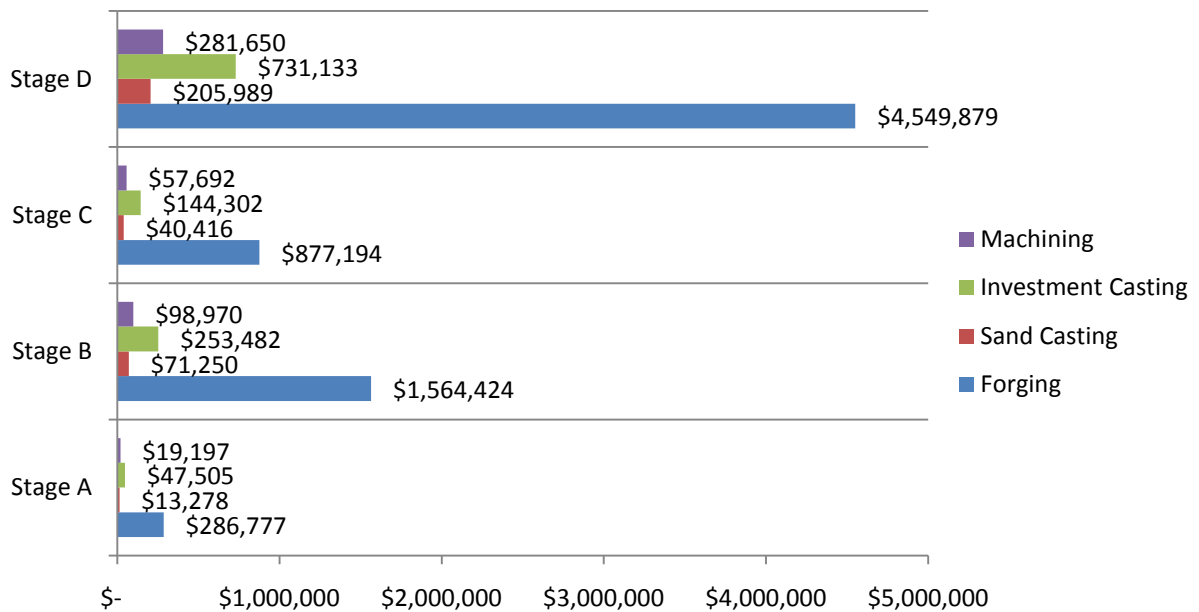


FIGURE O-3: DRIVE SYSTEM COST DECOMPOSITION VS. MANUFACTURING METHOD

TABLE O-5: FINAL MANUFACTURING COMBINATION

			Total Cost
139			
140	VASCOX2M (Sun)	Forging	\$1,167,712.52
141	VASCOX2M (Ring)	Forging	
142	VASCOX2M (Planet)	Forging	
143	AISI4340 (Carrier)	Forging	
144	Pyrowear53 (Pinon)	Casting	
145	VASCOMX2M (Gear)	Casting	

## O.2. Recurring cost and acquisition cost

The manufacturing phase along with the dynamic system, the engines integration, and avionics are considered part of the recurring production cost, and are generally associated with the acquisition cost or the price of the vehicle. The recurring cost for this vehicle was determined using the average unit production cost for 200 production units, produced over 4 years (50 units/year). The average unit cost with amortized non-recurring cost can be calculated using the learning curve applied to the quickstep method, as shown by the trend of the curve in Figure O-4. Targeting 200 units by 2029, the average unit cost is

evaluated at \$7,286,500 in 2011\$. Adding a profit of 12%, the unit price of Odyssey would be \$8,160,000 in 2011\$. The production cost breakdown is shown in Figure O-5. The flight controls, the power plant and the rotor design, including the Gurney flaps, represent more than 60% of the production cost, followed by the fuselage design which includes the duct fan and the drive system.

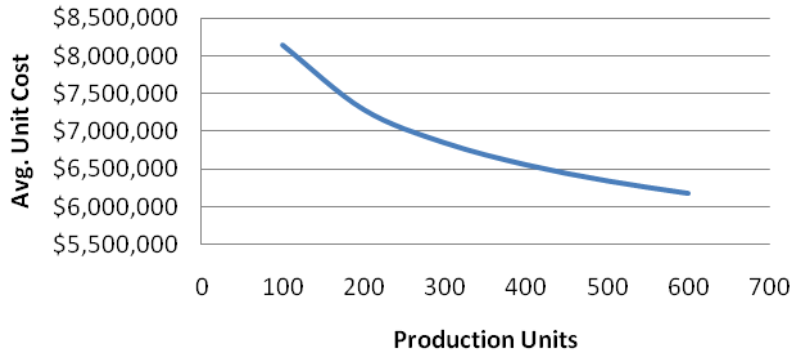


FIGURE O-4: ODYSSEY AVERAGE UNIT COST VS. PRODUCTION UNITS

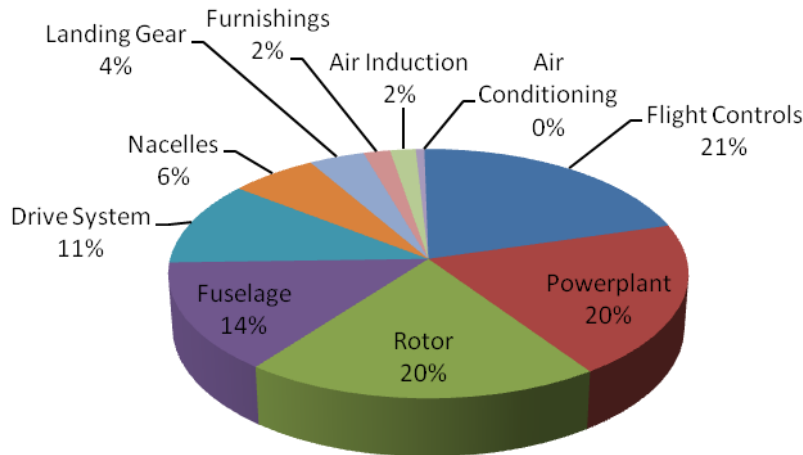


FIGURE O-5: AVERAGE PRODUCTION COST BREAKDOWN

### O.3. Direct operating cost

The final objective of the LCC analysis consists in studying the direct and indirect operating cost. Direct operating cost refers to the resources immediately required to drive the system or its independent units, such as fuel, lubricants, airframe maintenance, and engine overhaul. Indirect operating costs are more difficult to capture because they involve a broader category of cost that would occur if the vehicle did not exist. For example, flight crew labor, insurance policies, facilities maintenance, along with depreciation of the vehicle are considered indirect operating cost. Assuming a mission time between 3 and 4 hours on average, and assuming three missions per week as suggested by the RFP, it was possible to evaluate the minimum and maximum number of hours spent in flight over a year. The depreciation cost is difficult to estimate and depends on several other parameters that are out of scope of this study. However, assuming that Odyssey flies 600 hrs on average per year, the overall Operations & Support (O&S) costs can be estimated in Figure O-6.

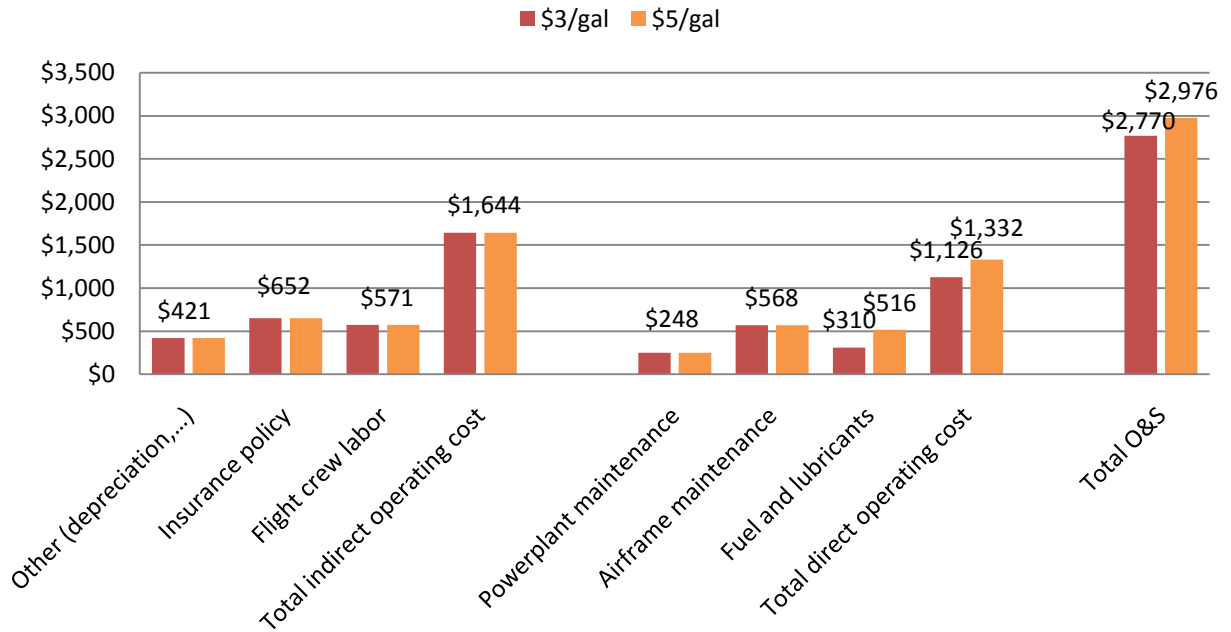


FIGURE O-6: OPERATIONS AND SUPPORT COST

Assuming the current fuel price (\$3/gallon), the total O&S cost is \$2,770/hr. However, due to recent forecast, it looks more sensible to conduct this analysis with a significant increase of fuel price (\$5/gallon). In this case, assuming the other cost to be insensitive to the fuel price, the O&S cost are estimated at \$2,976/hr. A sensitivity analysis was conducted and the results are presented in Figure O-7, showing that Odyssey’s total operating cost are less sensitive to the fuel price than the tilt rotor concept for example.

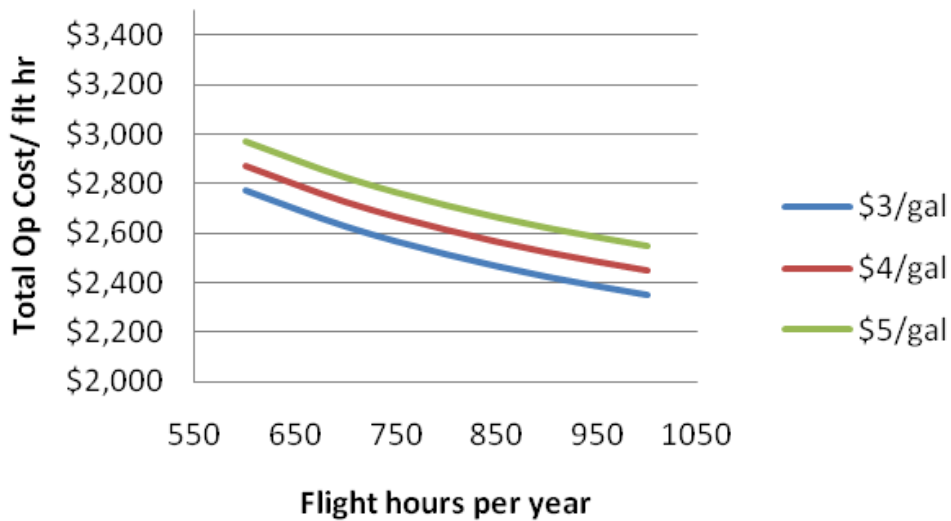


FIGURE O-7: SENSITIVITY ANALYSIS OF THE FUEL PRICE’S IMPACT ON THE O&S COST

## Appendix P CERTIFICATION CONSIDERATIONS AND TIMEFRAME

The purpose of this section is to provide some certification considerations to obtain the Type Certificate issued by the Federal Aviation Administration (FAA).

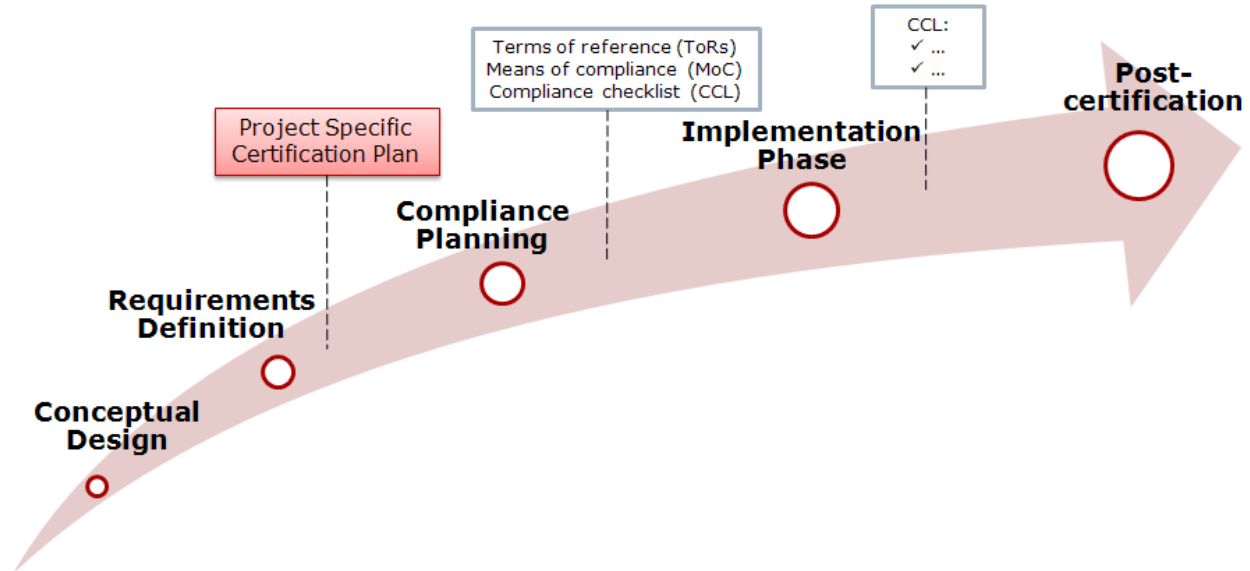
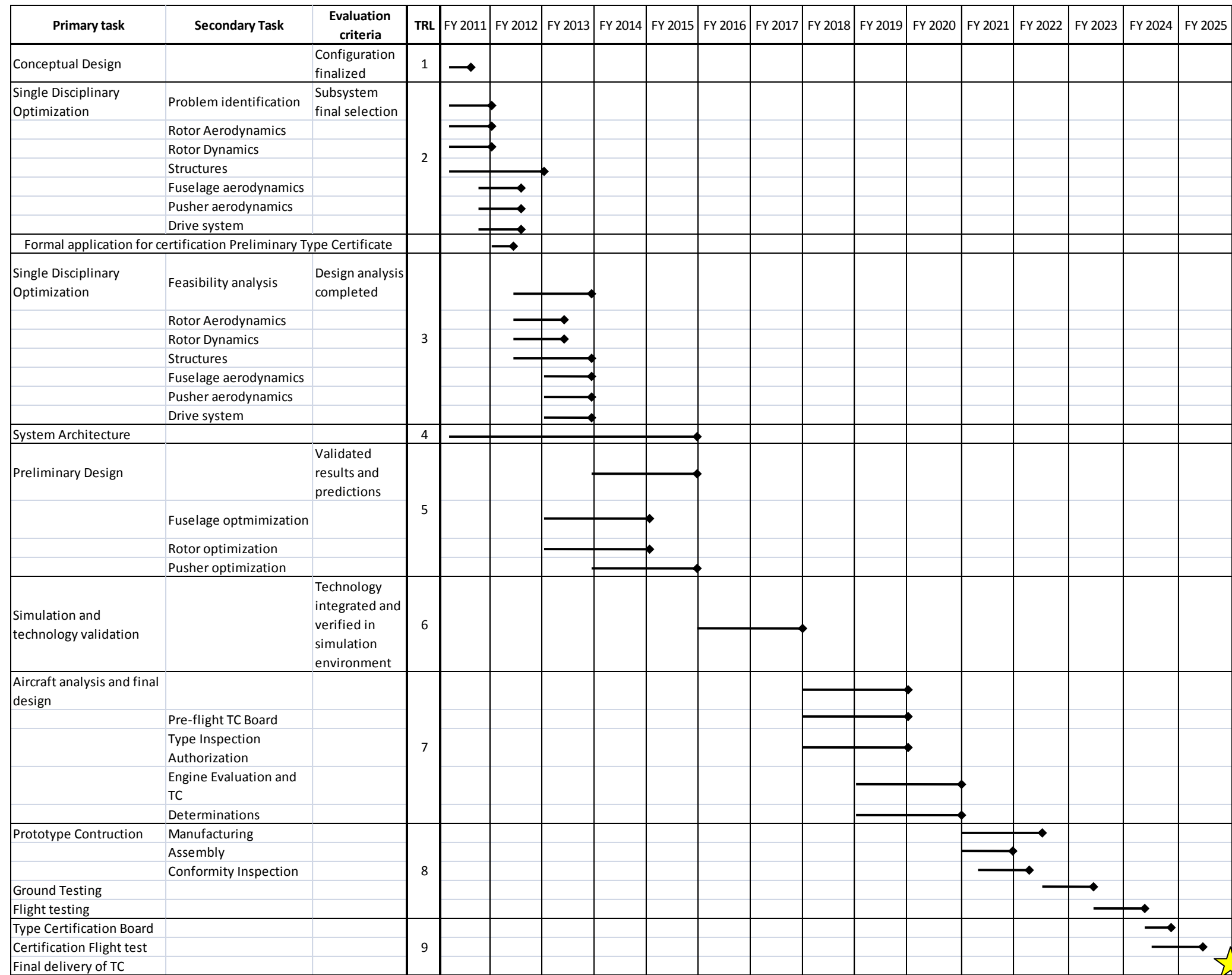


FIGURE P-1: FAA TYPE CERTIFICATE PROCESS

In order to understand the FAA Type Certification process depicted in Figure P-1, it is important to highlight that delegation has been a fundamental aspect of the FAA's organization. The FAA relies on both individual and organizational delegations in the certification process, and delegation is used to the maximum [34]. The applicant agrees to create a working environment where designers can make judgments on compliance and conformity problems, totally free from company pressure and with the support of the FAA.

DERs (Designated Engineering Representatives) are a group of experts acting within their disciplines during the certification process (for example structure, power plant, system and equipment, radio, engine, propeller, flight analysis, flight test pilot...). The DER may approve technical data, may witness FAA compliance tests and may perform investigations. Conceptual design is the early opportunity to bring together people involved in the certification process and to begin the formulation of a preliminary Project Specific Certification Plan (PSCP). The requirements definition phase aims at defining the product, the associated risks and converging towards a mutual agreement. Specific regulatory requirements and methods of compliance are formulated during this phase. The PSCP addresses the unique certification attributes of a design and the development of such a complete and elaborated document is beyond the scope of this design project. However an initial proposal timeframe was created to identify critical milestones in the certification procedure, as shown in Figure P-2.



TRL 1: Basic principles observed and reported.

TRL 2: Technology concept and/or application formulated.

TRL 3: Analytical and experimental critical function and/or characteristic proof-of-concept.

TRL 4: Technology component and/or basic technology subsystem validation in laboratory environment.

TRL 5: Technology component and/or basic technology subsystem validation in relevant environment.

TRL 6: Technology system / sub-system model or prototype demonstration in a relevant environment.

TRL 7: Technology prototype demonstration in an operational environment.

TRL 8: Actual technology system completed and qualified through test and demonstration.

TRL 9: Actual technology system qualified through successful mission operations.

FIGURE P-2: TENTATIVE DEVELOPMENT SCHEDULE AND CERTIFICATION TIMEFRAME

## CONCLUSIONS AND RECOMMENDATIONS

Odyssey is a multi-mission aircraft system designed to replace numerous current utility and SAR helicopters in the US armed forces by 2025. The requirements are driven by recent events following natural disasters, such as the recent tsunami in Japan, and by the current needs for a more efficient and affordable vehicle capable of performing different civilian and military missions everywhere in the world. The reconfiguration capability is a critical aspect of Odyssey which can be deployed anywhere on the US territory in less than 10 hours following a major emergency and can be self-deployed to locations outside the US. A military version, heavier and bigger, could also be developed in the next couple of years to address the US Army desire to progressively replace the current attack helicopters to provide Close Air Support to the ground troops.

The objective of going faster requires much more money for development and production efforts, along with an increase in direct operating costs. Odyssey would be more sensitive to the price of maintenance than the price of fuel and trades productivity for a mix of more modest speed improvement and competitive costs.

The micro flaps represent a promising technology in terms of vibration and noise reduction and would require further analysis. The Odyssey design team also recommends implementing Active Vibration Control in the airframe to counter the main rotor forces in hover and in forward flight. Verification and expansion of the Aircraft Flight Control System to include IBC and micro flaps may be also necessary in the next iteration of the Odyssey design process.

The main attributes of Odyssey are:

- A very compact, adaptable, high speed multi-mission advanced rotorcraft sizeable for future military needs
- Hybrid variable speed transmission with power regeneration for propeller
- Best-in-class high-speed performance
- Micro flaps for yaw control and enhanced maneuverability at low thrust settings
- Easily reconfigurable cabin layout for joint service deployment
- Ducted counter-rotating propellers to provide the translational thrust in high speed forward flight
- ICAO noise standards (Level 4) compliant vehicle
- IR suppression technologies for low detectability and improved survivability in hostile territories
- Crashworthy retractable landing gears and efficient lightweight primary structure
- Level 1 and 2 handling qualities for high speed and low speed agility
- Robust flight control system for enhanced flight safety and handling qualities
- Low direct and indirect operating costs, and acquisition price



*“ODYSSEY’s attributes makes it the next generation advanced helicopter with superior performance, affordability and multi-mission capability”*

## REFERENCES

- [1] Ashish Bagai, *Aerodynamic Design of the X2 Technology Demonstrator™ Main Rotor Blade*, 64<sup>th</sup> Annual Forum of the American Helicopter Society, International, Montreal, Canada, April 29-May 1, 2008.
- [2] Ashok, S. V., Schrage, D. P., and Robledo, A. *A Systems Engineering Modeling and Simulation Approach for Rotorcraft Drive System Optimization*, American Helicopter Society 67th Annual Forum. Virginia Beach, VA, May 2011.
- [3] Ashok, S. V., Wade, B., and Schrage, D. P., *Variable Speed Transmission using Planetary Gear System for High Speed Rotorcraft Application*, American Helicopter Society 66th Annual Forum. Phoenix, AZ, May 2010.
- [4] Bagai A., *Aerodynamic Design of the X2 Technology Demonstrator Main rotor blade*. AHS Annual Forum 2008
- [5] Bellocchio, A. T. *Drive System Design Methodology for a Single Main Rotor Heavy Lift Helicopter*, Master of Science Thesis, Aerospace Engineering. Georgia Institute of Technology, Atlanta, December 2005.
- [6] Blackwell R., Millot T., *Dynamics Design Characteristics of the Sikorsky X2 Technology™ Demonstrator Aircraft*, 64<sup>th</sup> Annual Forum of the American Helicopter Society, International, Montreal, Canada, April 29-May 1, 2008.
- [7] Borst, Henry V. *Summary of Propeller Design Procedures and Data*, Volume I. Aerodynamic Design and Installation. Henry V. Borst & Associates, 1973.
- [8] Bousman W., *Aerodynamic Characteristics of SC1095 and SC1094 R8 Airfoils*. NASA Technical Report, NASA/TP2003-212265 AFDD/TR-04-003, December 2003.
- [9] Chase N., *JMR Demonstrator Presentation*. International Powered Lift Conference, 5 October 2010.
- [10] Clancy L.J., *Aerodynamics*. Pitman Publishing Limited, London ISBN 0-273-01120-0, 1975.
- [11] Crosby W., *PEO Aviation SFL Overview*, Program Executive Office Aviation, May 12, 2009
- [12] Dalziel M. et al., "*Peregrine*": *Alternative Drive Rotor System*. Technical content, Georgia Tech Graduate report, 26h Annual AHS Student Design Competition, June 2009.
- [13] Davis Joseph, *Design Methodology for developing concept independent rotorcraft analysis and design software*. Master's thesis, Georgia Institute of Technology, School of Aerospace Engineering, December 2007
- [14] Dudley, D. W. *Handbook of Practical Gear Design*, Technomic Publication, 1994.
- [15] Fanucci, J. B. *Navy V/STOL Aerodynamics: Final Report*. West Virginia University, Aerospace Engineering. Report TR-40. February 1974.
- [16] Federal Aviation Administration official website, *Part29 - Airworthiness Standards: transport category rotorcraft*. Chapter I, Subchapter C, Regulations as of March 7, 2011
- [17] Federal Aviation Administration official website, *Part36.6*, Regulations as of March 7, 2011
- [18] Federal Aviation Administration official website, *Part91 - General operating and flight rules*. Regulations as of March 7, 2011.
- [19] Goldschmeid, F. R. 1987. *Fuselage Self-Propulsion by Static-Pressure Thrust: Wind Tunnel Verification*. AIAA Paper 87-2935, AIAA/AHS/ASEE Aircraft Design, Systems and Operations Meeting, St. Louis, MO, September 14-16.
- [20] Goodman, R.K. and Millott, T.A., *Design, Development, and Flight Testing of the Active Vibration Control System for the Sikorsky S-92*, American Helicopter Society 56th Annual Forum, Virginia Beach, VA, May 2000.
- [21] Gracey and Associates website, *Noise and Vibration glossary*. Accessed on March 10 2011.
- [22] Hennes Christopher, Leonard Lopes, Justin Shirey, James Erwin, and Kenneth S. Brentner, *PSU-WOPWOP 3.3.3 User's Guide*, The Pennsylvania State University, 2009.
- [23] Johnson Wayne, *Principles of Helicopter aerodynamics*. Chapter 13 Rotary Wing Aerodynamics, Dover publications, 1980
- [24] Leishman G., *Principles of Helicopter Aerodynamics*. Shyy W. & Rycroft M. edition, Cambridge Aerospace Series, 2006.
- [25] Levine Larry S., *Application of the ABC helicopter to the emergency medical service role*. 81-2653, presented at the AIAA/NASA Ames V/STOL Conference, Palo Alto, CA, December 1981

- [26] Litwin J. et al., *2011 AHS Design Competition: Coaxial Compound Concept*. AE 6333 Final Team Report, Fall Semester 2010, Georgia Institute of Technology, December 2010.
- [27] Matalanis Claude G., Wake Brien E., Opoku Daniel, Min B.Y., Yeshala Nandita, Sankar Lakshmi, *Aerodynamic Evaluation of Miniature Trailing-Edge Effectors for Active Rotor Control*, American Helicopter Society 66th Annual Forum. Phoenix, AZ, May 2010
- [28] Maurice L. et al., *Advanced aviation fuels: a look ahead via a historical perspective*. Propulsion and Power Directorate, Air Force Research Laboratory, August 2000.
- [29] McKay Mike and Luke Preisner. *Joint Transport Rotorcraft: sizing and parameter estimation*. AE 6331, School of Aerospace Engineering, Georgia Institute of Technology, Atlanta, GA, 2000.
- [30] McLemore, H.C. *Wind Tunnel Tests of a 1/20-Scale Airship Model with Stern Propellers*. NASA TN D-1026, January 1962.
- [31] Millott, T.A., Goodman, R.K., Wong, J.K., Welsh, W.A., Correia, J.R., and Cassil, C.E., *Risk Reduction Flight Test of a Pre-Production Active Vibration Control System for the UH-60M*, American Helicopter Society 59th Annual Forum, Phoenix, AZ, May 2000.
- [32] Min Byung-Young, Sankar Lakshmi, Bauchau Olivier, *A CDF-CSD coupled-analysis of HART-II Rotor Vibration Reduction using Gurney Flaps*, American Helicopter Society 66th Annual Forum. Phoenix, AZ, May 2010
- [33] Minor et al., "Athena". Technical content, Georgia Tech Graduate Report, 25th Annual AHS Student Design Competition, June 2008.
- [34] Mugnier Marc, *An investigation on the current certification procedures and ATA24 considerations for highly-integrated airborne systems*, Technical report submitted to Hispano-Suiza, Aerospace Systems Design Laboratory, Georgia Institute of Technology, School of Aerospace Engineering, April 2011
- [35] Norton, R. L. *Machine Design - An Integrated Approach*, Pearson Prentice Hall, Third Edition, 2006.
- [36] Patel N., Zaidi T., Bernardo J., Chen P., Jackson D., Oh S., Tsai E., *Formulation and implementation of a methodology for aircraft subsystem architecture selection*, External Advisory Board Presentation, Aerospace Systems Design Laboratory, Georgia Institute of Technology, April 29, 2009.
- [37] Pretto Ernesto, Peter Safar, *National Medical Response to Mass Disasters in the United States: Are we prepared?* Journal of the American Medical Association (JAMA), no 266, pp 1259-1262, 1991
- [38] Prouty R.W. 1986. *Helicopter Performance, Stability, and Control*, PWS Engineering Publishing, Boston, MA.
- [39] Runge W. et al., *Configuration Analysis of Coaxial Compound Rotorcraft for AHS Future Mission Requirements*, AE 6333 Final Team Report, Fall Semester 2010, Georgia Institute of Technology, December 2010
- [40] *Sample Industry Conceptual Design Study of Helicopter, Compound Helicopter and Tilt Rotor Aircraft*. LHX Concept Definition, Boeing Vertol Company, January 1983.
- [41] Sankar Lakshmi, *Vehicle Performance methods*. School of Aerospace Engineering, Georgia Institute of Technology, Atlanta, AE 6070 Rotary Wing Design Course Notes, Fall Semester 2010.
- [42] Schaeffler Norman W., Brian G. Allan, Caroline Lienard and Arnaud Le Pape, *Progress Towards Fuselage Drag Reduction via Active Flow Control: A Combined CFD and Experimental Effort*, 36<sup>th</sup> European Rotorcraft Forum, Paris, France, Sep. 7-9, 2010.
- [43] Schrage Daniel P., *Extension of Rf Method for Advanced VTOL Aircraft*. School of Aerospace Engineering, Georgia Institute of Technology, Atlanta, AE 6333 Rotorcraft Systems Design I Course Notes, Fall Semester 2010.
- [44] Schrage Daniel P., *Extension of RF method to VTOL Aircraft Conceptual and Preliminary Design*. School of Aerospace Engineering, Georgia Institute of Technology, Atlanta, AE 6333 Rotorcraft Design I Course Notes, Fall Semester 2010.
- [45] Schrage Daniel P., *Georgia Tech IPPD process guidelines for rotorcraft preliminary design*. School of Aerospace Engineering, Georgia Institute of Technology, Atlanta, AE 6333 Rotorcraft Design I Course Notes, Fall Semester 2009.
- [46] Schrage Daniel P., *Rotorcraft Modeling for Hover and in Forward Flight*. School of Aerospace Engineering, Georgia Institute of Technology, Atlanta, AE 6333 Rotorcraft Design I Course Notes, Fall Semester 2010.

- [47] Schrage Daniel P., *Vehicle Synthesis for advanced VTOL Aircraft*. School of Aerospace Engineering, Georgia Institute of Technology, Atlanta, AE 6333 Rotorcraft Systems Design I Course Notes, Fall Semester 2004.
- [48] Sikorsky official website, accessed on March 9th 2011.
- [49] Sikorsky UH-60L Black Hawk, *UH-60A/L Comparison at mission gross weight*. Sikorsky official website, December 2001
- [50] Thiel Michael R., Lesieutre George A., Maughmer Mark D., Koopmann Gary H., *Actuation of an Active Gurney Flap for Rotorcraft Application*, 47<sup>th</sup> AIAA Structures, Structural Dynamics and Materials Conference, Newport, Rhode Island, May 2006
- [51] US Department of Transportation Federal Aviation Administration, *Type certificate Data Sheet H2NE Sikorsky Aircraft*. Revision 3, S-70 (UH-60A, UH-60L), October 24, 1995.
- [52] Wilson Ronald and James McKay, *Landing loads and accelerations of the XB-70-1 Airplane*. National Aeronautics and Space Administration (NASA) Technical note No 4336